A Thesis for the Degree of Ph.D. in Engineering

Response of shock loading and effect of pressure on ultrasonic propagation in magnetorheological fluids

September 2013

Graduate School of Science and Technology
Keio University

Ahmad Isnikurniawan

SUMMARY OF Ph.D. DISSERTATION

School Integrated Design Engineering	Student Identification Number	First name Surname Ahmad Isnikurniawan

Title

Response of shock loading and effect of pressure on ultrasonic propagation in magnetorheological fluids

Abstract

In this research, the behavior of magnetorheological fluid when subjected to high excitation or shock loading is investigated experimentally. In order to fully understand the behavior of cluster formation in this fluid under pressure that caused by shock loading, another experimental analysis is performed. Ultrasonic measurement technique is applied since magnetorheological fluid is opaque. The properties of ultrasonic propagation change when cluster structures formed in magnetorheological fluid. Therefore, cluster formation in this fluid under various magnetic fields and pressures can be analyzed based on the change of ultrasonic propagation properties. This dissertation is organized into six chapters.

Chapter 1 introduces the basic characteristic of magnetorheological fluid, background and objectives of the research, contributions and outline of this dissertation.

Chapter 2 summarizes the previous studies on the behavior of magnetorheological fluid under shock loading. The experimental apparatus, experiment procedure, preliminary results and repeatability of the experiment system are also described.

Chapter 3 discusses the effect of magnetic field, orifice inner diameter and volume fraction on the performance of magnetorheological fluid to handle the shock loading. At low impact velocity, magnetic field has significant effect. However, the effect becomes not significant at high impact velocity. Damping force is relatively similar under different field. It because the force, which caused by shock loading, is much higher than the viscous force, which generated by the magnetic field. Performance of magnetorheological fluid under shock loading is also affected by orifice inner diameter and volume fraction of this fluid. The smaller orifice inner diameter is stronger to handle the shock loading. Moreover, the higher volume fraction, the bigger cluster is formed. In addition, bigger cluster is stronger to handle the shock loading.

Chapter 4 summarizes the previous studies about the inner structure in magnetorheological fluid. It also describes the experimental apparatus and method of ultrasonic technique, procedure and experiment results. Temperature has significant effect on the cluster formation. The cluster size becomes smaller when higher temperatures are applied. In the application of magnetic field, magnetic particles begin to form cluster in seconds. The cluster size becomes bigger when higher magnetic fields are applied. Frequency of alternating magnetic field also affects the cluster size. The cluster size becomes smaller when higher frequencies are applied.

Chapter 5 describes the experimental apparatus, procedure and the results of the investigation of cluster formation in magnetorheological fluid under pressures. At low magnetic flux densities (100 and 200 mT), the cluster size becomes smaller under higher pressures. However, at high magnetic flux densities (300 and 400 mT), the effect of pressure becomes not significant. At that range of magnetic field, cluster formation is strong enough to handle the pressure. These results confirm that magnetic field has effect on the performance of MR fluid to handle pressure that caused by shock loading. The higher magnetic flux densities produces bigger cluster. The bigger clusters are stronger to handle the amount of pressures that caused by the shock loading.

Chapter 6 summarizes the results in this study.

Acknowledgments

First of all, I am grateful to Almighty Allah Ta'ala for providing me this opportunity and granting me the capability to finish this work successfully.

I would not have been able to complete this work without the support of many people over the past three years. Therefore, I would like to offer my sincere thanks to all of them. First, I would like to express my deepest gratitude and appreciation towards my supervisor, Prof. Tatsuo Sawada, whose expertise, understanding and patience, added considerably to my graduate experience. Without his valuable advice, warm encouragement, thoughtful guidance and critical comments, this work would not have been completed.

I would like to express my great appreciation to Prof. Toshihiko Sugiura, Assoc. Prof. Kazuo Nakazawa and Assoc. Prof. Kenjiro Takemura for the valuable advice, comment and discussions. I would also like to convey my appreciation to Prof. Yasushi Ido of Nagoya Institute of Technology and Dr. Masaaki Motozawa of Shizuoka University for their valuable discussion and advice.

Thanks to all member and former member of Sawada Laboratory for their help, guidance and support during the whole period of my study, particularly for Dr. Kenichi Ohno, Dr. Muhammad Agung Bramantya, Mr. Jun Kuroiwa, Mr. Yoshitaka Moroka, Mr. Hiromichi Ohba, Mr. Shunsuke Kaneko, Mr. Yasuhiro Fujita, Mr. Hiro Kaneko, Mr. Sachio Tanimoto, Mr. Shin-Ichiro Takemoto, Mr. Ryo Yoshizawa, Mr. Kanta Moriyama and Mr. Yuzo Shimizu. I would also like to acknowledge to all workshop staffs of Faculty of Science and Technology, Keio University, whose expertise in machining works, particularly for Mr. Aihara, Mr. Morita, Mr. Saita and Mr. Yoshida. Because of their guidance, this work can run very well.

Over the past three years, I have enjoyed the aid of scholarship, which supported me during my PhD program. I express my gratitude to Japan International Cooperation Agency (JICA) for the financial support and JICA staff, especially Mrs. Maria Sutherland, Ms. Tomomi Nishigaki and Mr. Masataka Tsuchiya for their help and support. I would also like to thank the Asean University Network/Southeast Asia Engineering Education Development Network (AUN/SEED-Net) and AUN/SEED-Net staff for their help and guidance, particularly, Ms. Siriporn Rungreangtanya and Ms. Karnkitti Patanasuthikul. I would also like to thank Keio University for providing the research grant and also giving me the opportunity to attend many conferences and meet so many interesting people. Moreover, I would like to thank Gadjah Mada University, especially Department of Mechanical and Industrial Engineering as my sending institution.

Many thanks to all of my friends at Keio University, Dr. Gunawan, Dr. Khairul, Dr. Sofyan, Mr. Roni, Mr. Dhresta, Mr. Rosdzimin, Mr. Faizal, Mr. Ajib, Mr. Nazirul, Mr. Aifa, Mr.

Aizuddin, Mr. Ilmiawan, Mr. Alpha and the others for their warm friendship and provides a wonderful atmosphere in Keio University, especially in Yagami campus.

I would also like to thank my parents and my mother and father-in-law for their encouragement and support. I also thank my elder brother for his support and assistance in numerous ways.

Finally, I dearly thank to my wife Dr. Khusnun Widiyati and my son Muhammad Yahya for their love, patient, support, encouragement and understanding. May Allah Ta'ala give you all the best in return.

Contents

List of Figures

List of Tables

Nomenclatures

a	:	Radius of the particle (m)
B	:	Magnetic flux density (mT)
C_0	:	Concentration of magnetic particles (%)
Dp	:	Piston displacement (mm)
Dp_{max}	:	Maximum value of piston displacement or piston stroke (mm)
E	:	Energy (J)
Er	:	Measurement error
f	:	Frequency (Hz)
F	:	Damping force (N)
F_{max}	:	Peak value of transmitted force (N)
g	:	Gravity acceleration (m/s^2)
h	:	Drop height (mm)
H	:	Magnetic field intensity (A/m)
I	:	Electric current (A)
I_m	:	Moment of inertia density for the grains
m	:	Mass (kg)
m_{MR}	:	Mass of MR fluid and the piston (kg)
M	:	Drop mass (kg)
M_m	:	Magnetic moment (J/T)
n	:	Sample size
KE	:	Kinetic energy (J)
P	:	Momentum (J/s)
PE	:	Potential energy (J)
Pi	:	Sound pressure at the receiver with magnetic field (dB)
Pin	:	Inlet pressure (Pa)
Po	:	Sound pressure at the receiver without magnetic field (dB)
$Pout$	:	Outlet pressure (Pa)
r	:	Separation vector between the centers of the two particles (m)
s	:	Data interval
SD	:	Standard deviation
t	:	Time (s)

T	:	Temperature (°C)
W	:	Interaction energy between two dipoles (J)
T_i	:	Ideal value of one wavelength (s)
T_m	:	Averages value of one wavelength (s)
T_s	:	Propagation time from the experiment system (s)
v	:	Impact velocity (m/s)
V	:	Ultrasonic propagation velocity with magnetic field (m/s)
V_o	:	Ultrasonic propagation velocity without magnetic field (m/s)
Vp	:	Piston velocity (m/s)
Vp_{max}	:	Maximum value of piston velocity (m/s)
x_i	:	Data sample
$\bar{x}$	:	Mean or average value
β	:	Ratio of relative magnetic permeability and permeability of the fluid
β_e	:	Average elastic modulus of medium
θ	:	Angle between propagation direction and magnetic field direction (°)
ρ	:	Density (kg/m^3)
ϕ	:	Orifice inner diameter (mm)
Φ	:	Volume fraction (%)
λ	:	Ratio between the interaction energy of two particles with the thermal energy
μ	:	Viscosity (Pa $\cdot$ s)
μ_f	:	Permeability of fluid (H/m)
μ_0	:	Permeability of vacuum (H/m)
μ_p	:	Relative magnetic permeability
$\dot{\gamma}$	:	Shear rate
τ	:	Shear stress (Pa)
τ_t	:	Relaxation time
τ_y	:	Yield stress (Pa)
ΔP	:	Pressure difference between inlet and outlet of the orifice (Pa)
ΔP_{max}	:	Peak value of pressure difference (Pa)
$\Delta\alpha$	:	Change of ultrasonic propagation attenuation (dB/m)
$\Delta V/V_o$	:	Change of ultrasonic propagation velocity (%)
$(\Delta V/V_0)_{\max}$	:	Maximum value of change of ultrasonic propagation velocity (%)
ω	:	Natural frequency (Hz)
ω_C	:	Natural frequency for the orientation fluctuations (Hz)

Chapter 1

Introduction

1.1 Introduction

The main purpose of this chapter is to introduce magnetorheological (MR) fluid and other field responsive fluids, rheological properties and operational modes of MR fluid to the reader. In addition, the background, objectives and contributions are presented. Lastly, the outline of the dissertation is presented.

1.1.1 Field responsive fluids

Field responsive fluids are known as a class of smart materials since their properties can be altered or tuned using an external field [1]. These field responsive fluids include electrorheological (ER) fluid, MR fluid, magnetic fluid or ferrofluid and certain types of polymeric gels. These fluids typically consist of nano or micro sized solid particles dispersed in a carried liquid. ER fluids require the use of solid particles that responsive to an electric field while MR fluids and magnetic fluid require the use of solid particles that are magnetizable or responsive to magnetic field.

Electrorheological fluid

ER fluid is classified as field responsive fluids since its rheological properties can be controlled using electric field. This fluid was first reported by Winslow [2] in 1947. Apparent viscosity of this fluid increases very fast by several orders of magnitude when higher strength of electric field is applied [3, 4, 5].

ER fluid is formed by dielectric particles suspended in a non-conducting liquid. These dielectric particles migrate and lead to the formation of large particle aggregates elongated in the field direction under the influence of externally applied electric field [6, 7]. Particles are free to slide over each other when electric field is not applied [8]. The size of the particle is about 10 μm. When electric field is applied to the fluid, particles begin to form structure which parallel to the field direction. The structure formation has strong effect on the mechanical and physical properties of ER fluid. For example, the thick column structure has a higher shear stress than the single-chain structure [9].

According to their characteristic, ER fluid is classified into two types which are particle type

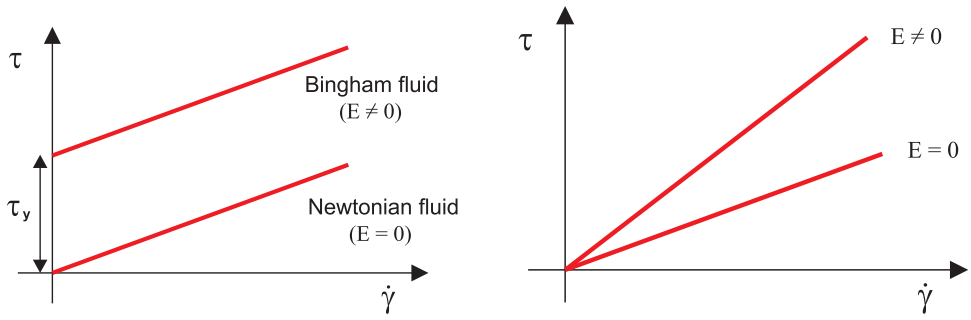

(a) Particle type (b) Homogeneous type

Figure 1.1: Characteristics of particle type (a) and homogeneous type (b) of ER fluid

and homogeneous type [10]. The exhibit characteristic of particle type ER fluid is fairly well described by Bingham plastic model [7, 11, 12]. According to the Bingham plastic model, this type of ER fluid does not flow until the applied shear stress (τ) reaches the critical value or yield stress (τ_y). ER fluid starts to flow and exhibit like Newtonian fluid when the fluid is stressed higher the yield stress. Figure 1.1 (a) illustrates a simple Bingham fluid and a Newtonian fluid model. A Newtonian fluid is a fluid which its stress at any point is proportional to the applied strain rate ($\dot{\gamma}$) at that point. The homogeneous type ER fluid have been developed by using low-molecule liquid crystal or macro-molecular liquid crystal [13]. The exhibit characteristic of this type of ER fluid is presented in Fig. 1.1(b). The shear stress nearly proportional to shear rate is generated, and its slope, namely viscosity can be controlled by electric field. As a result, it is possible to acquire a mechanical control force proportional to the speed under a constant electric field and to mechanically realize what is equivalent to the so-called differential control [10].

Due to the characteristic of ER fluid which capable of varying viscosity or even solidification in response of electric field and have a few millisecond of response time to the electric field, this fluid has been used in various application. Information of the current and potential application of ER fluid is presented in Table 1.1.

Magnetorheological fluid

MR fluid was first reported by Rabinow [14] in 1948. MR fluid is formed by micron-size of magnetic particles suspended in nonmagnetic fluid such as silicon oil. The most common magnetic material in preparation of MR fluids is high purity iron (Fe) powder [15, 16]. Small amount of additive or surfactants are usually added to improve the performance of MR fluid, for example to decrease the aggregation of magnetic particles.

The magnetorheological response of MR fluid results from the polarization induced in the suspended particles by application of an external field [17]. In the absence of magnetic field, MR fluid exhibits Newtonian-like behavior [18]. When magnetic field is applied, magnetic particles in MR fluid become magnetized, behave like tiny magnets and form particle clusters that parallel with the magnetic field direction. The cluster formation will grow with the strength of magnetic field. The increase in magnetic field strength increases the size of cluster formation in MR fluid.

Table 1.1: Application of ER fluid

Field	Device	Application
Automotive	Damper Clutch	Vehicle suspension and engine mount [19, 20, 21, 22]. Alternator clutch and engine accessory drive clutch [19].
Mechanical Engineering	Brakes Clutch	Exercise machine [23]. Turbine [24].
Machining	Damper Bearing Polishing	Machine tool table and cutting test [25, 26]. Guideways and spindles of machine tools [26]. Surface finishing [27, 28, 29].
Robotic	Damper Brakes Actuator	Robot arm [10] and artificial muscle manipulator [30]. Passive force display for virtual reality [31]. Adaptive control of pneumatic muscle actuators for a robotic elbow [32, 33].
Medical	Actuator Spherical joint	Virtual reality and medical treatments [34]. Minimally invasive surgery [35].

The motion of the MR fluid becomes slower because of this cluster structure. A shear stress or a pressure difference is needed to disrupt this cluster formation in MR fluids. The strength of the fluid, such as the value of apparent yield stress, increases when the strength of applied magnetic field is increased.

Currently, MR fluid is considerably stronger than ER fluid, which has a yield stress at or below 10 kPa. This makes MR fluid very attractive [36]. Based on the apparent viscosity of MR fluid which changes rapidly with the application of magnetic field, this fluid has been applied in many applications such as in automotive, mechanical engineering, civil engineering, machining, robotic and medical applications. The detail of the current and potential application of MR fluid is presented in Table 1.2.

Magnetic fluid

Magnetic fluid is a stable colloidal dispersion of nano-sized of magnetic particle in liquid carrier, such water, kerosene and silicon oil. The most common magnetic particle materials used in a magnetic fluid are ferrites such as magnetite (Fe_3O_4) and maghemite (Fe_2O_3) and metallic particles such as cobalt and iron particles [37]. The magnetic particle in magnetic fluid will form chain-like cluster when magnetic field is applied. The mean diameter of magnetic particle in magnetic fluid is about 10 nm. In order to avoid agglomeration due to magnetic dipole interaction, the particles in magnetic fluid are coated with a surfactant [38, 39]. The typical thickness of the surfactant layer is about 2–3 nm. By coating with surfactant, a stable suspensions of magnetic particles in carrier liquids can be obtained [40].

The dependence of chain-like cluster formation on the magnetic field strength and shear stress applied to the fluid leads to strong changes of viscosity and to the appearance of viscoelastic effects in the fluids [41]. In comparation with MR fluid, magnetic fluid has smaller the magnetic particle size. Particles in magnetic fluid are in brownian motion and remain suspended under

Table 1.2: Application of MR fluid

Field	Device	Application
Automotive	Damper Clutch	Vehicle suspension [42, 43, 44, 45], engine mounts [46] and helicopter crew seat suspension [47, 48]. Transmission clutch [49, 50].
Mechanical Engineering	Brake	Aerobic exercise equipment [51, 52, 53, 54, 55].
Civil Engineering	Damper	Control of seismic vibration in structures [56, 57].
Robotic	Clutch Brake	Coupling the motor drive to the joint [58]. Haptic glove for virtual reality [59].
Medical	Clutch Brake	Leg robot for physiotheraphist of brain-injured patient [60]. Intelligent ankle-foot orthosis [61].

room condition [62]. Brownian motion is a random movement of particles which suspended in a fluid resulting from their constant activity of atoms or molecules in the gas or liquid [63]. Since particle material in MR fluid is in micron sized, the particles are too heavy for brownian motion to keep them suspended, and thus will settle over time due to the inherent density between the particle and its liquid carrier. Moreover, larger MR fluid particles allow for stable, highly magnetizable materials and reversible particle aggregation [17].

One of the most promising properties of ferrofluids is the possibility to significantly influence their flow behavior by moderate magnetic fields [64]. Magnetic fluid is commonly used in industries such as computers, loudspeakers, semiconductor, motion control, sensors and petrochemical [65, 66]. The application of magnetic fluid is presented in Table 1.3.

Mixing magnetic fluid and MR fluid

Particle distribution in magnetic fluid is more stable than that of MR fluid since magnetic fluid are synthesized by colloidal magnetic particles. However, apparent viscosity of magnetic fluid is smaller than that in MR fluid. In order to achieve larger apparent viscosity as well as a more stable distribution of particles while maintaining their behavior as fluids, Shimada et al. [67] proposed a new magnetically responsive fluid compound which called magnetic compound fluid (MCF) using nanometer-sized magnetite and micrometer-sized iron particles in a solvent. This fluid is produced by mixing magnetic fluid and MR Fluid. The magnetization of MCF and MR fluid under AC and DC magnetic field is larger than that of magnetic fluid [68]. This fluid can be applied for damper, polishing and as composite material [69, 70]. Another researcher also studied performance of nano-fluid based MR fluids [71]. Nano-fluid based MR fluid is more stable than conventional MR fluid, which subsequently increases their application potentiality.

Table 1.3: Application of magnetic fluid

Field	Device	Application
Mechanical engineering	Seal	Coatings system and heat treating furnaces [65, 66] and vacuum seals for rotary shafts [72, 73].
	Bearing	Journal bearings lubricated with ferrofluid [74].
	Damper	Vibration isolating table [75] and rotary shaft [76].
Machining	Grinding	Manufacturing process [77, 78].
	Polishing	Manufacturing process [79, 80].
Electrical engineering	Seal	Semiconductor processing, fiber optics, lasers, X-ray machines and avionics [65].
	Stepper	Permanent magnet stepping motor [66].
	Sensor	Avionics, robotics, machine tool, automotive and medicine industry[65, 66].
	Loudspeaker	Electronics devices [65, 66].
Medical	Cancer treatment	Targeting drug delivery and magnetic fluid hyperthermia [81, 82, 83, 84].

1.1.2 Rheological properties of MR fluid

Rheology is a study of the deformation and flow of matter in response to an applied force. Rheology can be used to describe the properties of a wide variety of materials. A rheometer is an instrument to measure the rheological properties of the fluid. Based on the measurement results, the stability of the rheological properties of the fluid can be analyzed. The stability of the rheological properties of the fluid is important to the product and process performance in industrial applications. The stability of the fluid is affected by many factors such as hydrodynamic forces, Brownian motion, volume fraction, electrostatic forces, size and shape of particles.

Rheological properties of MR fluid change quickly with the application of magnetic field. The rheological properties of this fluid depend on the concentration and density of particles, particle size and shape distribution, properties of the carrier fluid, additional additives, applied field, temperature and other factors [85].

The efficiency of an MR fluid is firstly judged through its yield stress, which determines the strength of the structure formed by the application of the magnetic field [86]. The yield stress depends on the magnetic field applied to the field. The value of yield stress is indicated by the maximum value of stress after the increases in magnetic field have no further effect. Similar to the ER fluid, the rheology of ER fluid under steady shear is usually well represented by a Bingham law [86]:

$$\tau = \tau_y + \eta\dot{\gamma},\ \tau > \tau_y \tag{1.1}$$

$$\dot{\gamma} = \frac{\partial u}{\partial y} \tag{1.2}$$

where τ is shear stress, τ_y is yield stress caused by the applied field, $\dot{\gamma}$ is shear strain rate and η is field dependent post yield plastic viscosity, which is defined as the slope of the measured shear stress versus the shear strain rate [57].

1.1.3 Operational modes of MR fluid

There are three different operational modes of MR fluid; valve mode, shear mode and squeeze mode, based on the fluid flow and the way of stress application [17, 18].

Valve mode

Figure 1.2 illustrates the valve mode of operational modes in MR fluid. In the valve mode, fluid flows inside a pipe or an orifice. The magnetic field is applied in perpendicular direction with the flow direction. By applying magnetic field in that area, the viscosity of the MR fluid can be controlled. Moreover, the flow of MR fluid also can be controlled. The examples of valve mode devices include servo-valves, dampers, shock absorbers and actuators [17, 51].

Shear mode

Figure 1.3 illustrates the shear mode of operational modes in MR fluid. In the shear mode, a plate moves or rotates in relation with other plate. The magnetic field is applied in perpendicular direction with the plate direction. Plate motion or rotation in the system can be controlled by changing the strength of magnetic field. The examples of shear mode devices include clutches, brakes, chucking and locking devices, dampers and structural composites [17, 51].

Squeeze mode

Figure 1.4 illustrates the squeeze mode of operational modes in MR fluid. In the squeeze mode, MR fluid is subjected to tension or compression loading. The magnetic field is applied in parallel direction with the loading direction. The distance between two plates under loading can be controlled by changing the strength of magnetic field. The examples of squeeze mode devices include small amplitude vibration and impact dampers [17].

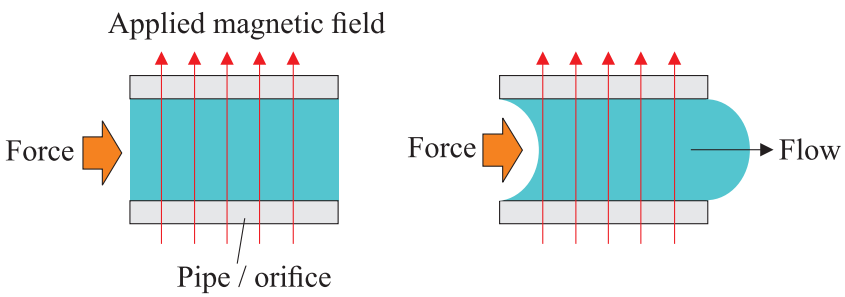

Figure 1.2: Concept of valve mode

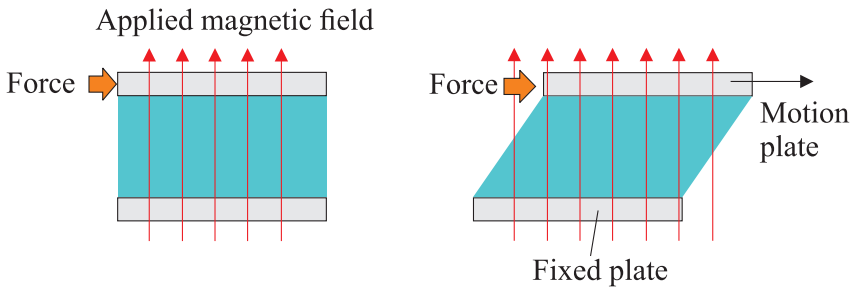

Figure 1.3: Concept of shear mode

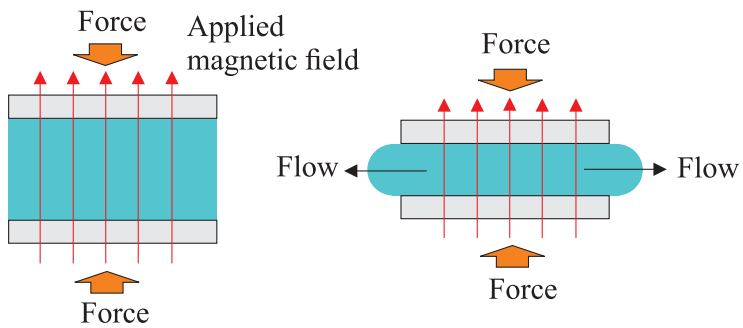

Figure 1.4: Concept of squeeze mode

1.2 Background

In recent years, MR devices have been attracting the attention of the marketplace. For example, MR damper has been developed by Lord Corporation. This damper has been applied in automotive primary and secondary suspensions, seat suspensions and military suspensions. In comparation to the conventional mechanical controllable devices, MR damper offers quick response time, continuously variable control of damping, simple design and relatively safe with extreme temperature.

In an automotive system, most conventional suspension uses passive spring and damper with rather limited vibration performance, both for linear and nonlinear restoring or damping characteristics [87]. In order to improve the vibration performance, semi-active MR damper has been introduced. Semi-active MR damper, which consists of a conventional spring and an adaptive damper, is capable of changing its response on demand and can provide the same performance as active suspensions without high power consumption and with only minor design variations from conventional passive systems [44].

In regard to the potential application of MR damper, a lot of study and investigation on MR damper have been conducted both theoretically and experimentally. The majority of the publication focused on the damping characteristic of MR damper, which subjected to cyclic and low excitation [88, 89]. Under the cyclic and low excitation, the magnitude of damping force increases when higher magnetic flux densities are applied. The performance of MR fluid devices under high excitation has been investigated by few researchers [90, 91] using commercial MR damper. However, the behavior and performance of MR fluid under high excitation is not fully

understand. Therefore, behavior and performance of MR fluid when subjected to high excitation or shock loading is investigated experimentally in this research.

In order to get fully understanding about the behavior of inner structure in MR fluid under pressure that caused by shock loading, another experimental analysis are conducted in this research. Due to the characteristic of MR fluid, which is opaque, ultrasonic measurement technique is applied. Moreover, in comparison to the optical observation technique, the ultrasonic techniques are especially advantageous when the number of particles is high [92]. The properties of ultrasonic propagation, such as propagation velocity and attenuation, change when clustering structures form in magnetic and MR fluids [93]. Therefore, inner structure in MR fluid under magnetic field can be analyzed based on the change of ultrasonic propagation properties. In order to explain about this measurement technique, experiments are conducted by applying DC and AC magnetic field. Investigation of inner structure in MR fluid under AC magnetic field is conducted since majority researcher investigate the behavior of MR fluid under DC magnetic field [92, 94, 95]. The effect of applied time, temperature, magnetic field, magnetic field sweep rate and frequency of AC magnetic field on the cluster formation in MR fluid is analyzed in this study.

There are few publications on the study of MR fluid characteristic under pressure. Several researchers [96, 97] conducted experiment by subjecting a load through a cylinder to the MR fluid. The load was moved from the initial position to a certain gap. Their experiment results confirmed that the type of MR fluids, the content of magnetic particle in MR fluids and the magnitude of the applied current have significant effect on the performance of MR fluid when subjected to compressive force. However, there is insufficient information about the characteristics of the inner structure in MR fluid under high pressure. In order to investigate the effect of pressure on a MR fluid, experiments in which various magnetic fields and various pressure are applied is conducted in this research. In the experiment setup, the gap of the MR fluid is set constant during the measurement. The ultrasonic propagation velocity in the MR fluid is measured and the influence of high pressure on the change of ultrasonic propagation velocity is clarified. From the change of ultrasonic propagation velocity, inner structure in MR fluid under pressure is analyzed.

1.3 Objectives

The main objective of this study is to investigate the behavior of MR fluid under shock loading. The cluster formation in MR fluid under pressure is also investigated experimentally using ultrasonic measurement technique. More specifically, the aims of this study can be summarized as follow:

1. To study the behavior of MR fluid under shock loading.
2. To investigate the effect of magnetic field, volume fraction of MR fluid and orifice inner diameter in terms of the behavior of MR fluid under shock loading.
3. To investigate the cluster formation in MR fluid under DC and AC magnetic field.
4. To investigate the cluster formation in MR fluid under pressure.

1.4 Contributions

In general, this study provides information on the behavior of MR fluid under shock loading. Moreover, the information of cluster formation in MR fluid under pressure is also provided. The new contributions to the scientific world that can be offered in this dissertation consist of:

- Experiment analysis of the effect of magnetic field, volume fraction of MR fluid and orifice inner diameter on piston displacement, velocity, damping force and pressure difference on orifice area in term of the behavior of MR fluid under shock loading.
- Ultrasonic propagation properties in MR fluids under AC and DC magnetic field.
- Experiment analysis of the effect of pressure and magnetic field on the ultrasonic propagation velocity in MR fluid.

1.5 Outline

This section provides brief information on each chapter. This dissertation is organized into six chapters which summarized as follow;

- Chapter 1 gives summary on the background, objectives and contributions of the research and the outline of dissertation.
- Chapter 2 starts with the explanation about the previous studies on the behavior of MR fluid under shock loading. Then, experimental apparatus, experimental procedure, preliminary experiment and repeatability of the experiment system are described.
- Chapter 3 discusses the experiment results in terms of the effect of magnetic field, orifice inner diameter and volume fraction of MR fluids. Discussion will be focused on the piston displacement, piston velocity, damping force and pressure difference on orifice area under shock loading.
- Chapter 4 starts with the explanation about the previous studies about the investigation of inner structure in MR fluid. Then, experimental apparatus, method and procedure are given. Last section on this chapter discusses on the experiment results. The experiment results consist of the effect of temperature, applied time, magnetic field, magnetic field sweep rate, volume fraction of MR fluids and frequency of AC magnetic field.
- Chapter 5 explains the ultrasonic propagation properties of MR fluid under pressure. The discussions are focused on the measurement results of ultrasonic propagation velocity under different pressures and different magnetic flux densities.
- Chapter 6 presents conclusions and future works.

Chapter 2

Experimental system of investigation of the behavior of MR fluid under shock loading

The main purpose of this chapter is to explain the previous study about the behavior of MR fluid under sinusoidal and shock loading. An explanation about experimental system is presented. The experimental apparatus in the system consists of three main parts, U-pipe, drop test tower and measurement devices, are used in this study. The results of the preliminary experiment are also presented. Preliminary experiments are conducted by applying water as the test fluid. Lastly, the repeatability of the experiment system is discussed. Experiments are conducted three times for similar conditions. The experiment results consist of piston displacement and velocity from laser displacement sensor, damping force from load cell and pressure difference in orifice area from the pressure sensors.

2.1 Introduction

In recent years, MR fluid has been widely used in the area of vibration control, such as suspension in automobiles [42, 43, 44, 45], seismic isolation in civil engineering [56, 57, 98, 99] and so on. In comparison to conventional oil as working liquid, a damper that utilizes MR fluid offers some advantages such as have faster response time and easier to control its damping characteristic. Most importantly, a MR fluid damper can be considered as a "fail-safe" device, that is, they can retain a minimum required damping capacity in the event of a power supply or electronic system failures [100].

In regard with the potential application of MR damper, many studies and investigation on MR damper have been conducted theoretically and experimentally. Chooi and Oyadiji [89, 101] presented the procedure for obtaining exact solutions to describe the flow of MR fluid through an annular gap. Their solution was validated by computational fluid dynamics analysis. They proposed a mathematical model of the double-tube MR damper using the annular flow solutions and incorporating fluid compressibility. Their proposed mathematical model was validated by carrying out experiments using MR damper [102]. They conducted experiment by subjecting

sinusoidal loading to MR damper. Performance of MR damper was investigated by measuring the damping force under different magnetic fields. They found that damping force increases when stronger magnetic fields are applied. Based on the value of damping force as the function of displacement and velocity, they observed that the comparison between the proposed model and experimental results are quite reasonably well. Wang and Gordaninejad [100] also developed theoretical model for predicting the behavior of field-controllable, MR and ER dampers by combining a fluid mechanics based approach and Herschel-Bulkley constitutive equation. Using the assumption of steady flow and one dimensional laminar, they presented the pressure drop as a function of material properties, geometry, and volumetric flow rate. Their theoretical model was validated by comparing the analytical results with experimental data for a prototype MR fluid damper. The prototype of MR damper was subjected to sinusoidal loading. Performance of MR damper was analyzed based on the value of damping force and pressure drop. As the expected, the damping force and pressure drop increases when stronger magnetic fields. They also observed that the proposed fluid-mechanics based model can accurately predict the dynamic response of a MR fluid damper over a wide range of operating conditions.

Several researchers designed MR damper for special purposes. Dogruer et al. [103] designed and developed new MR damper for high-mobility multi-purpose wheeled vehicle (HMMWV). The proposed MR damper was designed to HMMWV in terms of force characteristics, size and power consumption of the damper. They presented theoretical model to predict the performance of MR damper in terms of the damping force as the function of displacement and velocity for simple harmonic displacement input. Their theoretical predictions are in reasonably good agreement with the experiment results. Yang et al. [57] and Spencer et al. [104] designed and developed a large-scale 20 ton MR damper capable of providing semi-active damping for structural applications. The MR fluid was subjected to a sinusoidal displacement excitation. Their experimental results showed that MR dampers can provide large controllable damping forces, while requiring only a small amount of energy. They also proposed mechanical model based on the BoucWen hysteresis model to predict for the force-velocity relationship of the MR damper. Their proposed mechanical model presented results which closely match the experimental data.

Most of the publication in the previous study focused on the performance of MR damper subjected to cyclic excitation. The performance of MR damper under cyclic excitation is evaluated from the value of damping force. Under the cyclic excitation, the magnitude of damping force increases when stronger magnetic fields are applied [57, 89, 100, 104]. The increasing damping force means the resistance of MR fluid flow through the narrow gap becomes higher at higher magnetic flux density. The behavior and performance of MR fluid under shock loading is not fully understand. Few researchers have studied experimentally about the behavior and performance of MR fluid when subjected to shock loading. Ahmadian and Norris [91, 105] and El Wahed et al. [90] investigated the performance of MR fluid under shock loading. These studies were concerned about validating the capability of a specific MR fluid device using commercial MR dampers. The performance of MR damper was evaluated based on the value of damping force as the function of magnetic fields.

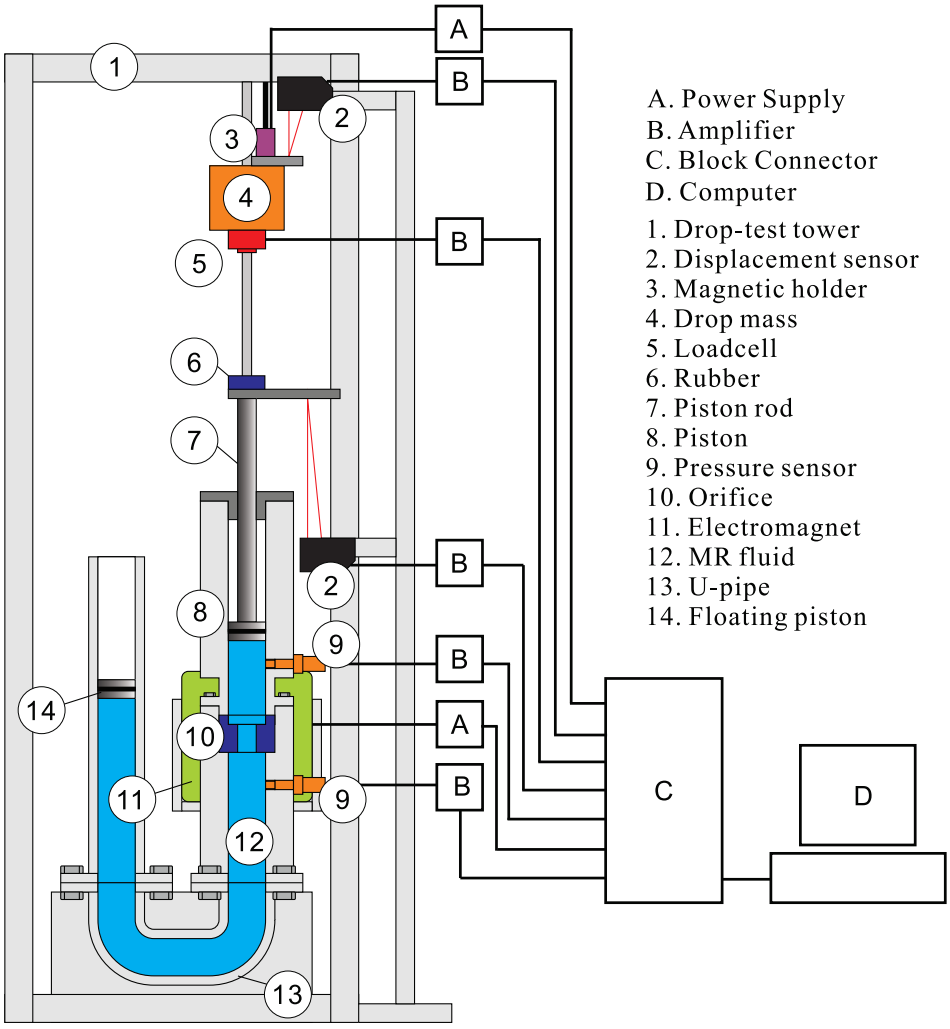

Figure 2.1: Experimental apparatus

2.2 Experimental apparatus

Figure 2.1 illustrates the experimental apparatus developed in this study. The experimental apparatus consists of a drop-test tower, a U-pipe, electromagnet and measurement devices. The experimental apparatus is set up as follow. First, piston head and piston rod are placed on one side of the U-pipe. Then, the U-pipe is filled with MR fluid partially. The MR fluid in the U-pipe is subjected to the shock loading through the piston rod. In this experiment, the shock loading is produced by dropping a drop-mass from its initial position onto the piston rod. Kinetic energy and impact force from this action can be controlled easily by varying the release heights and weights of the drop masses.

2.2.1 Drop-test tower

Drop-test tower is fabricated to simulate shock loading to the MR fluid. The main material of the tower is aluminum extrusions that are assembled using screws. A drop mass is attached in the tower. In order to minimize the effect of friction, a guide rail is attached in the tower.

When drop mass is released from the initial condition, it will go through along the rail. Small electromagnet is applied to hold the drop mass. By shutting down the power supply, the drop mass can be released easily.

If m is the mass of drop mass, v is impact velocity, g is the gravity acceleration and h is the distance between the initial position of the drop mass with the piston or drop height, the relationship between kinetic energy ($KE = \frac{1}{2}mv^2$) and potential energy ($PE = mgh$) when the drop mass hit the piston is derived using equation below;

$$\begin{aligned} KE &= PE \\ \frac{1}{2}mv^2 &= mgh \end{aligned} \tag{2.1}$$

The Eq. (2.1) is valid by neglecting the frictional effects during the release of the drop mass. From this equation, the impact velocity can be calculated using the equation below;

$$v = \sqrt{2gh} \tag{2.2}$$

In order to accommodate the effect of frictional effects and to confirm the real value of impact velocity for different drop mass, measurement is conducted. First, the drop mass is released from the initial position. The impact velocity of the drop mass, which measured by laser displacement sensor, is determined when drop mass hit the piston road. The impact velocity of the drop mass is varied by changing the drop height h. The value of the h is varied every 1 mm for every measurements. The value of h as a function of impact velocity for different drop mass is presented in Table 2.1.

The damping force in the MR fluid and position of the piston under shock loading is illustrated in Fig. 2.2. During the shock loading, if Dp is the piston displacement, the amount of the absorbed energy (E) by the MR fluid is expressed by the following equation;

$$E = \int_0^{Dp} F(x)dx. \tag{2.3}$$

The damping force that provided by the MR fluid can be calculated from Eq. (2.3) and the kinetic energy of the dropping a mass from the certain position.

$$F(x) = \frac{mv^2}{2Dp} \tag{2.4}$$

Table 2.1: The value of h as function of impact velocity for different drop mass

M (kg)	h (mm)			
	$v = 0.5$ m/s	$v = 1.0$ m/s	$v = 1.5$ m/s	$v = 2.0$ m/s
5.57	16	63	146	265
7.24	16	63	140	253
8.91	16	61	135	240
10.58	16	61	132	235

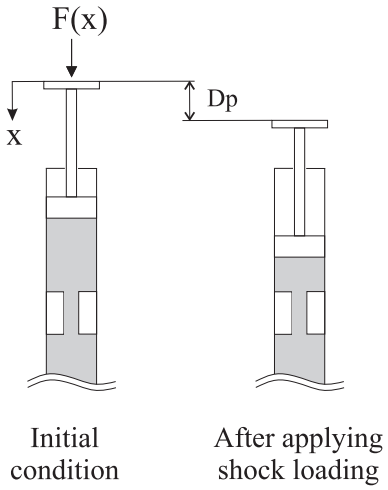

Figure 2.2: Damping force and position of the piston after shock loading

From the Eq. (2.4), the damping force increases when the heavier drop masses (m) and the higher impact velocities (v) are applied. The damping force also becomes higher as the piston displacement (Dp) is shorter.

In a collision involving two or more objects, the sum of the total momentum (P) before the collision equals the sum of the total momentum after the collision.

$$\Sigma\,(mv)_{before} = \Sigma\,(mv)_{after} \tag{2.5}$$

When a force acts on an object for a certain amount of time, it imparts an impulse (J) to the object. The impulse changes the existing momentum of the object.

$$\text{Impulse} = \text{Change of momentum} \tag{2.6}$$

If $J = F\Delta t$ and $P = m\Delta v$, the Eq. (2.6) will change as follows;

$$F\Delta t = m\Delta v \tag{2.7}$$

If v is impact velocity, V_p is piston velocity, M is the drop mass and m_{MR} is the total mass of piston and the MR fluid, the impulse of the collision between the drop mass and the piston is calculated using as follows;

$$F\Delta t = Mv - (M + m_{MR})V_p \tag{2.8}$$

$$F = \frac{Mv - (M + m_{MR})V_p}{\Delta t} \tag{2.9}$$

Based on the Eq. (2.9), the peak value of damping force can be calculated from the measurement results from the laser displacement sensor.

2.2.2 U-pipe

A U-pipe is designed to keep the MR fluid inside the pipe under shock loading. The U-pipe consists of four different parts. Each part is connected using screws. An orifice and two pressure

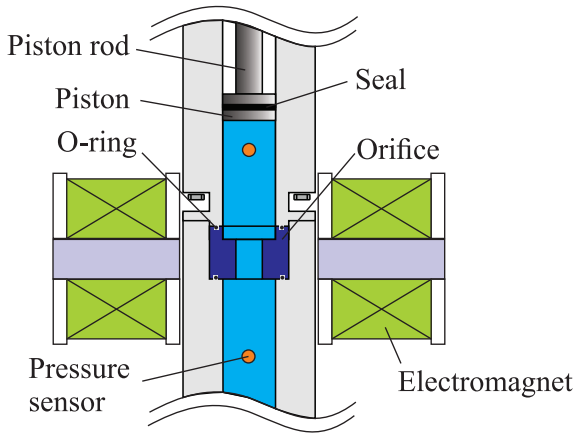

Figure 2.3: Detail of test section

sensors are attached in the one side of the U-pipe (Fig. 2.3). Two O-rings are mounted at lower and upper side of the orifice to avoid the leaking of MR fluid. Two pressure sensors are mounted 50 mm from the inlet and outlet part of the orifice. Also, a set of piston and piston rod is inserted in this pipe. A seal is attached in the piston to avoid leaking during the shock loading.

It is considered that noises due to vibration might occur when shock loading is produced. Because of this reason, it is necessary to minimize the effect of vibration noises. This is conducted by locating the drop-test tower separately from the set of U-pipe. U-pipe is mounted to the floor to minimize the effect of vibration to the tower.

2.2.3 Electromagnet

An electromagnet is utilized for applying magnetic field to the MR fluid. The strength of magnetic field in the electromagnet is controlled by changing the current in power supply. In this experiment, a pair of electromagnet is applied to ensure a uniform and strong magnetic field (Fig. 2.3). The magnetic field is applied to the MR fluid through the orifices. The direction of the magnetic field is perpendicular with the flow direction. Figure 2.4 shows the dimension of the electromagnet.

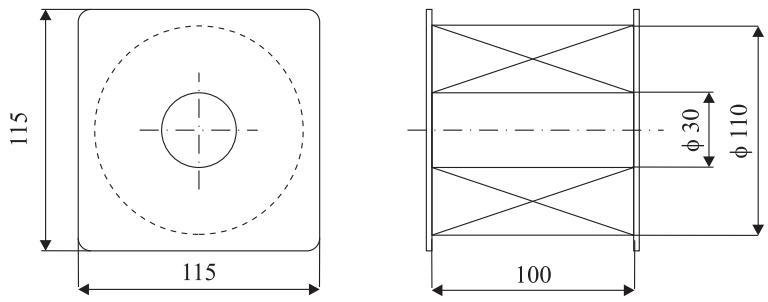

Figure 2.4: Dimension of electromagnet

2.2.4 Measurement devices

In this experiment, the event of shock loading is captured by measuring the piston rod displacement using laser displacement sensor, by measuring damping force using load cell and also by measuring the pressure in the inlet and outlet of the orifice using pressure sensors. Each of the measurement devices will be explain as follows:

Laser displacement sensor

In this experiment, two laser displacement sensors are applied. First sensor is used to measure the displacement of piston rod and another sensor is used to measure the displacement of drop mass. Figure 2.5 shows two laser displacement sensors. The sensors are attached separately with the drop-test tower to minimize the effect of vibration during the shock loading. The sensors are located based on the specification of the sensor (reference distance and measurement range) in respect to the position of piston rod and drop mass. The sensors have different model. The specification of laser displacement sensors is presented in Table 2.2. Measurement range of the laser indicates the upper and lower limit of the sensor to measure the distance. For example, laser LK-G505 can measure displacement at range 250 mm to 1000 mm. The illustration of reference distance and measurement range of sensor LK-G505 can be seen in Fig. 2.6.

The velocity and acceleration of the piston is calculated from the piston displacement data. The data from laser displacement sensor records the plot number with the time. The data interval is constant. In order to find the function from the plot data, a numerical differentiation is conducted. Three-point differentiation is determined. Figure 2.7 illustrates three points of data (x_{i-1}, x_i and x_{i+1}) and its function $f(x)$. If x_i express a certain point and the data interval is expressed by s, point of x_j which several times ($n = 0,1,2,\cdots$) from the x_i is expressed by the following equation:

$$x_j = x_i \pm ns \, (n = 0, 1, 2, \cdots) \tag{2.10}$$

Figure 2.5: Laser displacement sensor: LK-G505 (left) and LB-300 (right)

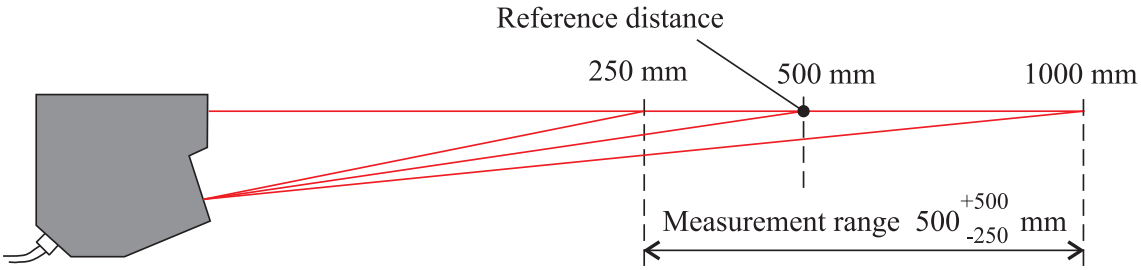

Figure 2.6: Reference distance and measurement range of laser displacement sensor LK-G505

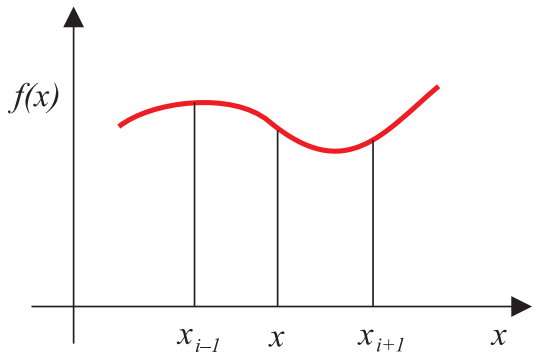

Figure 2.7: Reference point

The function of these points (x_j) can be derived using Taylor series equation:

$$\begin{aligned} f_j &= f(x_i \pm ns) \\ &= f_i \pm nsf_i' + \frac{(ns)^2}{2!}f_i'' \pm \frac{(ns)^3}{3!}f_i^{(3)} + \cdots \end{aligned} \tag{2.11}$$

If $n = \pm 1$, the following equation is obtained.

$$f_{i+1} = f_i + sf_i' + \frac{1}{2}s^2 f_i'' + \frac{1}{6}s^3 f_i^{(3)} + \frac{1}{24}s^4 f_i^{(4)} + \cdots \tag{2.12}$$

$$f_{i-1} = f_i - sf_i' + \frac{1}{2}s^2 f_i'' - \frac{1}{6}s^3 f_i^{(3)} + \frac{1}{24}h^4 f_i^{(4)} + \cdots \tag{2.13}$$

From Eqs. (2.12) and (2.13), new equation is obtained as bellow:

$$f_{i-1} - f_{i+1} = 2sf_i' + 2\left(\frac{s^3}{6}f_i^{(3)} \cdots\right) \tag{2.14}$$

Table 2.2: Detail specification of laser displacement sensor

Model	Reference distance	Measurement range	Time response	Accuracy
LK-G505	500 mm	$-250 \sim +500$ mm	0.02 ms	2 μm
LB-300	300 mm	$-100 \sim +100$ mm	0.07 ms	50 μm

From Eq. (2.14), the value of f_i' and the error value (e_i) is obtained.

$$f_i' \simeq \frac{1}{2s}(f_{i+1} - f_{i-1}) \tag{2.15}$$

$$e_i \simeq -\frac{h^2}{6} f_i^{(3)} \tag{2.16}$$

From Eqs. (2.12) and (2.13), another equation is obtained as bellow:

$$f_{i+1} + f_{i-1} = 2f_i + s^2 f_i'' + \frac{1}{12} s^2 f_i^{(4)} + \cdots \tag{2.17}$$

From Eq. (2.17), the value of f_i'' and the error value (e_i) are obtained.

$$f_i'' \simeq \frac{1}{s^2}(f_{i+1} - 2f_i + f_{i-1}) \tag{2.18}$$

$$e_i \simeq \frac{1}{12} s^2 f_i^{(4)} \tag{2.19}$$

If value of s is calculated from the sample rate value (SR) and by using Eqs. (2.15) and (2.18), piston velocity and acceleration can be calculated using equation below:

$$s = \frac{1}{SR}$$

$$a_i = \frac{1}{s^2}(f_{i+1} - 2f_i + f_{i-1}) \tag{2.20}$$

$$v_i = \frac{1}{2s}(f_{i+1} - f_{i-1}) \tag{2.21}$$

Load cell

Load cell is applied to measure the damping force during the shock loading. In this experiment, load cell is mounted on the bottom side of the drop mass (Fig. 2.8). When the drop mass contacts with the upper side of the piston rod (shock loading event), the load cell starts to measure the damping force. In order to minimize the damage on the load cell during the shock loading, a rubber piece is attached on the upper side of the piston rod. The specification of load cell is presented in Table 2.3. Rated capacity of the test cell is 5 kN. Since the safe overload is 200 %, it can measure up to 10 kN.

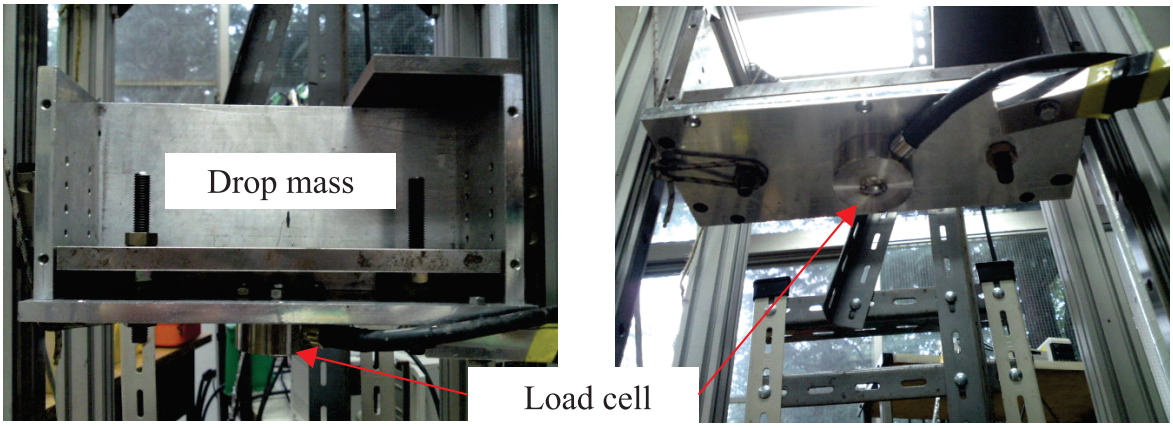

Figure 2.8: Position of load cell in experimental apparatus

Table 2.3: Specification of load cell

Model	LCN-A-5kN
Rated capacity	5 kN
Time response	0.077 ms
Safe Overload Rating	200 %
Accuracy	0.3 % from rated output
Manufacturer	Kyowa

Pressure sensor

Two pressure sensors are used to measure the pressure in the inlet and outlet of the orifice. The sensors are mounted 30 mm from the upper side and lower side of the orifice, respectively (Fig. 2.9). Rated capacity of the pressure sensor is 10 MPa. Since the safe overload is 150 %, it can measure up to 15 MPa. The specification of the pressure sensor is presented in Table 2.4

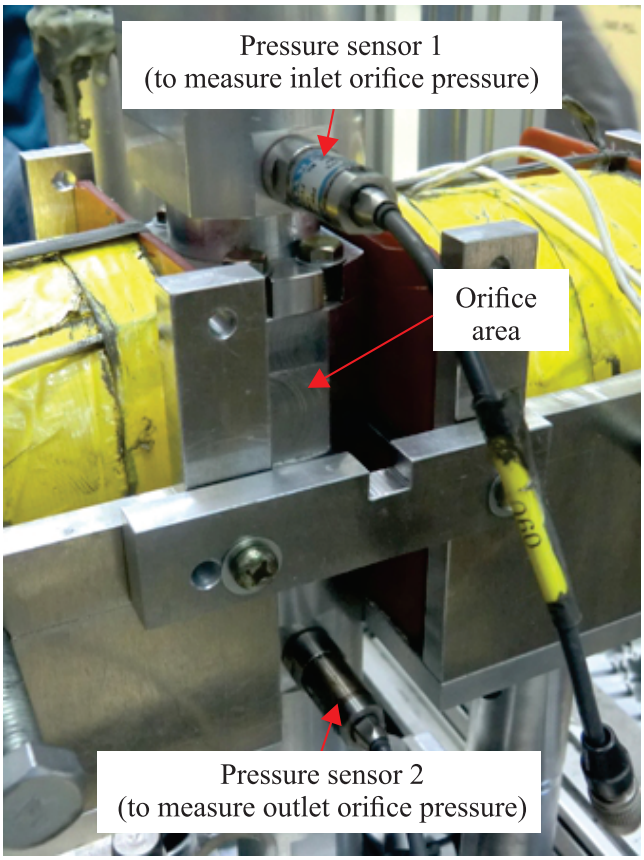

Figure 2.9: Pressure sensor

Table 2.4: Specification of pressure sensor

Model	PGM-100KD
Rated capacity	10 MPa
Time response	0.0088 ms
Safe Overload Rating	150 %
Accuracy	0.65 % from rated output
Manufacturer	Kyowa

Data processing

The measurement data is transferred from the laser displacement sensor, load cell and pressure sensors to connector block. Figure 2.10 shows the connector block from national instrument (NI BNC-2110). The connector block is also connected to the power supply which sends electric current to the magnet holder (use to hold the drop mass) and a pair of electromagnet (use to generate magnetic field at orifice area). The connector block is connected to the computer using data acquisition (DAQ) board from national instrument (NI PCI-6221).

By utilizing visual programming language, called LabVIEW (Laboratory Virtual Instrumentation Engineering Workbench) from national instrument, electric current of the power supply can be controlled easily. Moreover, the measurement data from the sensors can be monitored directly in the computer. In this study, LabVIEW is also utilized to analyze the measurement data. Figure 2.11 shows the front panel of the developed LabVIEW program.

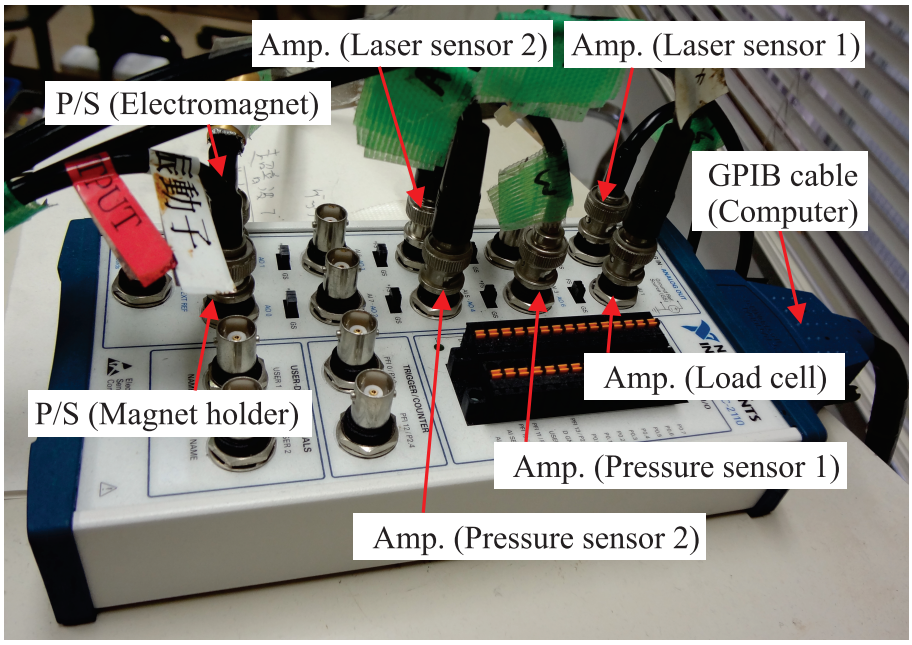

Amp. = Amplifier P/S = Power supply

Figure 2.10: Block connector (NI BNC-2110)

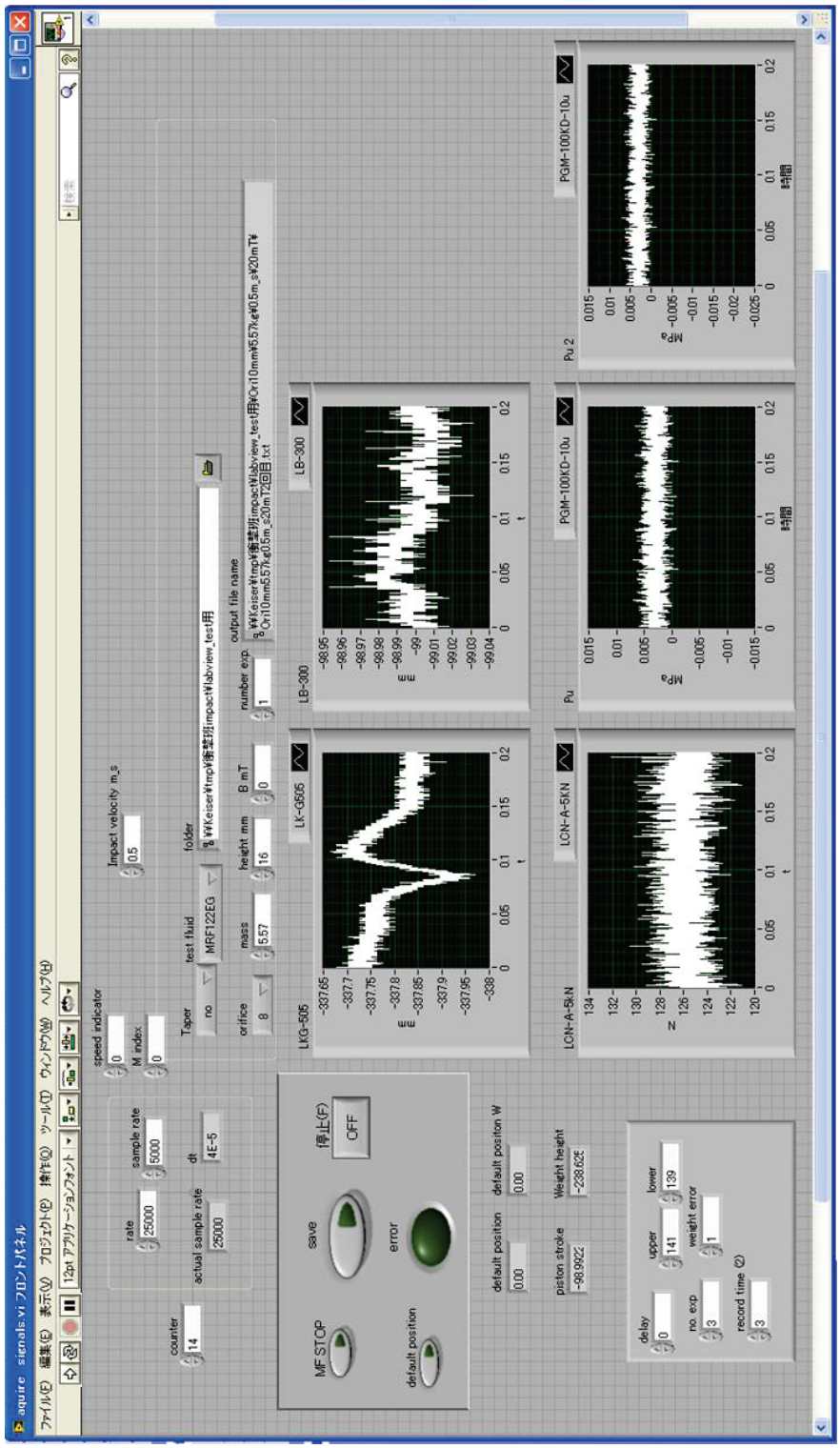

Figure 2.11: Front panel of LabVIEW program to acquire signal from the sensors

2.2.5 Magnetic field distribution

Measurement is conducted to know the magnetic field distribution in test section area. Gauss meter is used to measure the distribution of magnetic flux density (Fig. 2.12). Figure 2.13 shows the area of magnetic field measurement. The area of the magnetic field measurement is between poles. Measurement is conducted along the x and y direction.

Figure 2.14 shows the distribution of magnetic flux density in x direction at different distance at y direction. The measurement is taken at 2 A of electric current. From the figure, it shows that magnetic field distribution in test section area is relatively uniform. The length of the test area is 10 mm since maximum inner diameter of inner orifice in this experiment is 10 mm. The values of magnetic flux density decrease at further area from 0 point in y directions.

Magnetic flux density of the electromagnet is controlled by varying current of the power supply. In the process of developing VI (virtual instrument) in this experiment, the correlation of magnetic flux density and electric current in power supply is necessary to know. The correlation between magnetic flux density and electric current is presented in Fig. 2.15. Since power supply is able to supply electric current from 0 – 2.8 A, therefore, the maximum value of magnetic flux density generated is 125 mT.

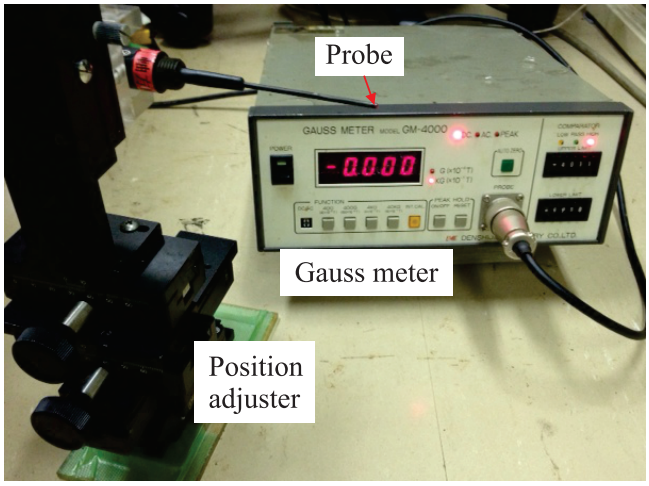

Figure 2.12: Gauss Meter

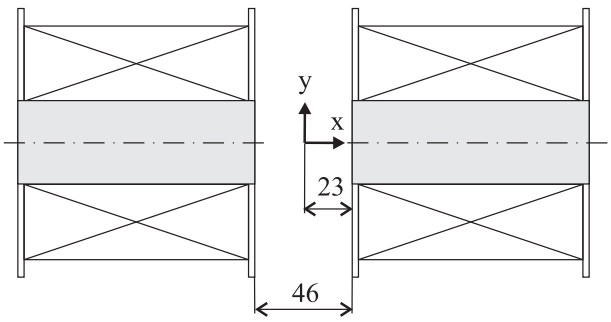

Figure 2.13: Area of magnetic field measurement

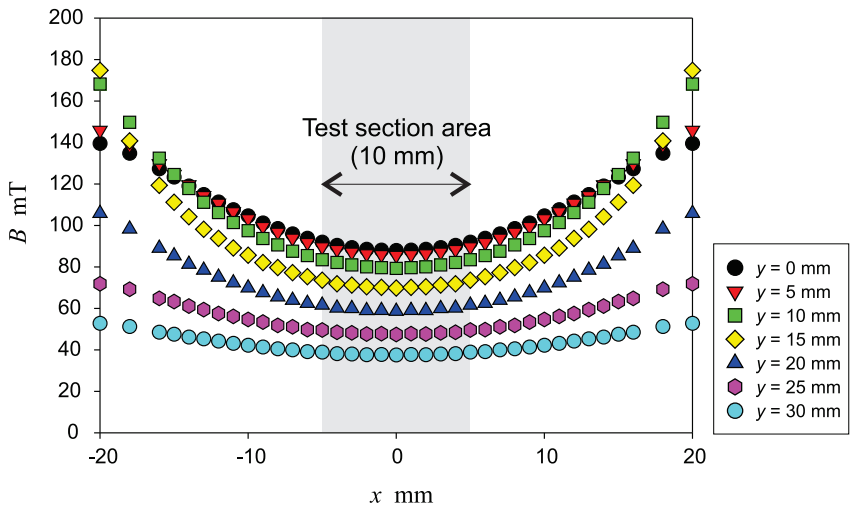

Figure 2.14: Distribution of magnetic flux density in x direction at 2 A of electric current

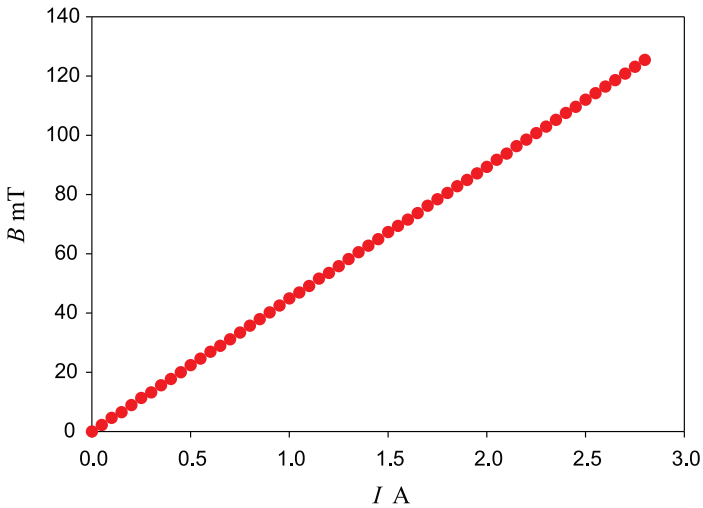

Figure 2.15: Correlation of magnetic flux density and electric current

2.2.6 Properties of MR fluids

In this study, two series of commercial MR fluids, MRF-122EG and MRF-132DG, are applied. Both series are produced by Lord Corporation. The two series of MR fluids are used in order to investigate the effect of volume fraction under shock loading. At 40 °C, the properties of the MR fluids is presented in Table 2.5. In addition, the yield stress versus magnetic field strength and typical magnetic properties of two MR fluids are presented in Figs. 2.16 and 2.17, respectively [106].

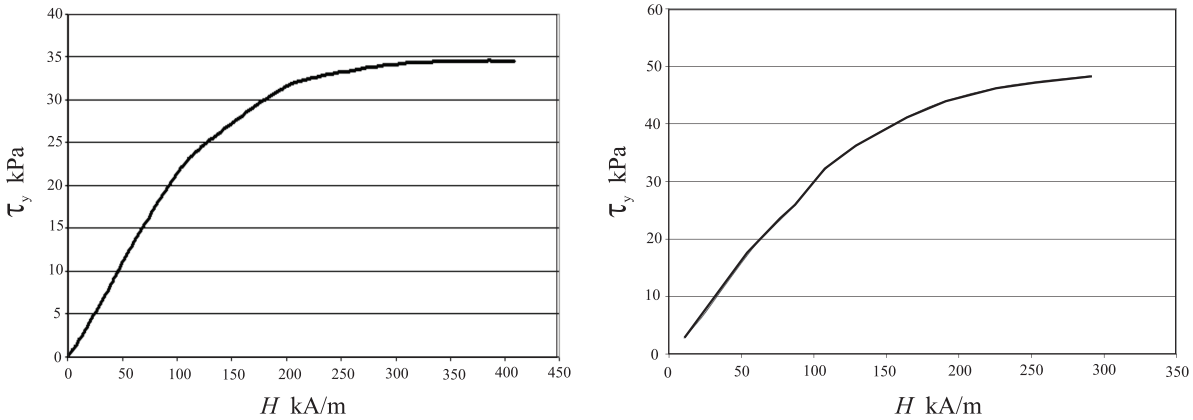

(a) MRF-122EG (b) MRF-132DG

Figure 2.16: Yield stress vs. magnetic field strength of MRF-122EG (a) and MRF-132DG (b) [106]

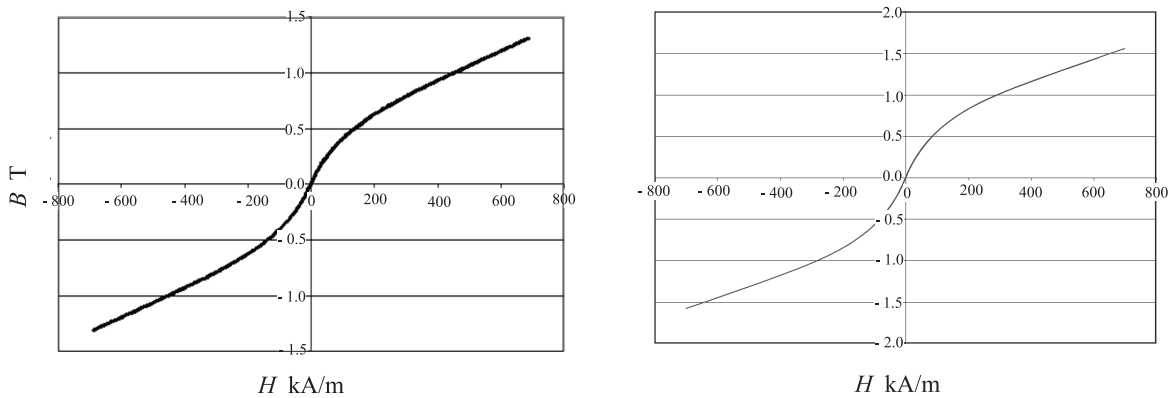

(a) MRF-122EG (b) MRF-132DG

Figure 2.17: Typical magnetic properties of MRF-122EG (a) and MRF-132DG (b) [106]

Table 2.5: Properties of MR fluids at 40 °C.

Property	Value	
Serial name	MRF-122EG	MRF-132DG
Particle material	Iron	Iron
Mean particle size	3 - 10 μm	3 - 10 μm
Volume fraction	0.22	0.32
Carrier liquid	Hydrocarbon oil	Hydrocarbon oil
Viscosity	42 ± 20 mPa $\cdot$ s	92 ± 15 mPa $\cdot$ s
Density	$2.28 - 2.48 \times 10^3$ kg/m^3	$2.98 - 3.18 \times 10^3$ kg/m^3

2.3 Experimental procedure

In this study, the experimental procedures follow these steps:

1. In order to minimize the effect of sedimentation, process of stirring of MR fluid is conducted for 30 minutes before the experiment is started. Figure 2.18 shows how MR fluid is stirred using a stirring machine.
2. Drop weight is subjected to the piston for several times (more than 30 times) to ensure no leaking on the U-pipe.
3. Experiments are conducted three times for similar condition to get the result properly.

In order to investigate the effect of magnetic field, the effect of volume fraction and the effect of orifice inner diameter on the damping characteristic of MR fluid under shock loading, different setup of experiments are developed. The experimental parameter are varied during the experiment as shown in Table 2.6.

Table 2.6: Experimental parameter.

No	Parameter	Value
1	Magnetic flux density	0, 40, 80 and 120 mT
2	Working fluid	MRF-122EG and MRF-132DG
3	Drop mass	5.57, 7.24, 8.91 and 10.58 kg
4	Impact velocity	0.5, 1.0, 1.5 and 2.0 m/s
5	Orifice inner diameter	5, 8.6 and 10 mm

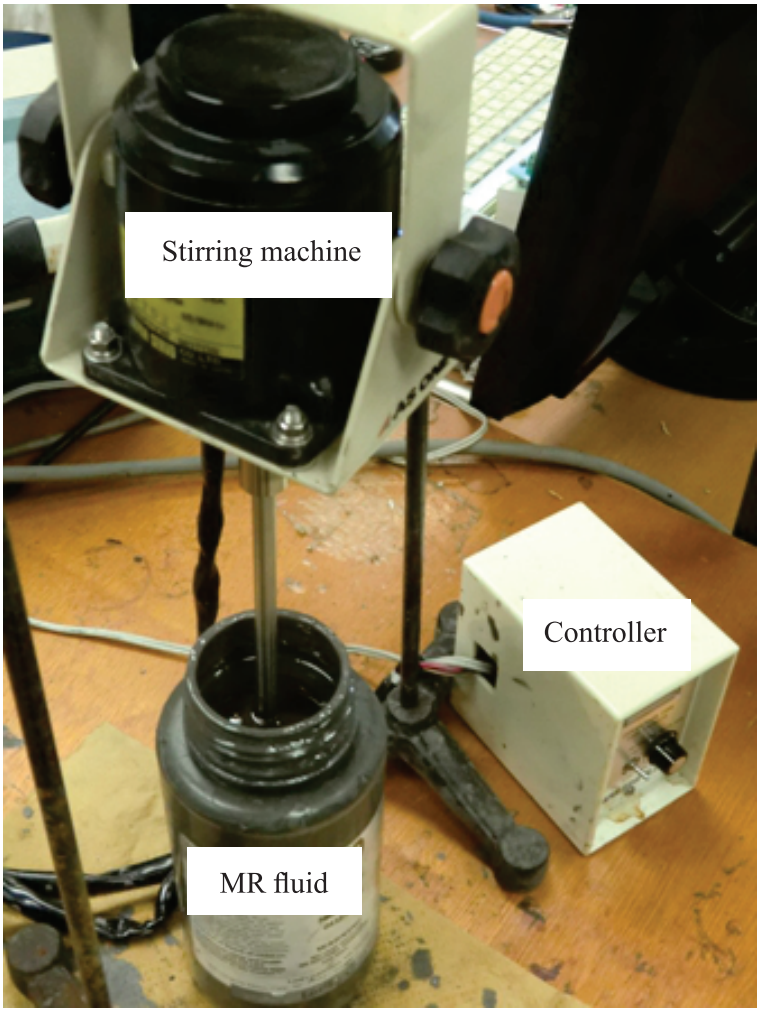

Figure 2.18: Stirring MR fluid

2.4 Preliminary experiment

Preliminary experiments are conducted to check the performance of the experimental apparatus such as the sensors can perform properly and no leaking of the working fluid under shock loading. The experiments are conducted using water as the working fluid. Condition of the experiments is presented in Table 2.7.

Figures 2.19 and 2.20 show piston displacement (Dp) over time (t) at drop mass (M) 5.57 kg and 10.58 kg, respectively. Piston moves at maximum stroke (140 mm) for both drop masses. However, the time required to reach maximum stroke (Dp_{max}) is different. The value of Dp_{max} decreases with the value of impact velocity and drop masses. The value of Dp_{max} as the function of impact velocity is presented in Fig. 2.21 (a). The value of Dp_{max} is similar for different impact velocity and drop masses since piston moves at maximum value.

Figures 2.22 and 2.23 show piston velocity (Vp) over time (t) at drop mass (M)5.57 kg and 10.58 kg, respectively. Piston velocity increases abruptly and reaches the peak value during the shock loading. The peak value of velocity (Vp_{max}) as function of impact velocity is presented in Fig. 2.24. The value of Vp_{max} is dependent with the value of impact velocity and drop mass. The value of Vp_{max} tends to increase at higher impact velocity, because the force from the shock loading is greater at higher impact velocity.

Figures 2.25 and 2.26 show force (F) over time (t) at drop mass (M)5.57 kg and 10.58 kg, respectively. The value of peak force (F_{max}) as the function of impact velocity is presented in Fig. 2.27. The value of F_{max} is dependent with the value of impact velocity. The value of Vp_{max} tends to increase at higher impact velocity due to the force from the shock loading is greater at higher impact velocity.

Figures 2.28 and 2.29 show pressure difference (ΔP) over time (t) at drop mass (M) 5.57 kg and 10.58 kg, respectively, for different impact velocity (v) = 0.5 $\sim$ 2.0 m/s. The pressure difference (ΔP) is calculated by subtracting the inlet pressure (Pin) with the outlet pressure ($Pout$).

$$\Delta P = Pin - Pout \tag{2.22}$$

The value of peak pressure difference (ΔP_{max}) as function of impact velocity is presented in Fig. 2.30. The value of ΔP_{max} is dependent with the value of impact velocity. The value of ΔP_{max} tends to increase at higher impact velocities. It because the higher impact velocities causes the greater of shock loading.

Table 2.7: Preliminary experiment condition

No	Parameter	Value
1	Working fluid	Water
2	Drop mass	5.57., 7.24, 8.91 and 10.58 kg
3	Impact velocity	0.5, 1.0, 1.5 and 2.0 m/s
4	Orifice inner diameter	8 mm
5	Piston stroke	140 mm

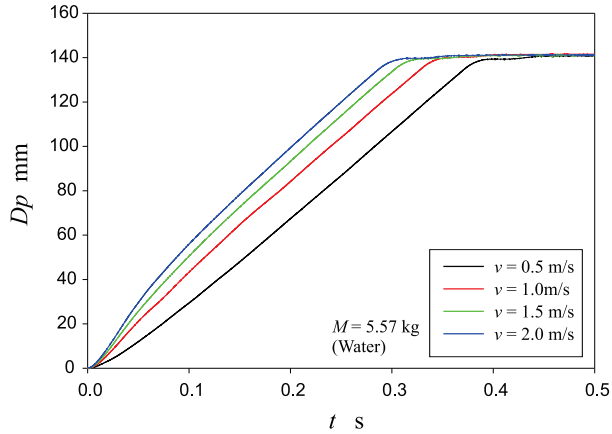

Figure 2.19: Piston displacement vs. time under $M = 5.57$ kg

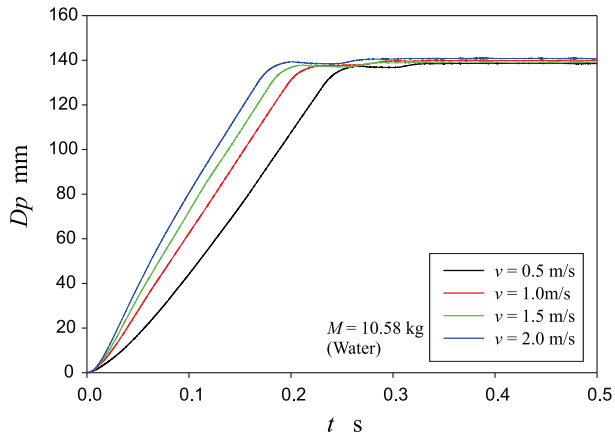

Figure 2.20: Piston displacement vs. time under $M = 10.58$ kg

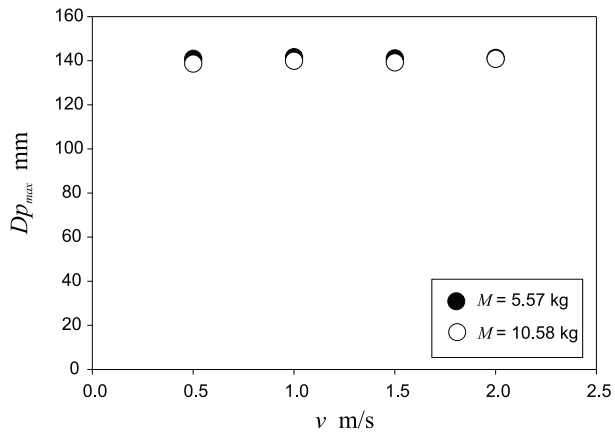

Figure 2.21: Maximum piston displacement as function of impact velocity

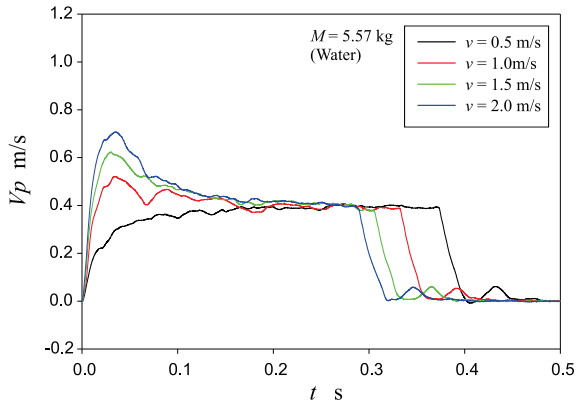

Figure 2.22: Piston velocity vs. time under $M = 5.57$ kg

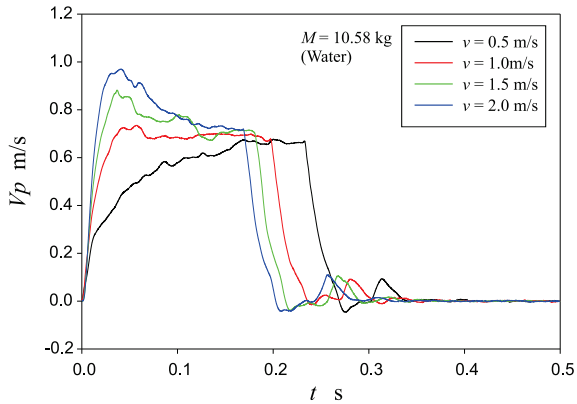

Figure 2.23: Piston velocity vs. time under $M = 10.58$ kg

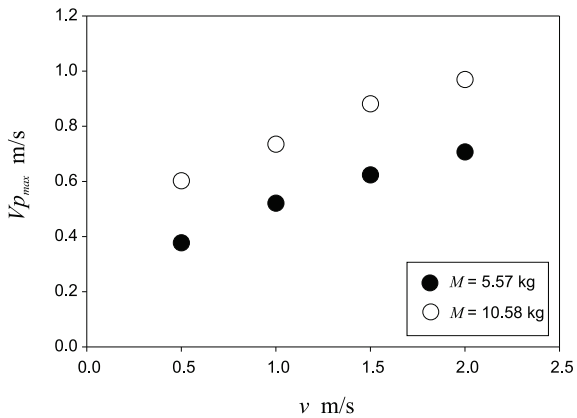

Figure 2.24: Maximum piston velocity as function of impact velocity

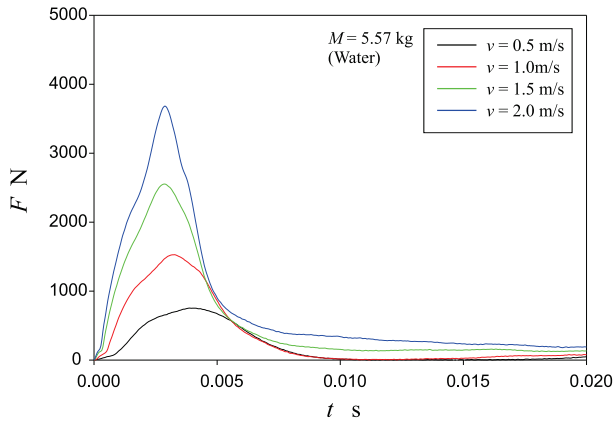

Figure 2.25: Force vs. time under $M = 5.57$ kg

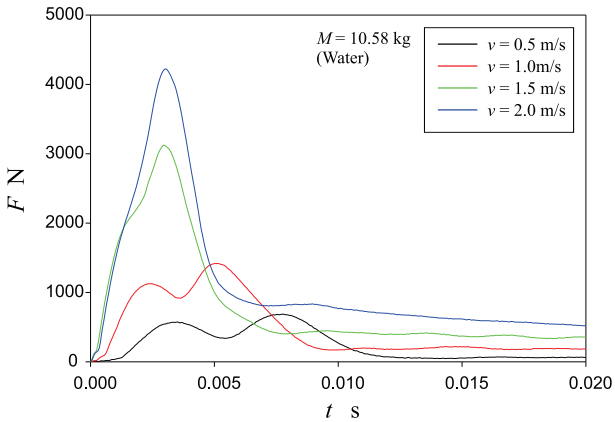

Figure 2.26: Force vs. time under $M = 10.58$ kg

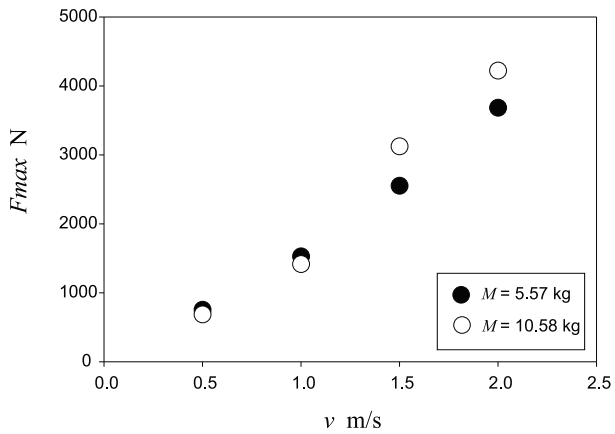

Figure 2.27: Maximum force as function of impact velocity

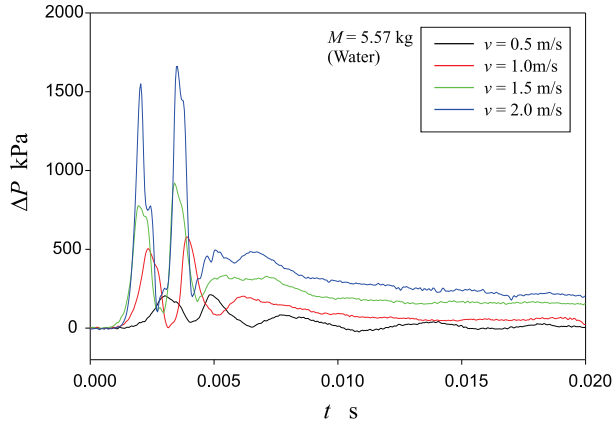

Figure 2.28: Pressure difference vs. time under $M = 5.57$ kg

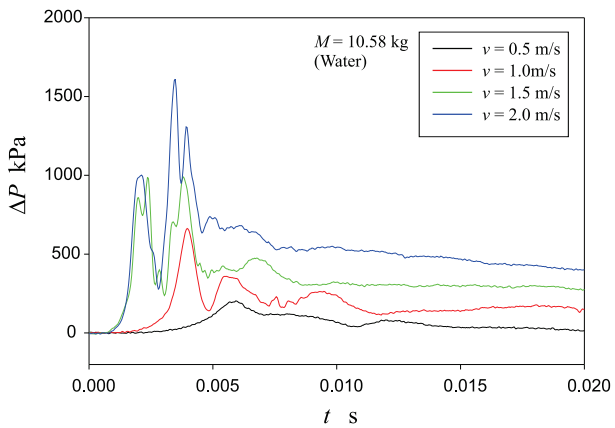

Figure 2.29: Pressure difference vs. time under $M = 10.58$ kg

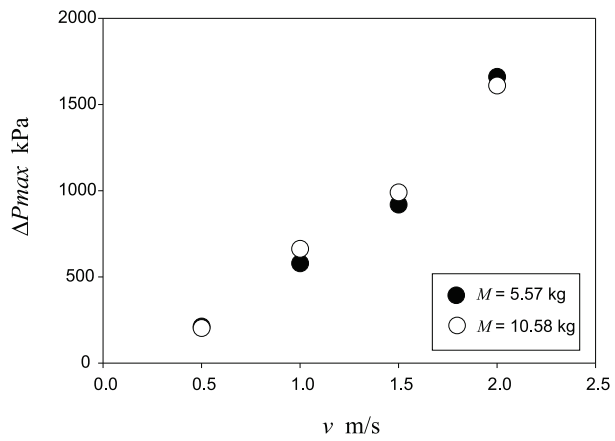

Figure 2.30: Maximum pressure difference as function of impact velocity

2.5 Repeatability of the experiment system

Repeability defines how consistent the measurement results taken under similar conditions. These condition include [107]:

- the same measurement procedure
- the same observer
- the same measuring instrument, used under the same conditions
- the same location
- repetition over a short period of time

The best way to examine repeatability is to take repeated measurements on a series of subjects [108]. In order to check the repeatibility of the experiment system, experiments are conducted three times for similar conditions. The experiment data of repeatability for the value of measurement result from laser displacement sensor (piston displacement and velocity), load cell (damping force) and pressure sensors (pressure difference) are presented in Figs. 2.31 $\sim$ 2.33.

If n is the number of repeated measurement and x_i is the measurement data, the average value ($\bar{x}$) can be calculated using the below equation.

$$\bar{x} = \sum_{i=1}^{n} x_i \tag{2.23}$$

The values of the deviation of the average value are used to calculate the experimental error (Er_x). The quantity that is used to estimate these deviations is known as the standard deviation (SD_x) and is defined as:

$$SD_x = \sqrt{\frac{1}{n}\sum_{i=1}^{n}(x_i - \bar{x})^2} \tag{2.24}$$

Based on the value of standard deviation, the value of experimental error can be calculated using this equation:

$$Er_x = \frac{SD_x}{\sqrt{n}} \tag{2.25}$$

The values of standard deviation (SD_x) and experimental error (Er_x) of the experiment results are presented in Tables 2.8 $\sim$ 2.11, respectively.

Table 2.8: Standard deviation and experimental error of the piston displacement

B	SD_x	Er_x
0 mT	0.6797	0.0110
40 mT	0.6919	0.0112
80 mT	1.0487	0.0171
120 mT	0.0459	0.0007

Table 2.9: Standard deviation and experimental error of the piston velocity

B	SD_x	Er_x
0 mT	0.0181	0.0002
40 mT	0.0151	0.0002
80 mT	0.0156	0.0002
120 mT	0.0018	0.00003

Table 2.10: Standard deviation and experimental error of the damping force

B	SD_x	Er_x
0 mT	93.7111	1.5296
40 mT	58.7747	0.9594
80 mT	14.8277	0.2420
120 mT	4.2124	0.0687

Table 2.11: Standard deviation and experimental error of the pressure difference

B	SD_x	Er_x
0 mT	46.6653	0.7617
40 mT	36.4662	0.5952
80 mT	17.5593	0.2866
120 mT	6.4590	0.1054

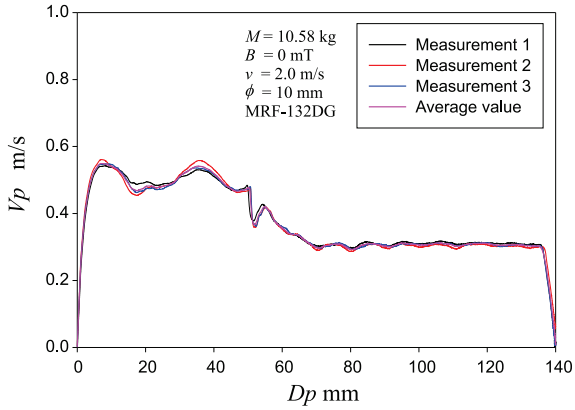

(a) $B = 0$ mT

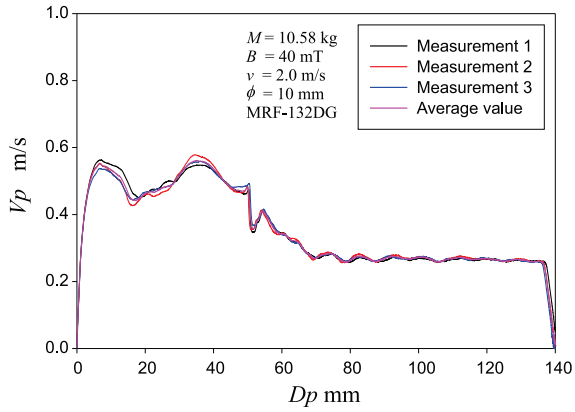

(b) $B = 40$ mT

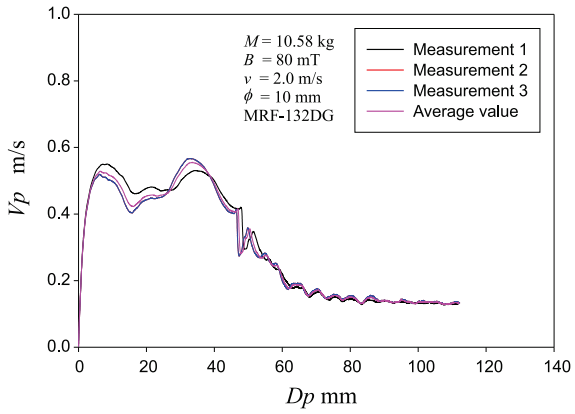

(c) $B = 80$ mT

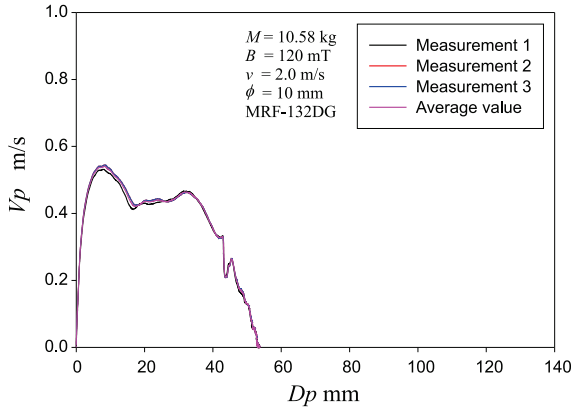

(d) $B = 120$ mT

Figure 2.31: Piston velocity vs. piston displacement of $M = 10.58$ kg at $B = 0$ mT (a), $B = 40$ mT (b), $B = 80$ mT (c) and 120 mT (d)

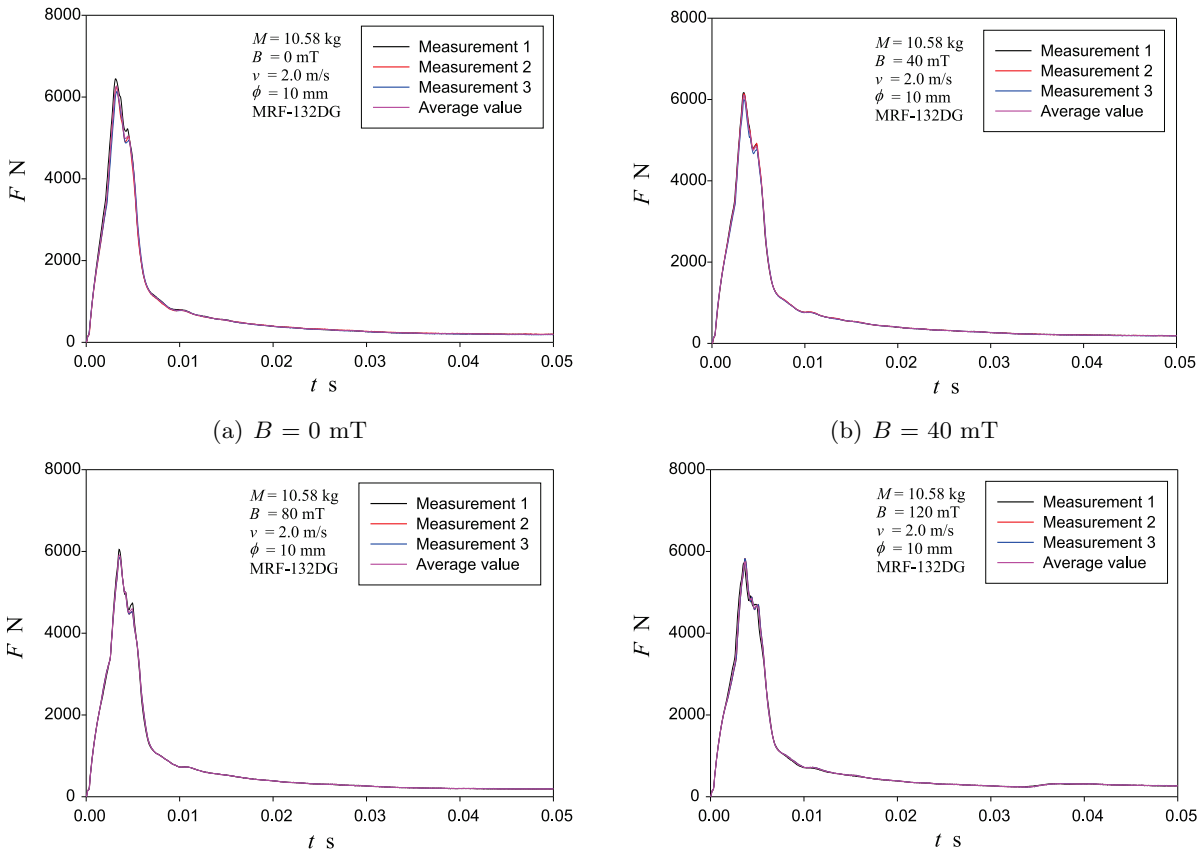

(a) $B = 0$ mT (b) $B = 40$ mT

(c) $B = 80$ mT (d) $B = 120$ mT

Figure 2.32: Force vs. time of $M = 10.58$ kg at $B = 0$ mT (a), $B = 40$ mT (b), $B = 80$ mT (c) and 120 mT (d)

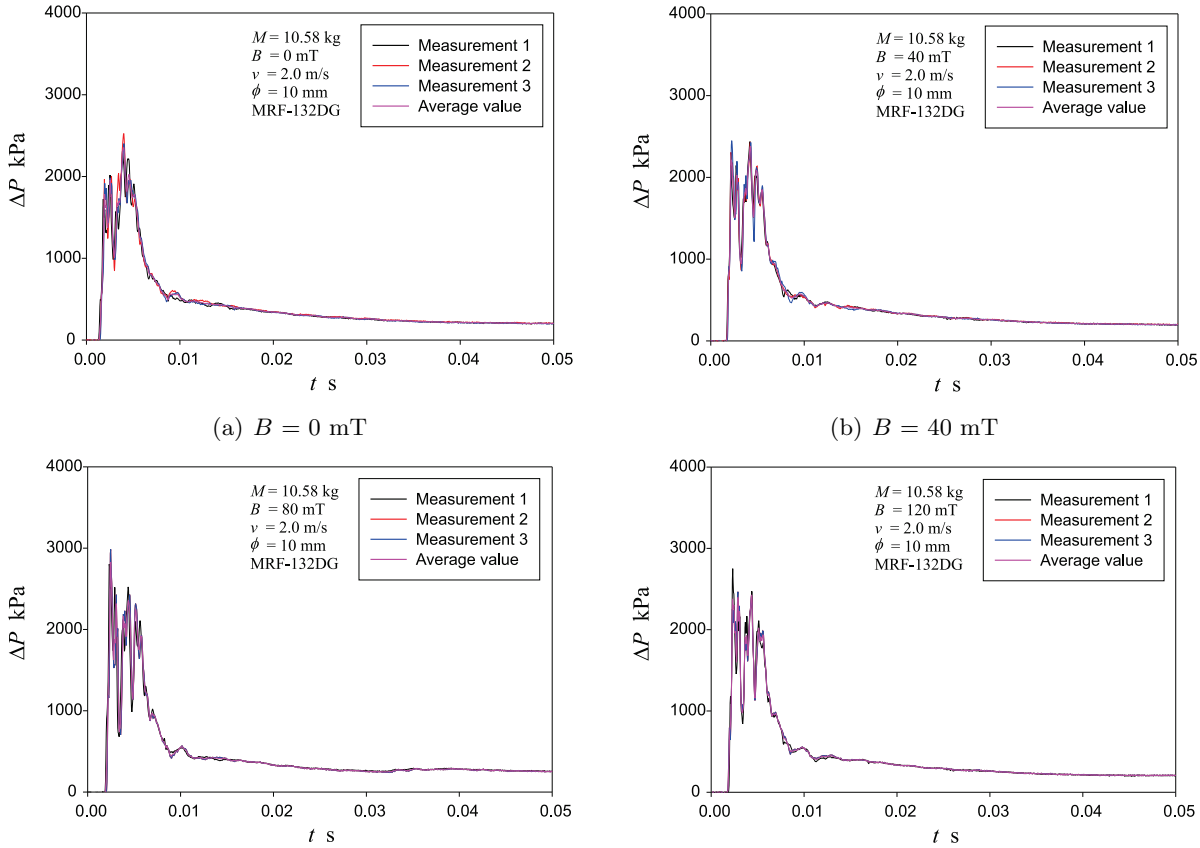

(a) $B = 0$ mT (b) $B = 40$ mT

(c) $B = 80$ mT (d) $B = 120$ mT

Figure 2.33: Pressure difference vs. time of $M = 10.58$ kg at $B = 0$ mT (a), $B = 40$ mT (b), $B = 80$ mT (c) and 120 mT (d)

Chapter 3

Analysis of MR fluid under shock loading

The purpose of this chapter is to explain the experiment results. In this study, three different experiments are conducted to investigate the behavior and performance of MR fluid to handle the shock loading. The discussions are focused on the some effects, which are magnetic flux density, orifice inner diameter and volume fraction of MR fluids, on the piston displacement, piston velocity, damping force and pressure difference.

This chapter is divided into three sections. First section discusses about the effect of magnetic field. Four different magnetic flux densities are applied for each experiment. Second section discusses about the effect of orifice inner diameter. Three different size of orifice inner diameter are applied. Third section discusses about the effect of volume fraction. Experiments are conducted by applying two different types of MR fluids (MRF-122EG and MRF-132DG).

3.1 Effect of magnetic field

Experiments are conducted to investigate the effect of magnetic field on the behavior of MR fluid under shock loading. Four different magnetic flux densities (0, 40, 80 and 120 mT) are applied in this experiment. The detail explanation about the experiment condition is presented in Table 3.1.

The effects of magnetic field are investigated based on the experiment results on piston

Table 3.1: Experiment condition to investigate the effect of magnetic field

No	Parameter	Value
1	Magnetic flux density	0, 40, 80 and 120 mT
2	Working fluid	MRF-132DG
3	Drop mass	5.57, 7.24, 8.91 and 10.58 kg
4	Impact velocity	0.5, 1.0, 1.5 and 2.0 m/s
5	Orifice inner diameter	10 mm
6	Piston stroke	80 mm

displacement, piston velocity, impact force and pressure difference in the orifice area.

3.1.1 Piston displacement and velocity

In this section, the effect of magnetic field is analyzed from the movement of the piston which measured using laser displacement sensor during the shock loading.

Figures 3.1 $\sim$ 3.4 show piston velocity (Vp) over piston displacement (Dp) at impact velocity (v) of 0.5 m/s (a) and 2.0 m/s (b) for different drop masses (M); 5.57 kg, 7.24 kg, 8.91 kg and 10.58 kg, respectively. Impact velocity of 0.5 m/s is selected to represent low impact velocity and impact velocity of 2.0 m/s is selected to represent high impact velocity. From these figures, it can be observed that piston velocity increases abruptly in the initial stage. There is no influence of the magnetic field on the initial increase of the velocity because the force caused by shock loading is much greater than the viscous force of the MR fluid, which is produced by the magnetic field. The piston velocity reduces after reaching the peak velocity. An almost constant velocity region appeared for every magnetic flux density. The gravitational force of the drop mass and the viscous force is balanced in this area. Subsequently, the velocity decreases suddenly in respect to the magnetic flux density. The decrease in the piston velocity at low impact velocity (v = 0.5 m/s) and at low magnetic flux density (B = 0 and 40 mT) is relatively small. However, the decrease becomes higher at higher magnetic flux densities (B = 80 and 100 mT)at low impact velocity and at different magnetic flux densities ($B = 0 \sim 120$ mT) at high impact velocity (v = 2 m/s). After the peak value of piston velocity, the velocity at 0 mT is higher than those at 40, 80, and 120 mT. At different impact velocities, the order of the velocity follows the magnetic flux density. As the density of the magnetic flux increases, the velocity decreases. This implies that the magnetic field affects the reduction in the piston velocity.

At high impact velocity, the piston velocity decreases significantly, followed by sudden increases for different magnetic flux densities (Figs. 3.1(b) $\sim$ 3.4(b)). This phenomenon seems to be caused by the second shock loading or bouncing from the drop mass. After first loading, the drop mass hit the piston one more times at high impact velocities. This phenomenon is not appeared at small impact velocities since there is no chance of drop mass to bouncing.

From Figs. 3.1 $\sim$ 3.4, it can be observed that the piston stroke decreases at higher magnetic flux density. The decrease in piston stroke or maximum value of piston displacement (Dp_{max}) is presented in Fig. 3.5. This figure shows piston stroke after subjected to shock loading as function of magnetic flux density for different drop mass at impact velocity 0.5 m/s (a) and 2.0 m/s (b). At low magnetic flux densities (B = 0 and 40 mT), the piston travels at maximum stroke (80 mm) for both impact velocity (v = 0.5 and 2 m/s) and different drop masses. It appears that 40 mT of magnetic flux density is not powerful enough to resist the movement of the piston. However, the piston travels at shorter distance when higher magnetic flux densities (B = 80 and 120 mT) are applied. This result agrees with the expected increase in apparent yield stress when higher magnetic flux density is applied.

The decrease in piston stroke becomes smaller at high impact velocity (v = 2.0 m/s). Figure 3.5(b) shows that piston nearly travels at similar distance ($\sim$ 80mm) at 10.58 kg of drop mass for different magnetic flux densities ($B = 0 \sim 120$ mT). The effect of magnetic field on the

movement resistance of MR fluid under shock loading reduces at higher impact velocities.

Figure 3.5 shows that the piston stroke decreases when heavier drop mass is applied. At 80 mT and 120 mT, the order of decrease in the value of the piston stroke follows the drop mass values. Moreover, at 80 mT and 120 mT, the piston stroke at 2.0 m/s of impact velocity is shorter than that at 0.5 m/s for different drop masses, respectively. These results indicate that drop mass and impact velocity have effect on the movement resistance of MR fluid under shock loading.

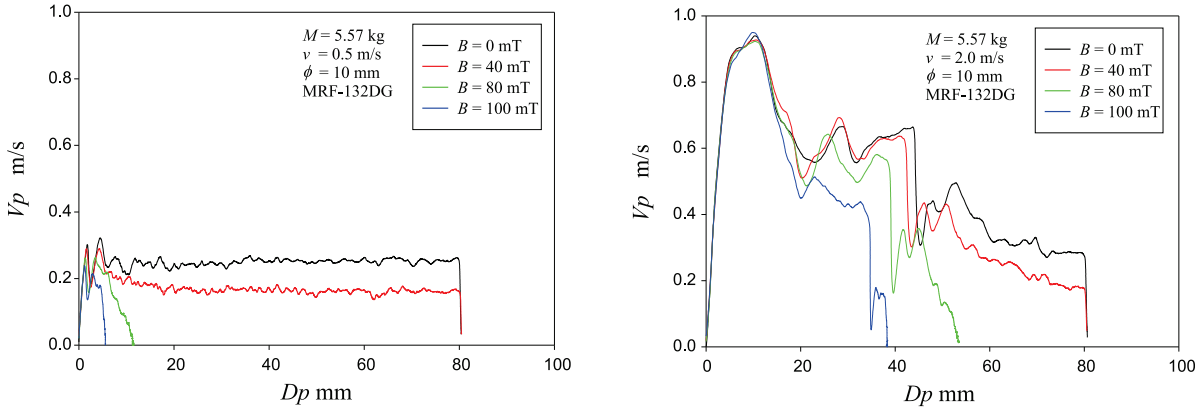

(a) $v = 0.5$ m/s (b) $v = 2.0$ m/s

Figure 3.1: Piston velocity vs. piston displacement of $M = 5.57$ kg at $v = 0.5$ m/s (a) and 2.0 m/s (b)

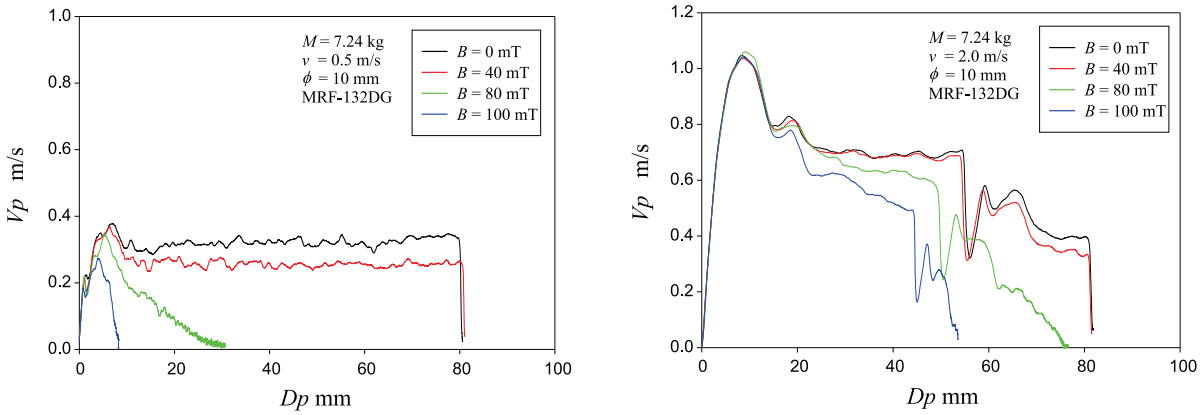

(a) $v = 0.5$ m/s (b) $v = 2.0$ m/s

Figure 3.2: Piston velocity vs. piston displacement of $M = 7.24$ kg at $v = 0.5$ m/s (a) and 2.0 m/s (b)

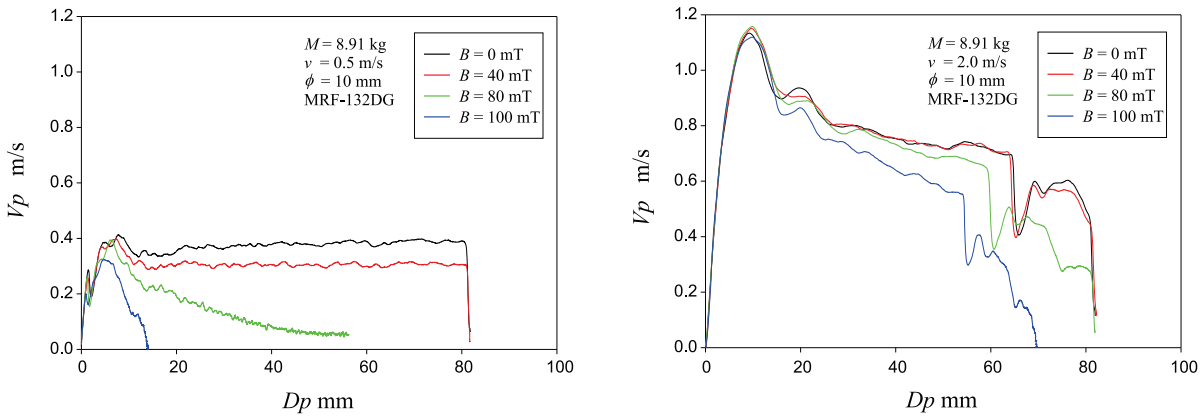

(a) $v = 0.5$ m/s (b) $v = 2.0$ m/s

Figure 3.3: Piston velocity vs. piston displacement of $M = 8.91$ kg at $v = 0.5$ m/s (a) and 2.0 m/s (b)

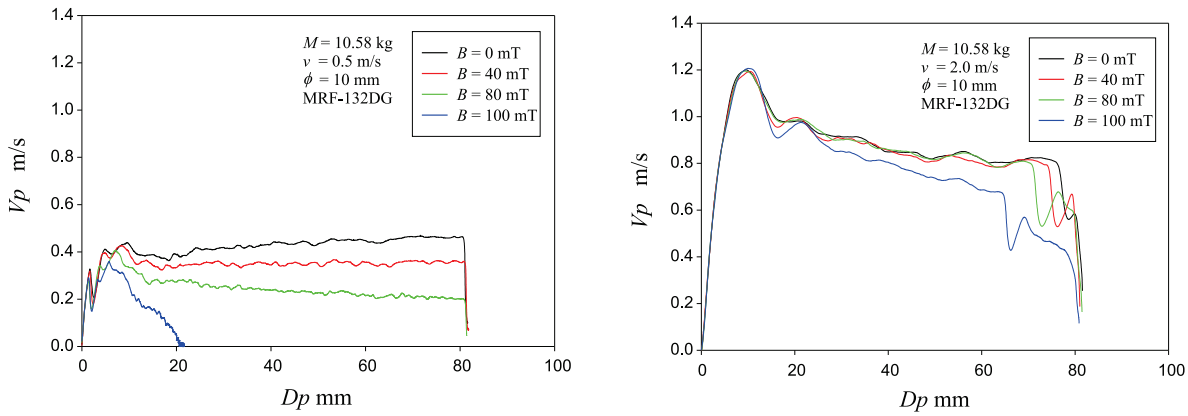

(a) $v = 0.5$ m/s (b) $v = 2.0$ m/s

Figure 3.4: Piston velocity vs. piston displacement of $M = 10.58$ kg at $v = 0.5$ m/s (a) and 2.0 m/s (b)

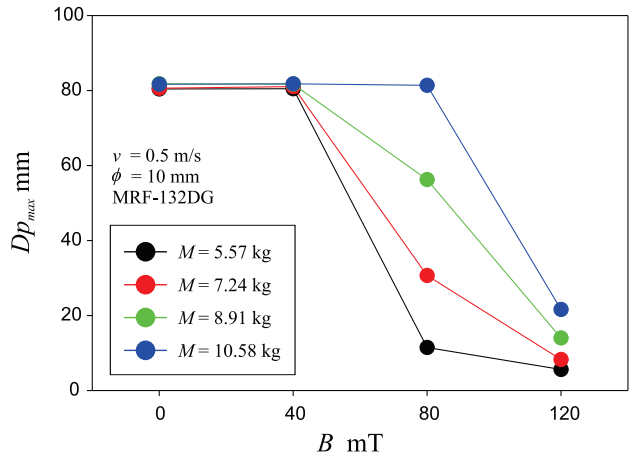

(a) $v = 0.5$ m/s

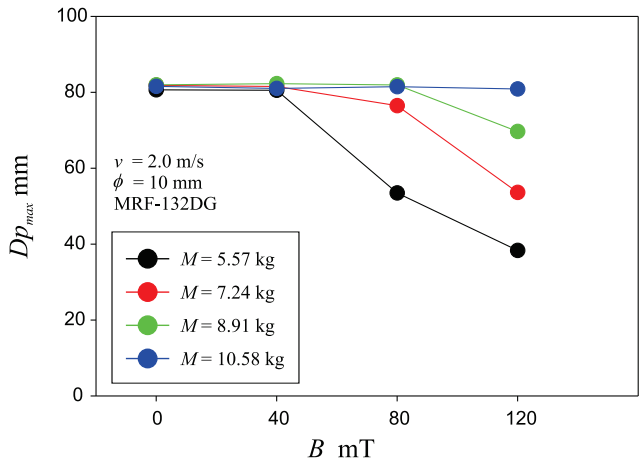

(b) $v = 2.0$ m/s

Figure 3.5: Maximum piston displacement as function of B for different M at $v = 0.5$ m/s (a) and 2.0 m/s (b)

3.1.2 Damping force

In this section, effect of magnetic field is analyzed from the damping force which is measured from load cell during the shock loading. Figures 3.6 $\sim$ 3.9 show the damping force (F) over time (t) at v = 0.5 m/s (a) and 2.0 m/s (b) for M = 5.57 kg, 7.24 kg, 8.91 kg and 10.58 kg, respectively. From Figs. 3.6(a) $\sim$ 3.9(a), it can be observed that the peak values of damping force (F_{max}) are occurred at 0.005 $\sim$ 0.01 s (depend on the value of impact velocity).

From Figs. 3.6(a) $\sim$ 3.9(a), at low impact velocity (v = 0.5 m/s), the value of F_{max} increases at higher magnetic flux density. The increasing value of damping force means that MR fluid with higher magnetic flux density has stronger when subjected to shock loading. It might be because at higher magnetic flux densities, the size of cluster in MR fluid is bigger. The bigger cluster is stronger to handle pressure that caused by shock loading. More more detail about the effect of pressure on the inner structure in MR fluid will be discussed in Chapter 5.

The trend of results is different at higher impact velocity (v = 2 m/s). From Figs. 3.6(b) $\sim$ 3.9(b), the value of F_{max} is relatively similar for different magnetic flux densities. These results imply that magnetic flux density has no remarkable effect on the damping force of MR fluid under shock loading at high impact velocities.

The value of F_{max} as the function of magnetic flux density of v = 0.5 m/s (a) and 2 m/s (b) is presented in Fig. 3.10. At low impact velocity (Fig. 3.10(a)), the value of F_{max} increases at higher magnetic flux density for different drop masses. The heavier of drop masses, the value of F_{max} becomes higher. However, at high impact velocity (Fig. 3.10(b)), the value of F_{max} is nearly similar for different magnetic flux density. The trend of these results is similar with the previous study [91]. During the initial stages of the shock loading, the MR fluid is not flowing through the orifice. Ahmadian and Norris [91] called this type of behavior as "fluid locking". In addition, these results suggest that the effect of magnetic field on the force resistance under shock loading becomes less significant at high impact velocities.

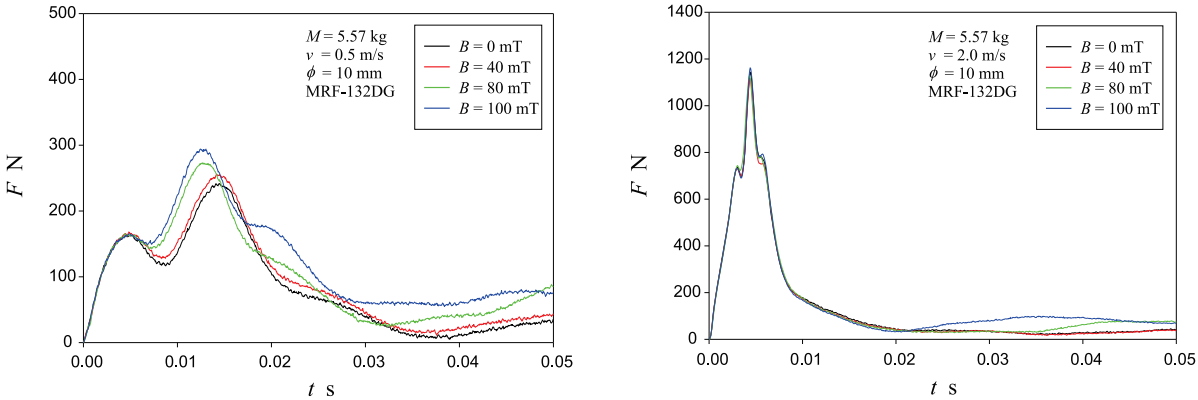

(a) $v = 0.5$ m/s (b) $v = 2.0$ m/s

Figure 3.6: Force vs. time of $M = 5.57$ kg at $v = 0.5$ m/s (a) and 2.0 m/s (b)

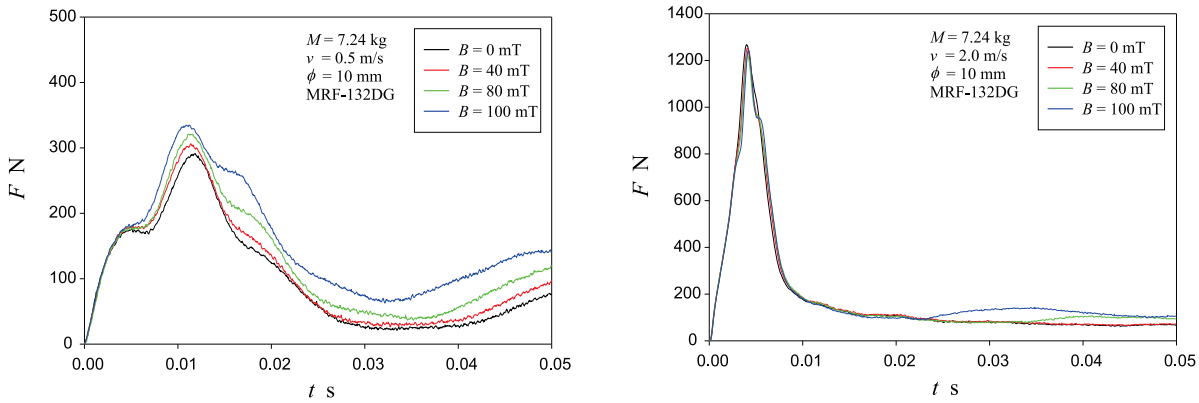

(a) $v = 0.5$ m/s (b) $v = 2.0$ m/s

Figure 3.7: Force vs. time of $M = 7.24$ kg at $v = 0.5$ m/s (a) and 2.0 m/s (b)

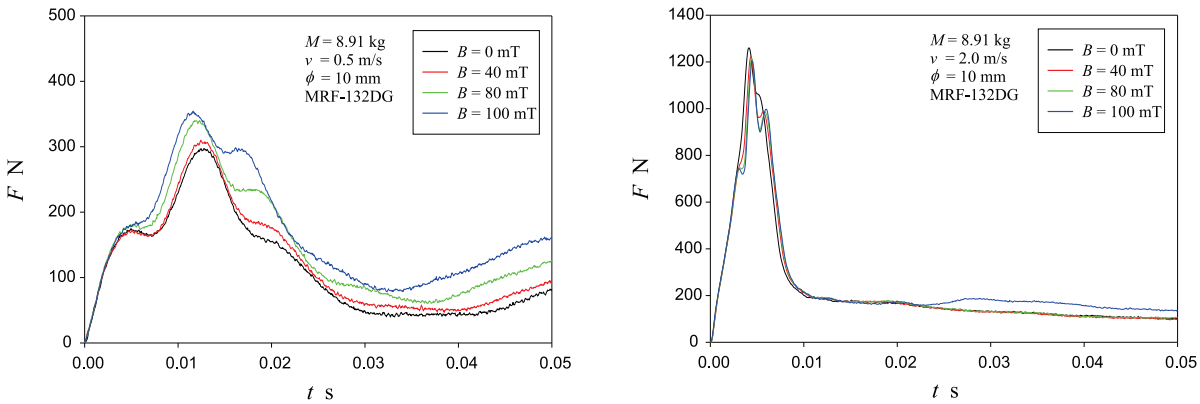

(a) $v = 0.5$ m/s (b) $v = 2.0$ m/s

Figure 3.8: Force vs. time of $M = 8.91$ kg at $v = 0.5$ m/s (a) and 2.0 m/s (b)

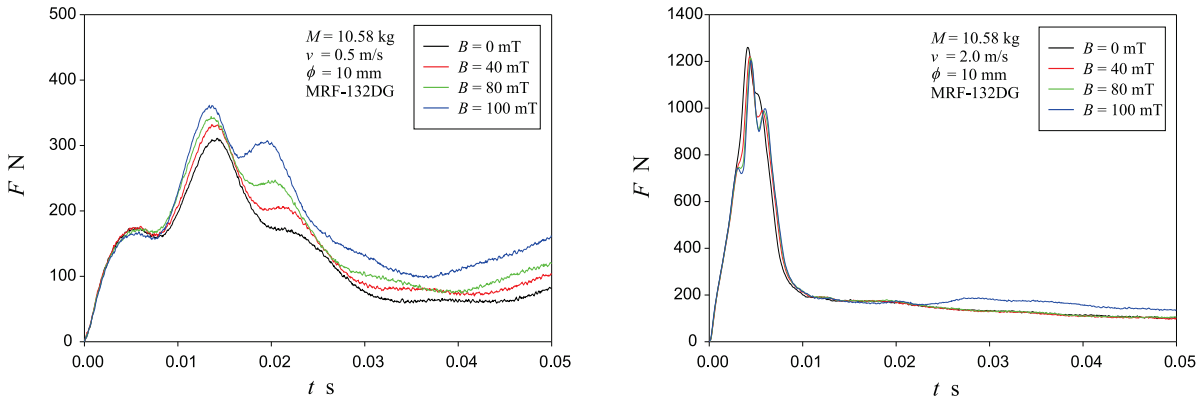

(a) $v = 0.5$ m/s (b) $v = 2.0$ m/s

Figure 3.9: Force vs. time of $M = 10.58$ kg at $v = 0.5$ m/s (a) and 2.0 m/s (b)

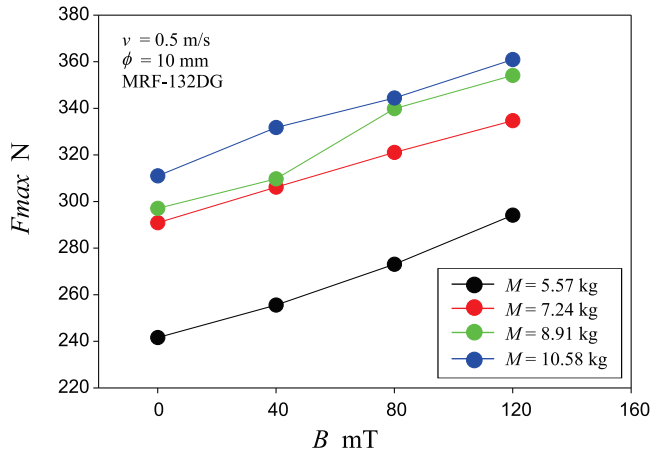

(a) $v = 0.5$ m/s

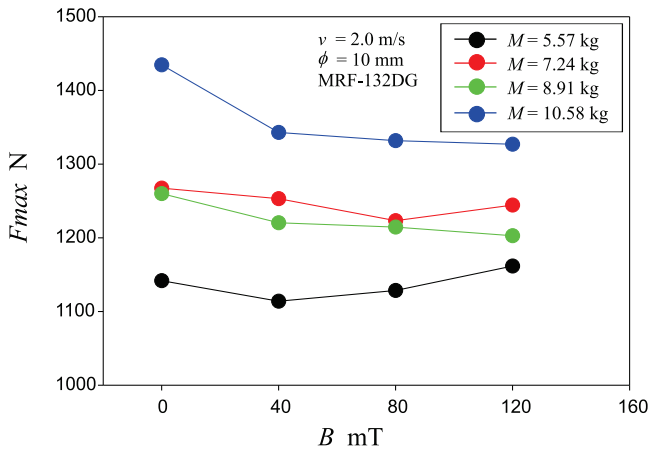

(b) $v = 2.0$ m/s

Figure 3.10: Peak value of F as function of B for different M at $v = 0.5$ m/s (a) and 2.0 m/s (b)

3.1.3 Pressure difference in the orifice

In this section, the effect of magnetic field is analyzed from the pressure in inlet (Pin) and outlet ($Pout$) of the orifice, which is measured from the pressure sensors. The pressure difference (ΔP) is calculated by subtracting the inlet pressure with outlet pressure.

Figures 3.11 $\sim$ 3.14 show the value of ΔP over time (t) at $v = 0.5$ m/s (a) and 2.0 m/s (b) for $M = 7.24$ kg, 8.91 kg and 10.58 kg, respectively. From these figures, it can be observed that the peak value of ΔP (ΔP_{max}) is occurred at around 0.005 $\sim$ 0.01 s, depends on the drop masses and impact velocities. The peak value of ΔP is occurred as the response to shock loading.

The value of ΔP_{max} as the function of magnetic flux density at $v = 0.5$ m/s (a) and 2.0 m/s (b) is presented in Fig. 3.15. At low impact velocity, the value of ΔP_{max} tends to increases with the increasing of magnetic flux density (Figs. 3.11(a) $\sim$ 3.14(a)). The increasing of the value of ΔP_{max} means that the higher magnetic flux density is more effective to restrict the flow of MR fluid under shock loading. However, at higher impact velocity, the value of ΔP_{max} is relatively similar for different magnetic flux densities (Figs. 3.11(b) $\sim$ 3.14(b)). This result confirms that at high impact velocities, the magnetic field has no remarkable effect to restrict the flow of MR fluid under shock loading.

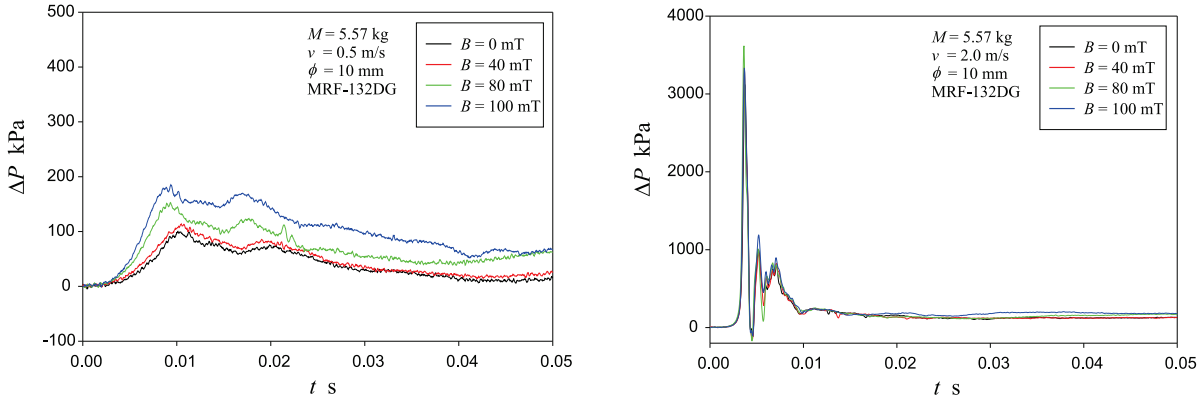

(a) $v = 0.5$ m/s (b) $v = 2.0$ m/s

Figure 3.11: Force vs. time of $M = 5.57$ kg at $v = 0.5$ m/s (a) and 2.0 m/s (b)

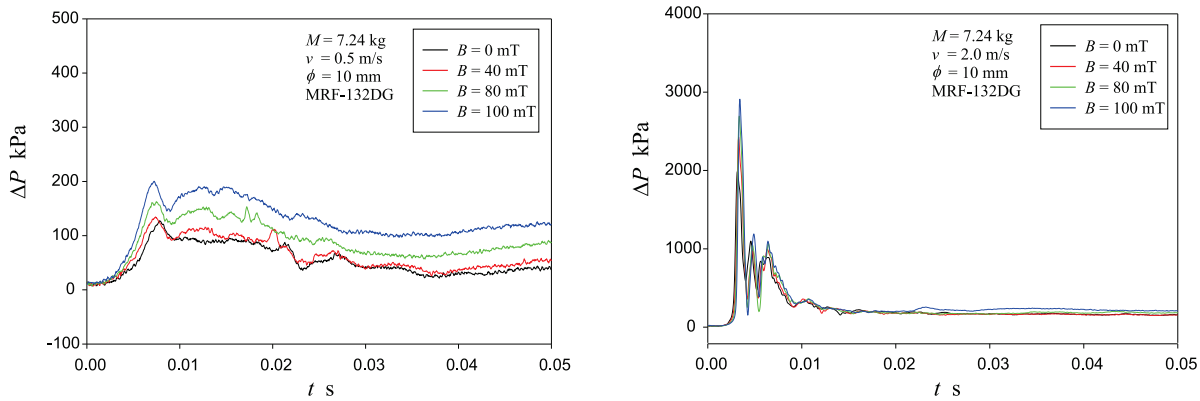

(a) $v = 0.5$ m/s (b) $v = 2.0$ m/s

Figure 3.12: Force vs. time of $M = 7.24$ kg at $v = 0.5$ m/s (a) and 2.0 m/s (b)

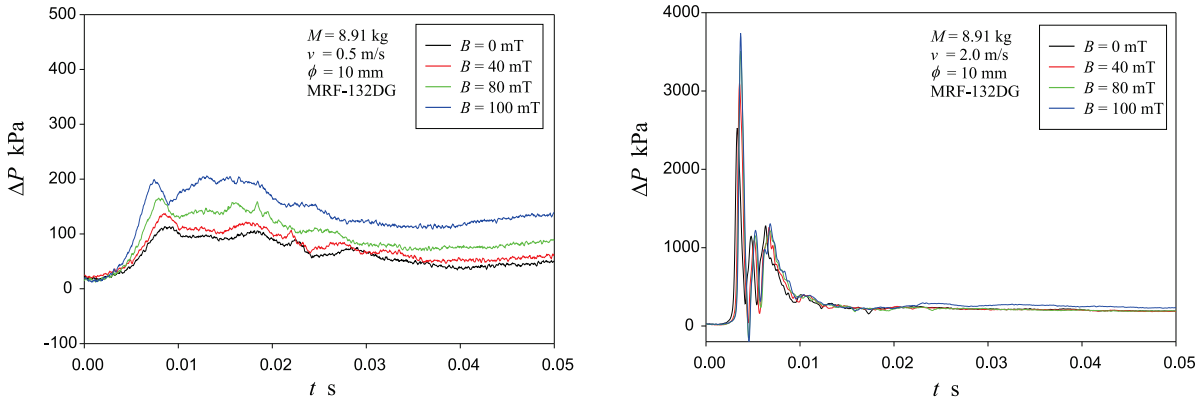

(a) $v = 0.5$ m/s (b) $v = 2.0$ m/s

Figure 3.13: Force vs. time of $M = 8.91$ kg at $v = 0.5$ m/s (a) and 2.0 m/s (b)

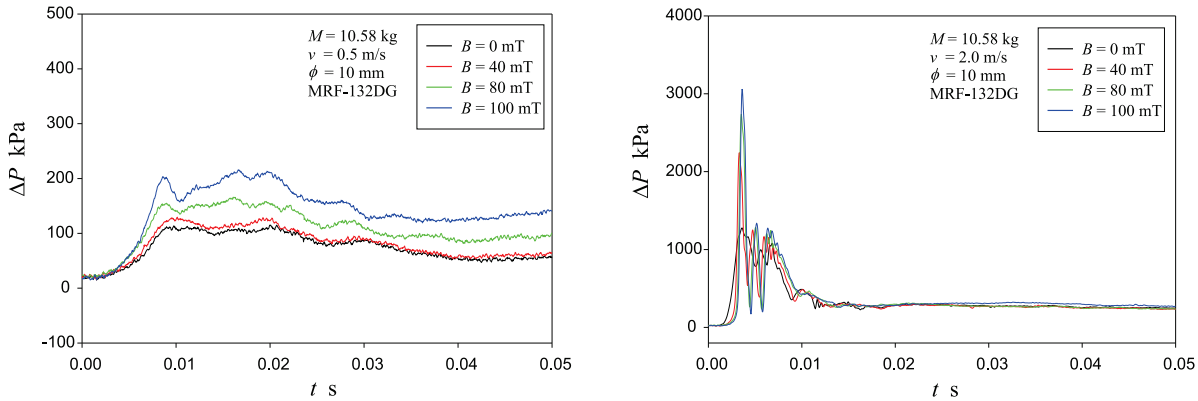

(a) $v = 0.5$ m/s (b) $v = 2.0$ m/s

Figure 3.14: Force vs. time of $M = 10.58$ kg at $v = 0.5$ m/s (a) and 2.0 m/s (b)

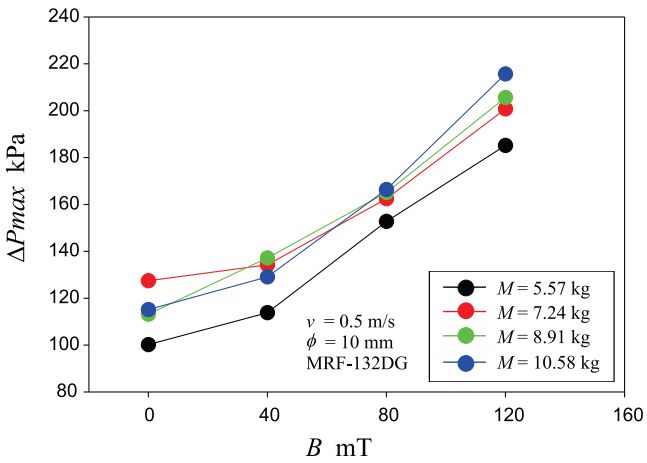

(a) $v = 0.5$ m/s

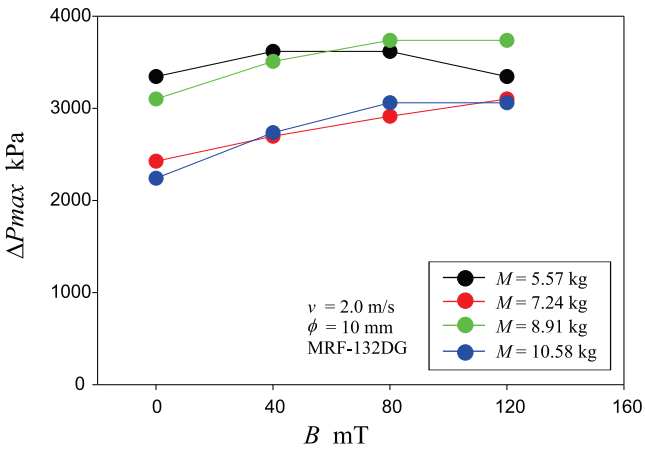

(b) $v = 2.0$ m/s

Figure 3.15: Peak value of ΔP as function of B for different M at $v = 0.5$ m/s (a) and 2.0 m/s (b)

3.2 Effect of orifice inner diameter

Experiments are conducted to investigate the effect of orifice inner diameter on the behavior of MR fluid under shock loading. Three different size of orifice inner diameter (5, 8.7 and 10 mm) are applied in this experiment. The information of the experiment condition is presented in Table 3.2.

3.2.1 Piston displacement and velocity

Figures 3.16 $\sim$ 3.18 show piston velocity (Vp) over piston displacement (Dp) at $v = 2.0$ m/s, at $B = 0$ mT (a) and 120 mT (b), for $M = 7.24$ kg, 8.91 kg and 10.58 kg, respectively. In order to represent strong shock loading, $v = 2$ m/s is selected. $B = 0$ mT and 120 mT are selected to represent low and high magnetic field, respectively. From these figures, it can be observed that the piston velocities reduce after reaching the peak velocity (Vp_{max}) for different orifice inner diameter. The value of Vp_{max} and Vp after the peak value at bigger orifice inner diameter (ϕ 10 mm) is higher than that at smaller orifice inner diameter (ϕ 8.7 and ϕ 5 mm). The order of the decreasing in Vp_{max} value follows the size of orifice inner diameter for different magnetic flux densities. The value of Vp_{max} as the function of orifice inner diameter is presented in Fig. 3.19. As the orifice inner diameter decreases, the velocity decreases. In other words, the peak velocity is dependent to the orifice size. This difference is caused by the flow resistance through the orifice. This implies that the orifice inner diameter affects the reduction in the piston velocity.

The maximum value of displacement (Dp_{max}) as the function of orifice inner diameter is presented in Fig. 3.20. At 0 mT, under different drop masses, the difference of piston stroke of ϕ 5 mm can be seen clearly (Fig. 3.20(a)). The difference of piston stroke of ϕ 8.6 mm and ϕ 10 mm is not clear because the piston reaches nearly the piston maximum stroke ($\sim$ 80 mm). However, at 120 mT, the difference of piston stroke of ϕ 8.6 mm and ϕ 10 mm can be seen (Fig. 3.20(b)). The increasing piston stroke follows the value of drop mass. The heavier of drop mass, the piston stroke becomes longer due to the potential energy of the drop mass. Generally, the travel length of the piston becomes shorter with smaller orifice inner diameter when the intensity of the applied magnetic field is the same. These results indicate the strong effect of orifice inner diameter on the piston displacement and velocity just after MR fluid is subjected to shock loading.

Table 3.2: Experiment condition to investigate the effect of orifice inner diameter

No	Parameter	Value
1	Orifice inner diameter	5, 8.7 and 10 mm
2	Magnetic flux density	0, 40, 80 and 120 mT
3	Working fluid	MRF-132DG
4	Drop mass	7.24, 8.91 and 10.58 kg
5	Impact velocity	0.5, 1.0, 1.5 and 2.0 m/s
6	Piston stroke	80 mm

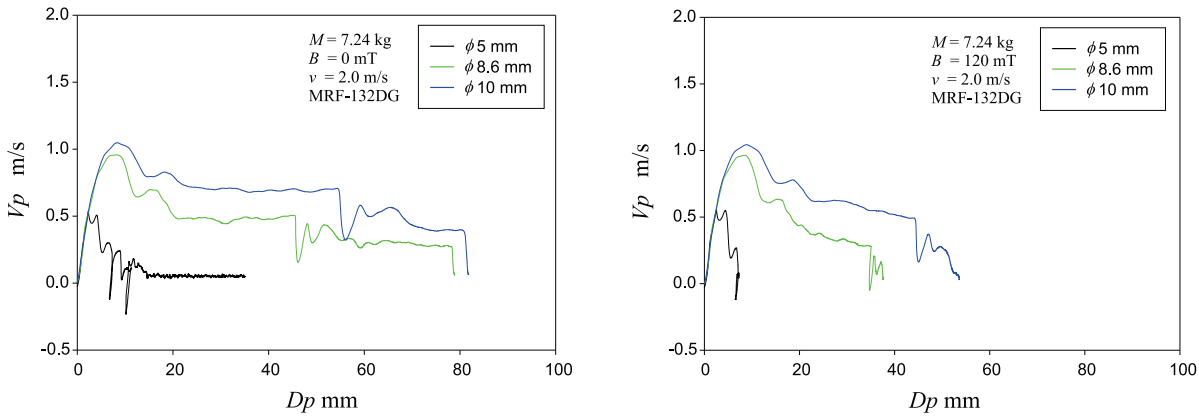

(a) $B = 0$ mT (b) $B = 120$ mT

Figure 3.16: Force vs. time of $M = 7.24$ kg at $B = 0$ mT (a) and 120 mT (b)

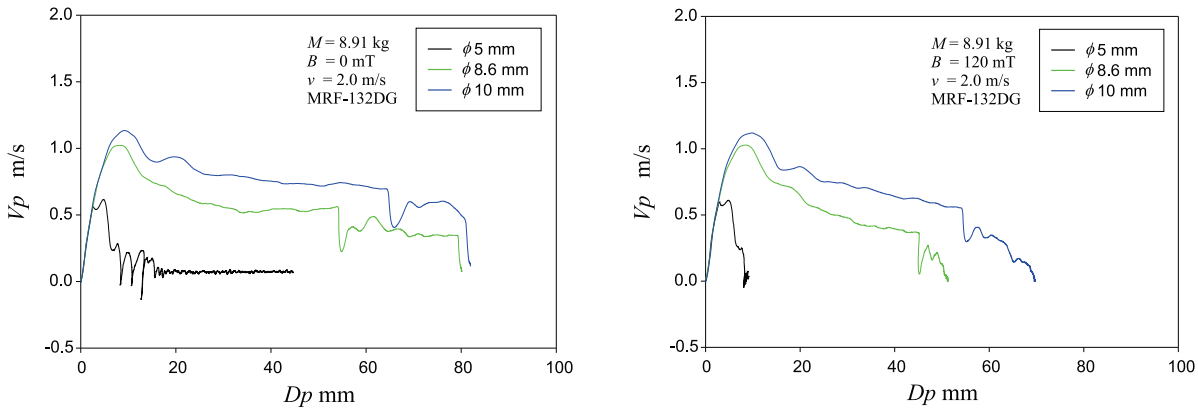

(a) $B = 0$ mT (b) $B = 120$ mT

Figure 3.17: Force vs. time of $M = 8.91$ kg at $B = 0$ mT (a) and 120 mT (b)

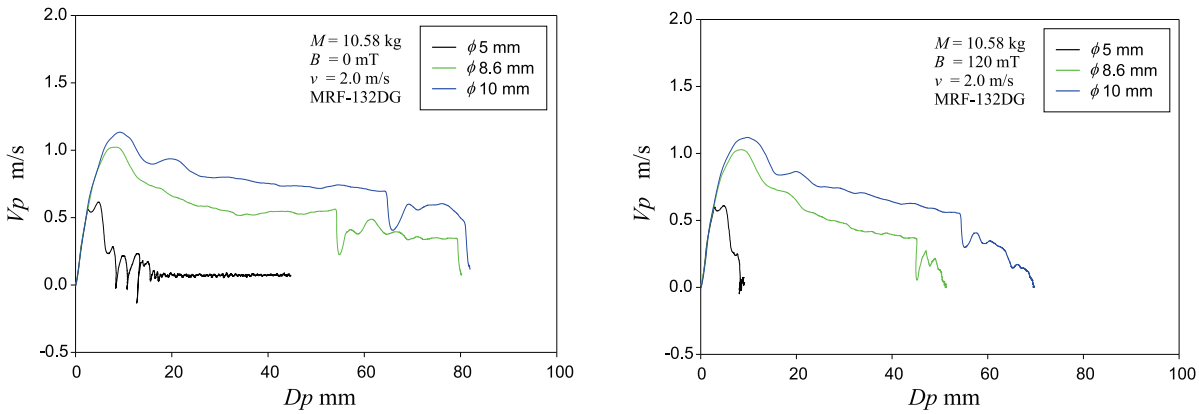

(a) $B = 0$ mT (b) $B = 120$ mT

Figure 3.18: Force vs. time of $M = 10.58$ kg at $B = 0$ mT (a) and 120 mT (b)

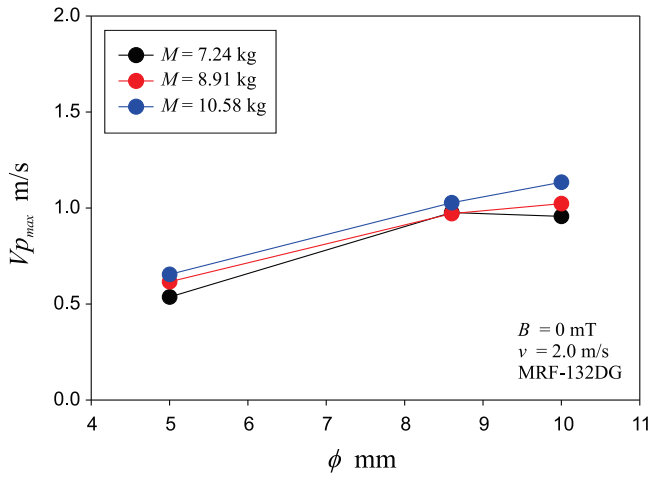

(a) $B = 0$ mT

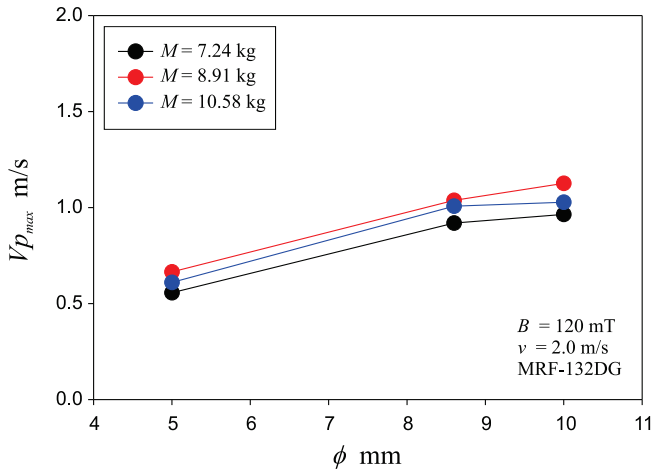

(b) $B = 120$ mT

Figure 3.19: Maximum piston velocity as function of ϕ at $B = 0$ mT (a) and 120 mT (b)

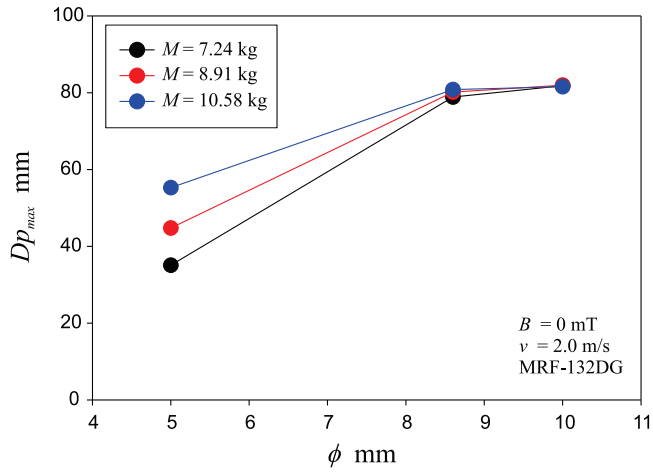

(a) $B = 0$ mT

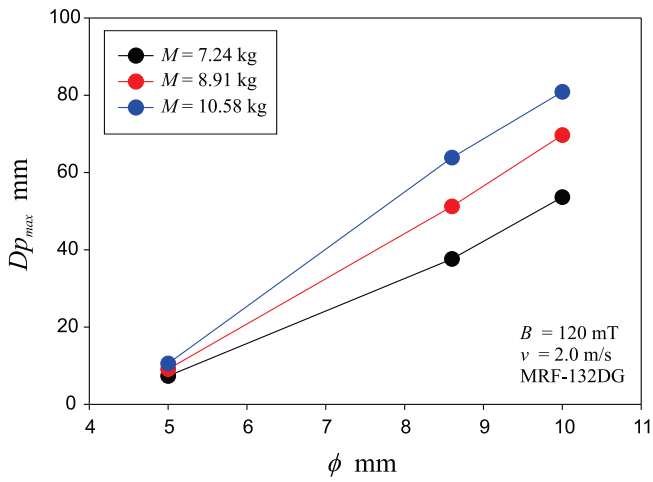

(b) $B = 120$ mT

Figure 3.20: Maximum piston displacement as function of ϕ at $B = 0$ mT (a) and 120 mT (b)

3.2.2 Damping force

Figures 3.21 $\sim$ 3.23 show damping force (F) over time (t) at v = 2.0 m/s for M = 7.24 kg, 8.91 kg and 10.58 kg, respectively. From these figures, it can be observed that the peak value of damping force (F_{max}) increases at smaller orifice inner diameter.

The value of F_{max} as function of orifice inner diameter at B = 120 mT is presented in Fig. 3.24. The value of F_{max} of ϕ 5 mm is much higher than that value of ϕ 8.6 mm and ϕ 10 mm for different drop masses. The order of the increasing value of F_{max} follow the value of drop masses. The increasing value of F_{max} means that smaller orifice inner diameter is more effective to resist the impact force caused by shock loading. These results indicate that orifice inner diameter has remarkable effects on the resistance force of MR fluid under shock loading.

3.2.3 Pressure difference in the orifice

Figures 3.25 $\sim$ 3.27 show the value of ΔP over time (t) at v = 2.0 m/s for M = 7.24 kg, 8.91 kg and 10.58 kg, respectively. From these figures, it can be observed that the peak value of ΔP (ΔP_{max}) tends to increases with the decrease in orifice inner diameter.

The value of ΔP_{max} as function of orifice inner diameter at B = 120 mT is presented in Fig. 3.28. The value of ΔP_{max} of ϕ 5 mm is higher than that value of ϕ 8.6 mm and ϕ 10 mm for different drop masses. The increasing value of ΔP_{max} means that smaller orifice inner diameter is more effective to restrict the flow of MR fluid under shock loading. These results indicate that orifice inner diameter has remarkable effects to restrict the flow of MR fluid under shock loading.

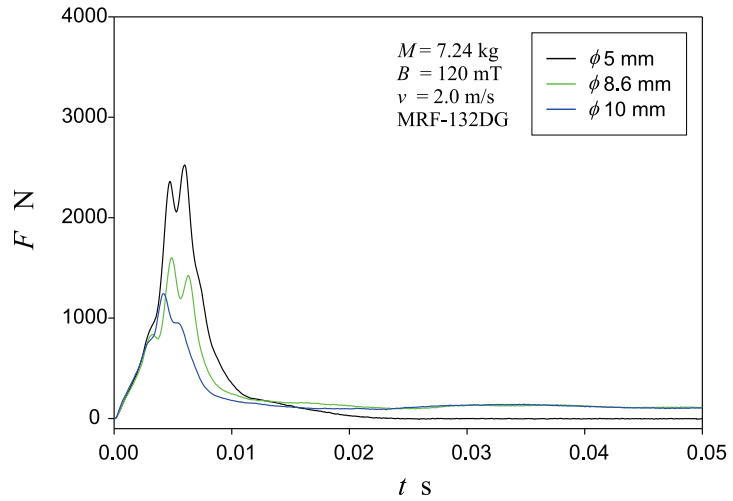

Figure 3.21: Force vs. time of $M = 7.24$ kg at $B = 120$ mT

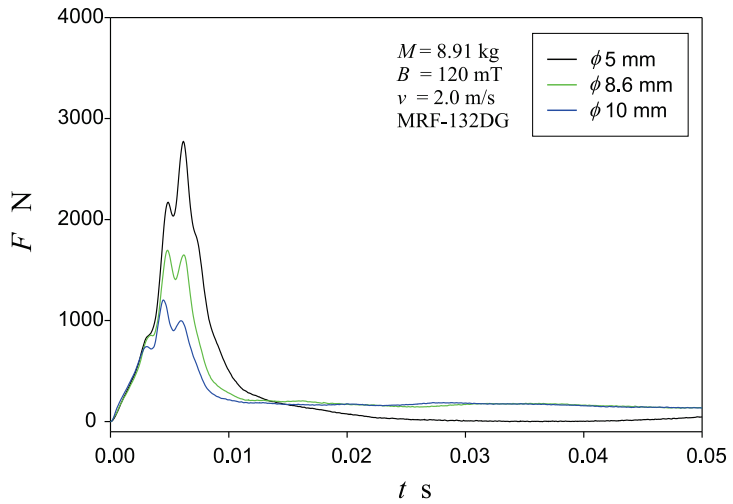

Figure 3.22: Force vs. time of $M = 8.91$ kg at $B = 120$ mT

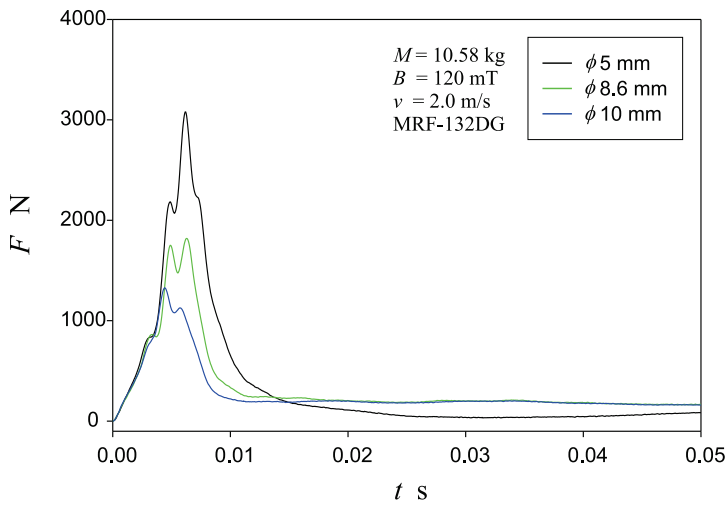

Figure 3.23: Force vs. time of $M = 10.58$ kg at $B = 120$ mT

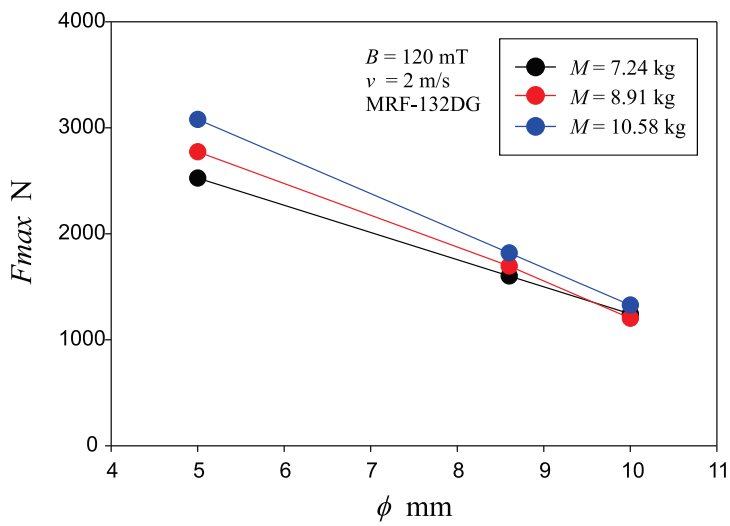

Figure 3.24: Peak value of F as function of ϕ at $B = 120$ mT

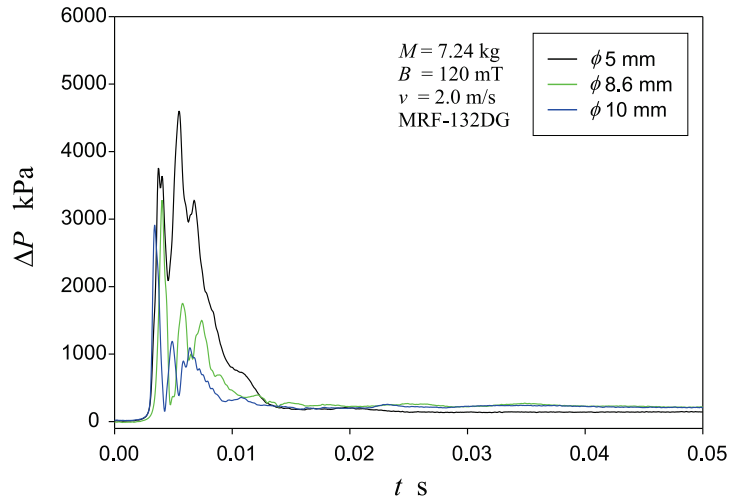

Figure 3.25: Pressure difference vs. time of $M = 7.24$ kg at $B = 120$ mT

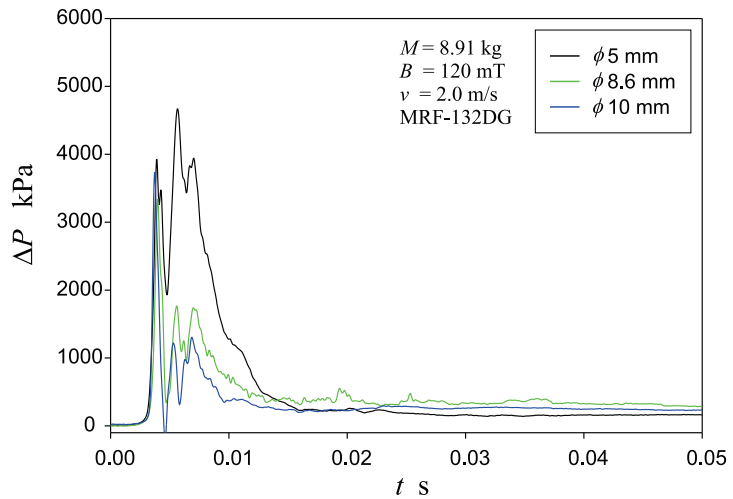

Figure 3.26: Pressure difference vs. time of $M = 8.91$ kg at $B = 120$ mT

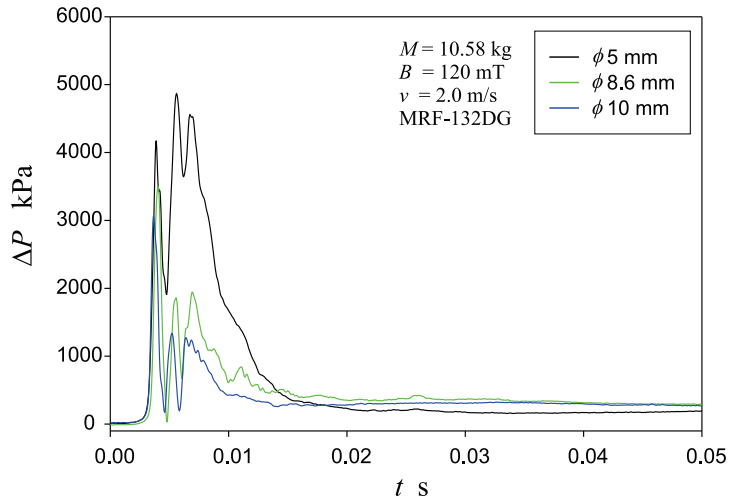

Figure 3.27: Pressure difference vs. time of $M = 10.58$ kg at $B = 120$ mT

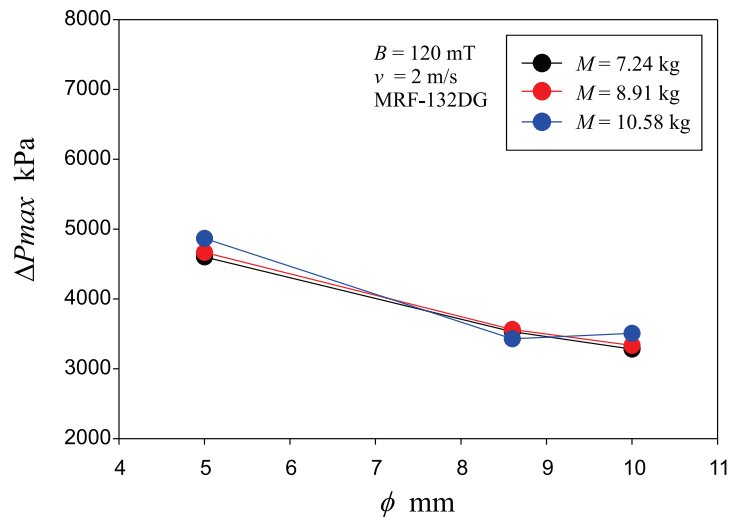

Figure 3.28: Peak value of ΔP vs. time at $B = 120$ mT

3.3 Effect of volume fraction of MR fluid

Experiments are conducted to investigate the effect of volume fraction of MR fluid on the behavior of MR fluid under shock loading. Two different series of MR fluid (MRF-122EG and MRF-132DG) are applied in this experiment. The information of the experiment condition is shown in Table 3.3. The main difference between the two MR fluids is their volume fraction or solid content on the fluids. MRF-122EG has 22 % and MRF-132DG has 32 % of volume fraction. The properties of these MR fluids is presented in Table 2.5.

3.3.1 Piston displacement and velocity

Figures 3.29 $\sim$ 3.32 show piston velocity (Vp) over piston displacement (Dp) at $B = 120$ mT of MRF-122EG (a) and MRF-132DG (b). From these figures, it can be observed that for different MR fluids, the order of increasing piston velocity and increasing piston stroke follows the order of impact velocity.

The values of Dp_{max} or piston stroke as the function of impact velocity for different MR fluids at $B = 0$ mT and 120 mT are presented in Figs. 3.33 and 3.34, respectively. At 0 mT, the value of Dp_{max} at $M = 7.24 \sim 10.58$ kg in MRF-122EG and at $M = 8.91$ and 10.58 kg is nearly 140 mm. It means that the piston travels at maximum stroke under these drop masses. However, under lighter drop mass ($M = 5.57$ kg in MRF-122EG and 5.57 kg and 7.24 kg in MRF-132DG), the value of Dp_{max} is lower than 140 mm. At that range, the value of Dp_{max} in MRF-132DG is lower than that value in MRF-122EG due to the viscosity of MRF-122EG is smaller than MR-132DG. As a result, the piston stroke is farther for smaller viscosity at 0 mT. In the contrary, at higher magnetic flux density (120 mT), cluster formation in MRF-132DG is thicker than its value in MRF-122EG. The thicker of cluster formation increases the viscosity of MR fluid. At higher viscosity, MR fluid becomes harder to flow in the orifice area. As a result, the piston travels in a shorter distance at higher volume fraction (Fig. 3.34). These results indicate that volume fraction affects the reduction of the piston stroke.

The values of peak value in piston velocity (Vp_{max}) as the function of impact velocity for different MR fluids at $B = 120$ mT are presented in Fig. 3.34. The value of Vp_{max} at smaller volume fraction (MRF-122EG) is higher than the value at higher volume fraction (MRF-132DG). It indicates that bigger volume fraction of MR fluid is more effective to reduce the velocity of the piston after reaching the peak velocity.

Table 3.3: Experiment condition to investigate the effect of volume fraction of MR fluid

No	Parameter	Value
1	Working fluid	MRF-122EG and MRF-132DG
2	Magnetic flux density	0, 40, 80 and 120 mT
3	Drop mass	7.24, 8.91 and 10.58 kg
4	Impact velocity	0.5, 1.0, 1.5 and 2.0 m/s
5	Orifice inner diameter	8 mm
6	Piston stroke	140 mm

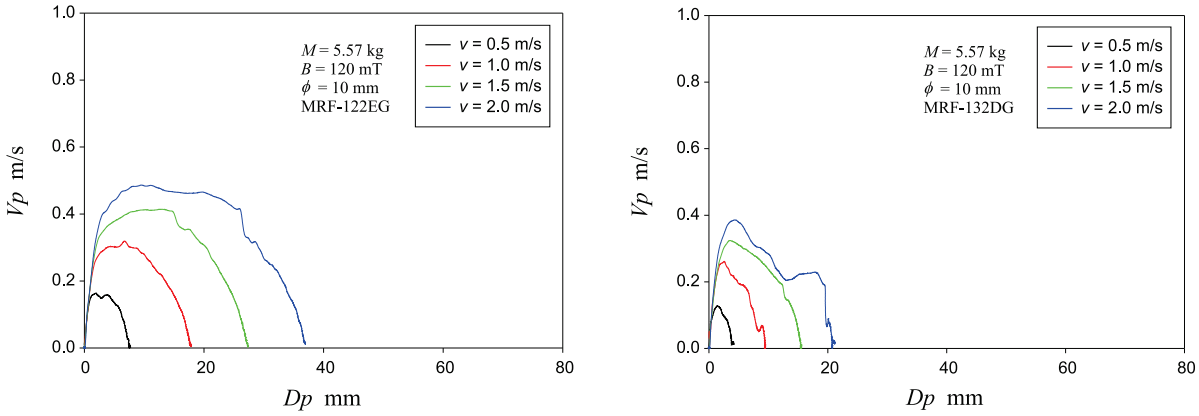

(a) MRF-122EG (b) MRF-132DG

Figure 3.29: Piston velocity vs. piston displacement of $M = 5.57$ kg of MRF-122EG (a) and MRF-132DG (b) at $B = 120$ mT

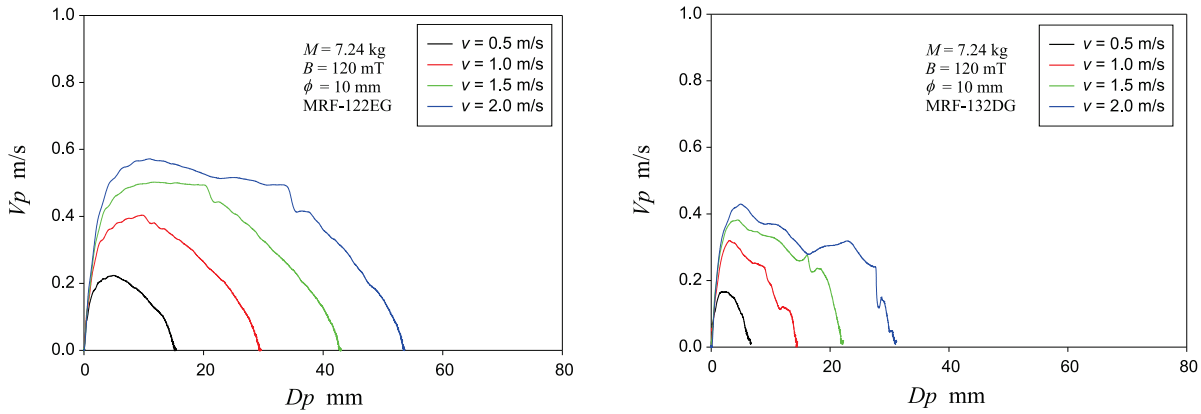

(a) MRF-122EG (b) MRF-132DG

Figure 3.30: Piston velocity vs. piston displacement of $M = 7.24$ kg of MRF-122EG (a) and MRF-132DG (b) at $B = 120$ mT

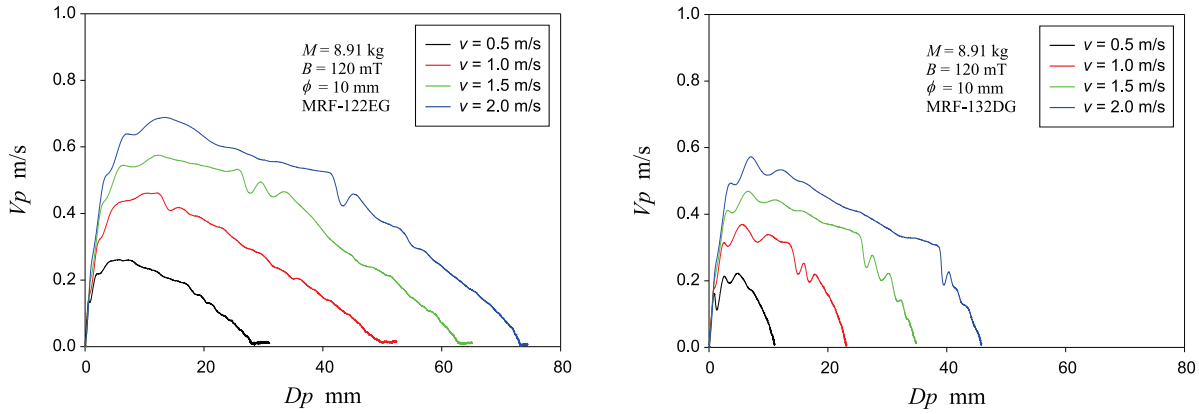

(a) MRF-122EG (b) MRF-132DG

Figure 3.31: Piston velocity vs. piston displacement of $M = 8.91$ kg of MRF-122EG (a) and MRF-132DG (b) at $B = 120$ mT

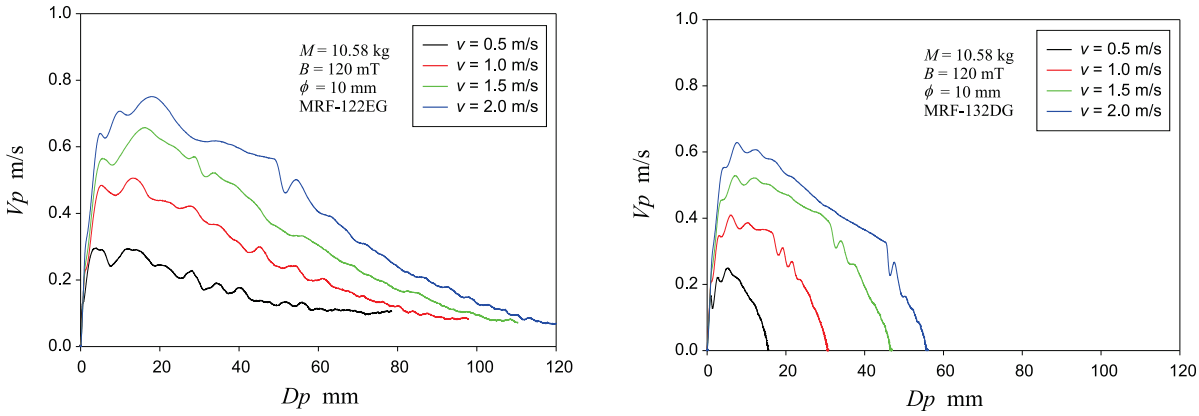

(a) MRF-122EG (b) MRF-132DG

Figure 3.32: Piston velocity vs. piston displacement of $M = 10.58$ kg of MRF-122EG (a) and MRF-132DG (b) at $B = 120$ mT

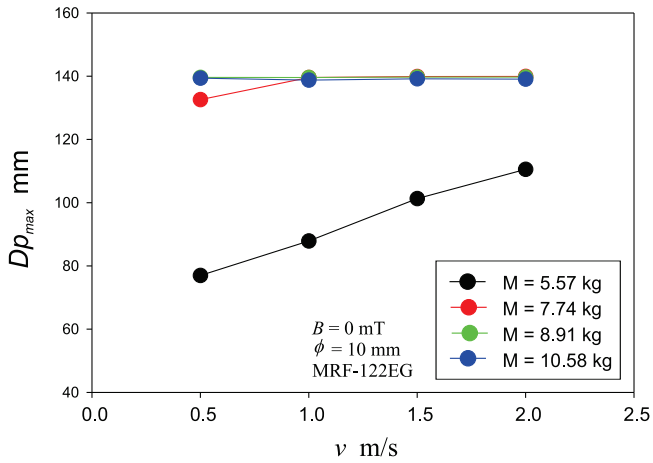

(a) MRF-122EG

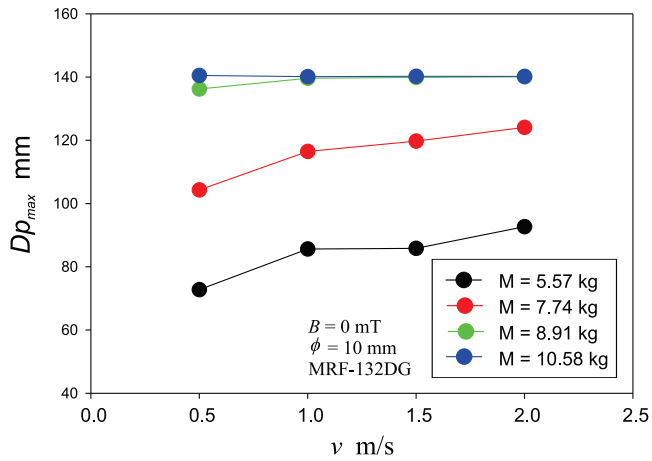

(b) MRF-132DG

Figure 3.33: Maximum piston displacement as function of v of MRF-122EG (a) and MRF-132DG (b) at $B = 0$ mT

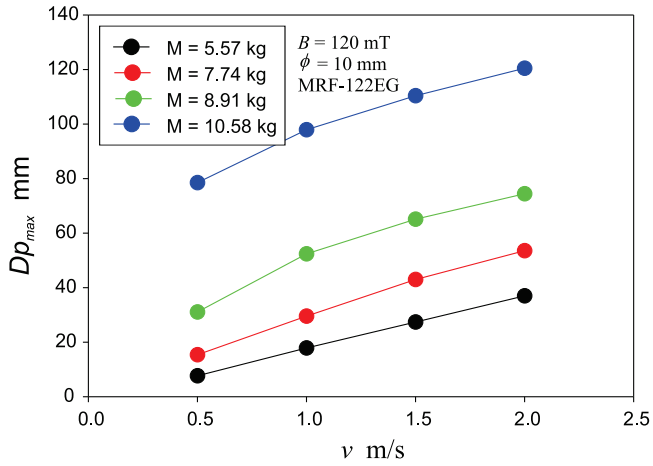

(a) MRF-122EG

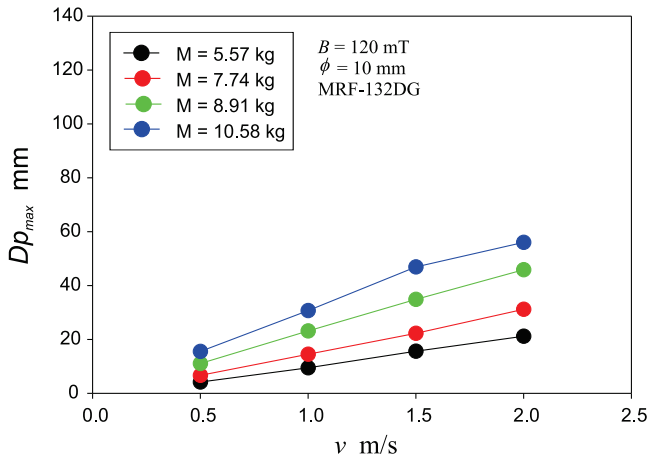

(b) MRF-132DG

Figure 3.34: Maximum piston displacement as function of v of MRF-122EG (a) and MRF-132DG (b) at $B = 120$ mT

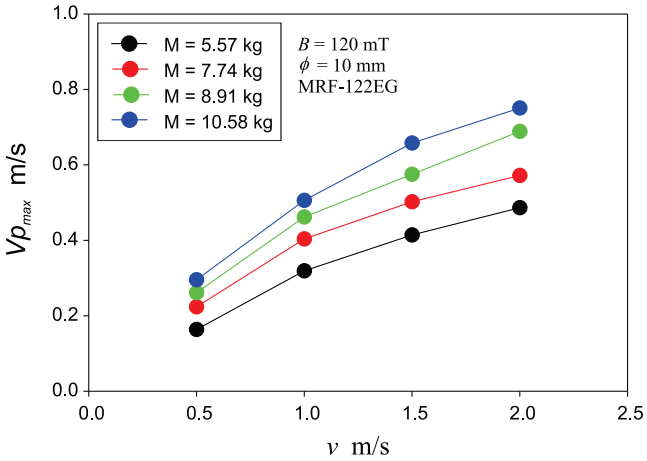

(a) MRF-122EG

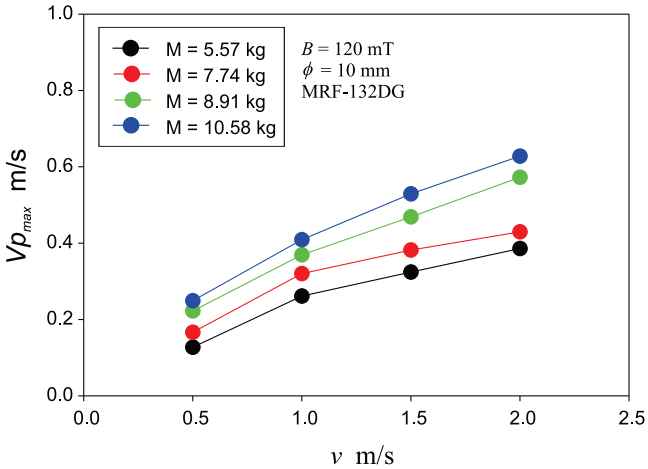

(b) MRF-132DG

Figure 3.35: Maximum piston velocity as function of v of MRF-122EG (a) and MRF-132DG (b) at $B = 120$ mT

3.3.2 Damping force

Figures 3.36 $\sim$ 3.39 show the damping force (F) over time (t) of MRF-122EG (a) and MRF-132DG (b) at B = 120 mT, v = 0.5 $\sim$ 2.0 m/s, M = 5.57 kg, 7.24 kg, 8.91 kg and 10.58 kg, respectively. From these figures, it can be observed that the peak value of damping force (F_{max}) increases at higher impact velocity for different MR fluids.

The value of F_{max} as the function of impact velocity of MRF-122EG (a) and MRF-132DG (b) is presented in Fig. 3.40. The value of F_{max} tends to increase at higher impact velocity for different MR fluids. The value of F_{max} of MRF-132DG is slightly higher than that value in MRF-122EG. The increasing value of F_{max} means that higher volume fraction of MR fluid (MRF-132DG) has the ability to resist more under shock loading. These results imply that volume fraction of MR fluid has significant effect on the resistance force of MR fluid under shock loading.

Moreover, the value of F_{max} also can be calculated using the Eq. (2.9). The measurement results from the laser displacement sensor such as piston velocity (Vp), impact velocity (v) and time (t) and also information of drop mass (M), total mass of MR fluid and the piston (m_{MR}) can be used to calculate the value of F_{max}. Figures 3.41(a) and 3.41(b) show comparison of the value of F_{max} of MRF-122EG (a) and MRF-132DG (b) at M = 10.58 kg and B = 0 mT. From these figures, the experiment results (data from the load cell) show slightly higher than the calculation results. The difference might be caused by the applying of floating piston as shown in Fig. 2.1. The floating piston is applied to avoid MR fluid to flow out during the shock loading. The application of floating piston will give resistance force to the piston. Therefore the value of F_{max} from the load cell is higher than that from the calculation.

3.3.3 Pressure difference in the orifice

Figures 3.42 $\sim$ 3.45 show the value of pressure difference (ΔP) over time (t) of MRF-122EG (a) and MRF-132DG at B = 120 mT, v = 0.5 $\sim$ 2.0 m/s, M = 5.57 kg, 7.24 kg, 8.91 kg and 10.58 kg, respectively. From these figures, it can be observed that the value of ΔP is higher at higher impact velocity for different MR fluids.

The maximum value of pressure difference (ΔP_{max}) as the function of impact velocity of MRF-122EG (a) and MRF-132DG (b) is presented in Fig. 3.46. The value of ΔP_{max} tends to increase at higher impact velocity for different MR fluids. At light drop mass (M = 5.57 kg), it shows that the value of ΔP_{max} of MRF-132DG is slightly higher than that value in MRF-122EG. However, at heavier drop mass (M = 7.24 $\sim$ 10.91 kg), the value of ΔP_{max} is nearly similar for different MR fluids. These results imply that under heavy drop mass (M = 7.24 $\sim$ 10.91 kg), the effect of volume fraction of MR fluid becomes less significant to restrict the flow of MR fluid under shock loading.

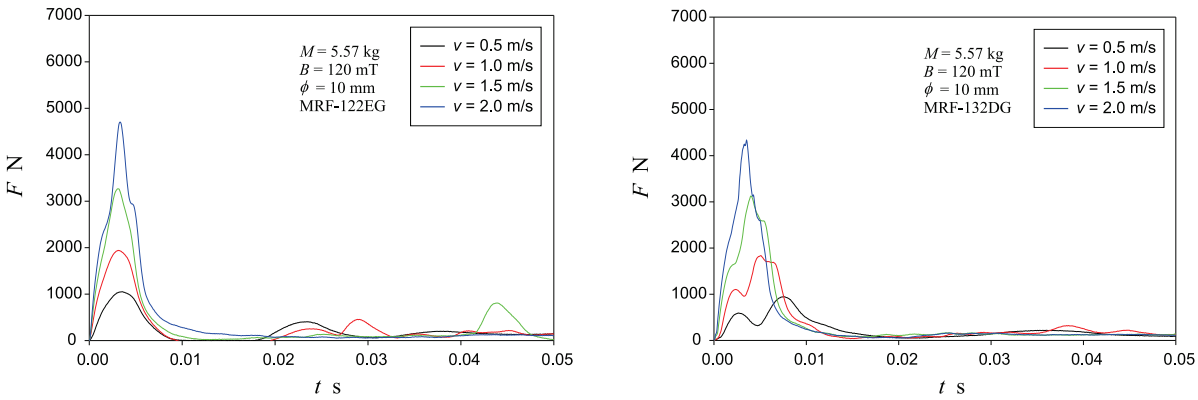

(a) MRF-122EG (b) MRF-132DG

Figure 3.36: Force vs. time of $M = 5.57$ kg of MRF-122EG (a) and MRF-132DG (b) at $B = 120$ mT

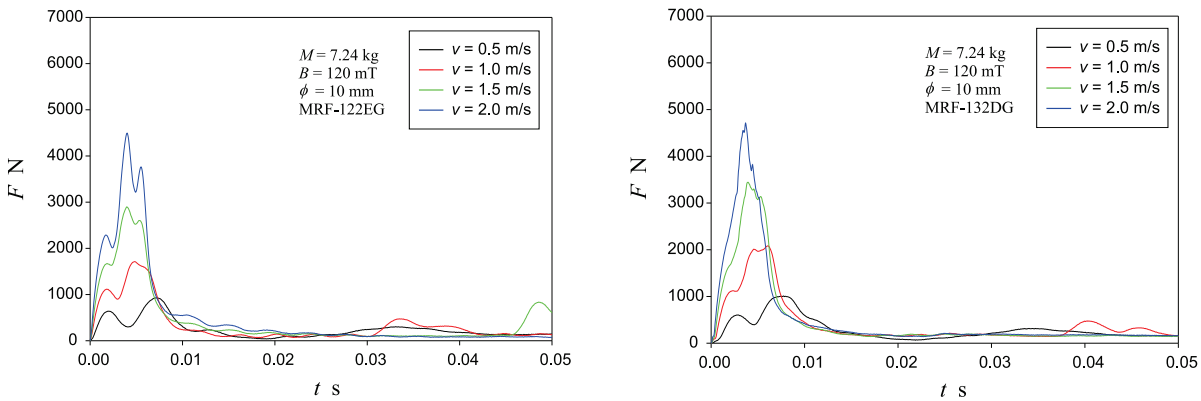

(a) MRF-122EG (b) MRF-132DG

Figure 3.37: Force vs. time of $M = 7.24$ kg of MRF-122EG (a) and MRF-132DG (b) at $B = 120$ mT

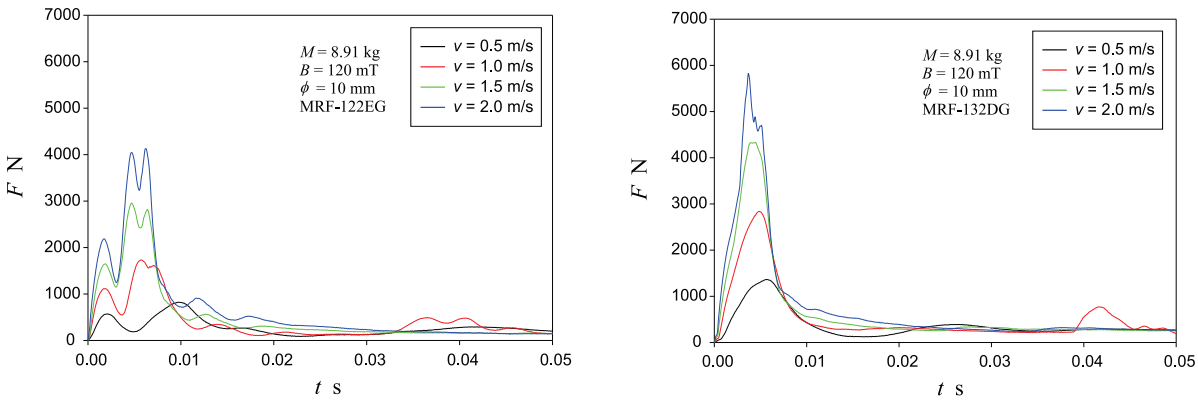

(a) MRF-122EG (b) MRF-132DG

Figure 3.38: Force vs. time of $M = 8.91$ kg of MRF-122EG (a) and MRF-132DG (b) at $B = 120$ mT

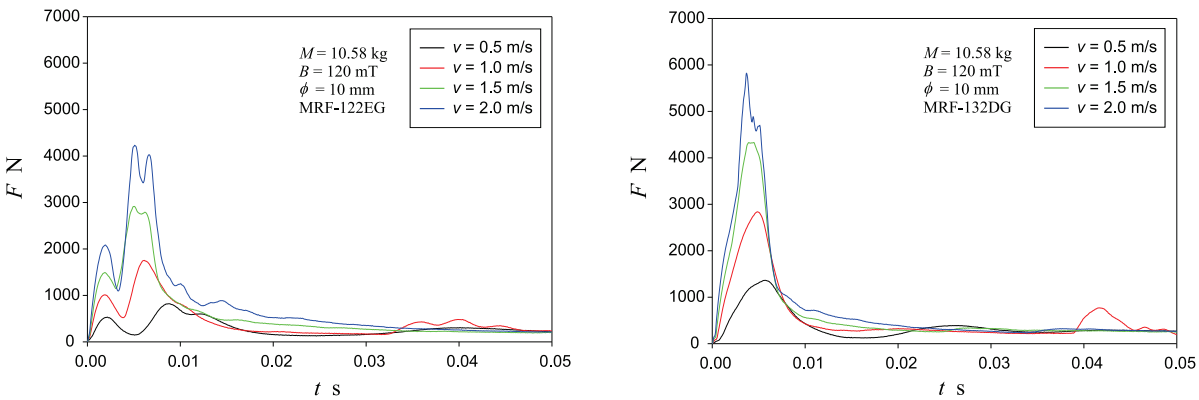

(a) MRF-122EG (b) MRF-132DG

Figure 3.39: Force vs. time of $M = 10.58$ kg of MRF-122EG (a) and MRF-132DG (b) at $B = 120$ mT

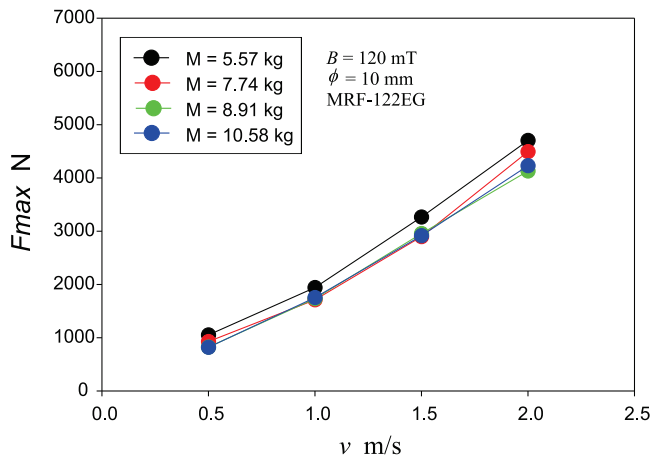

(a) MRF-122EG

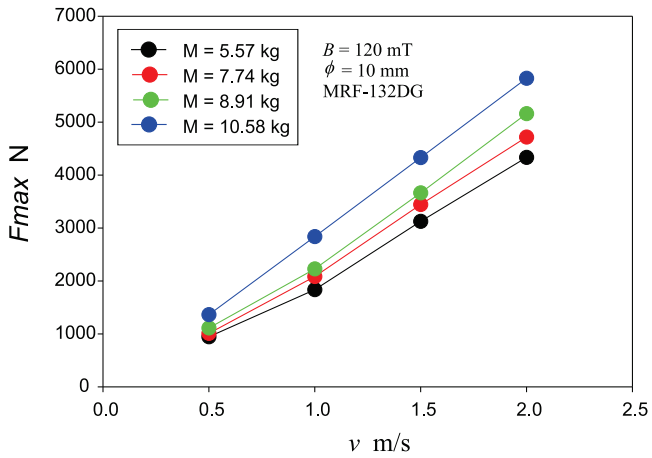

(b) MRF-132DG

Figure 3.40: Peak value of F as function of v of MRF-122EG (a) and MRF-132DG (b)at B = 120 mT

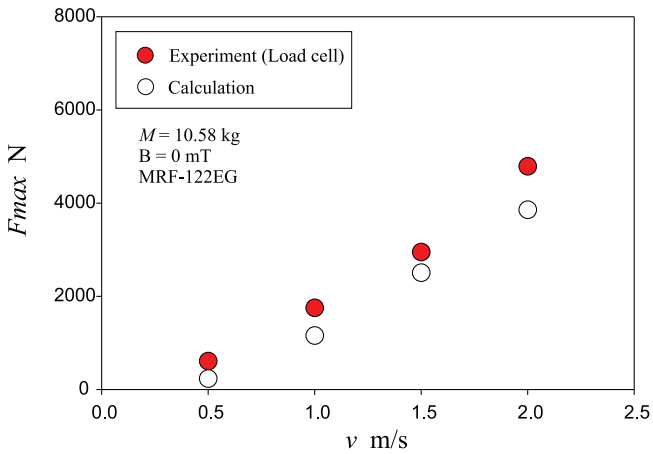

(a) MRF-122EG

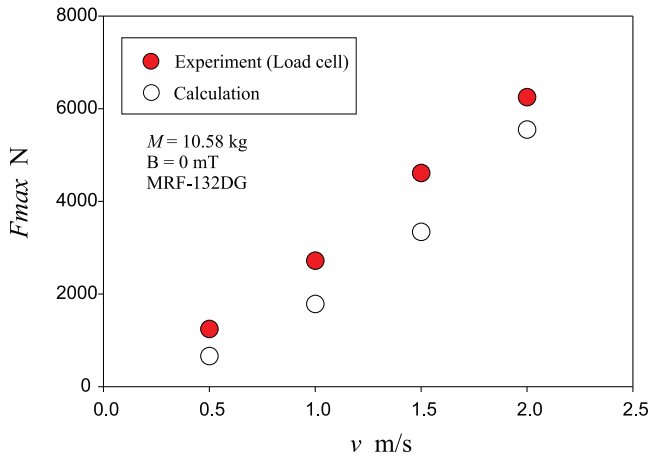

(b) MRF-132DG

Figure 3.41: Comparison of the peak value of F of MRF-122EG (a) and MRF-132DG (b) under $M = 10.58$ kg at $B = 0$ mT

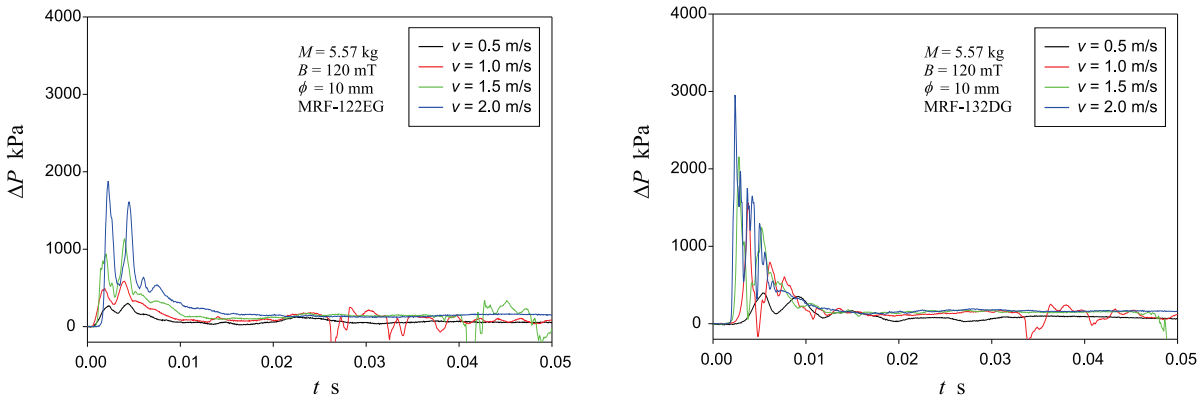

(a) MRF-122EG (b) MRF-132DG

Figure 3.42: Force vs. time of $M = 5.57$ kg of MRF-122EG (a) and MRF-132DG (b) at $B = 120$ mT

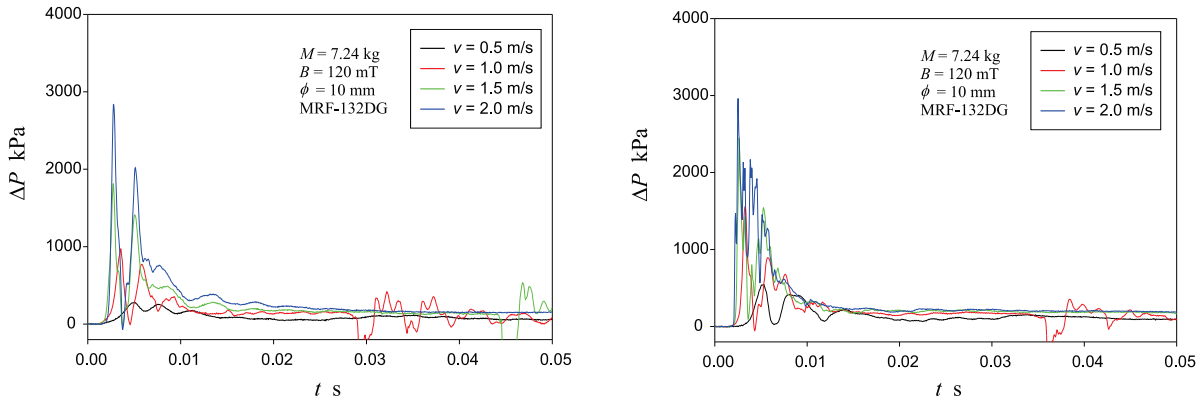

(a) MRF-122EG (b) MRF-132DG

Figure 3.43: Force vs. time of $M = 7.24$ kg of MRF-122EG (a) and MRF-132DG (b) at $B = 120$ mT

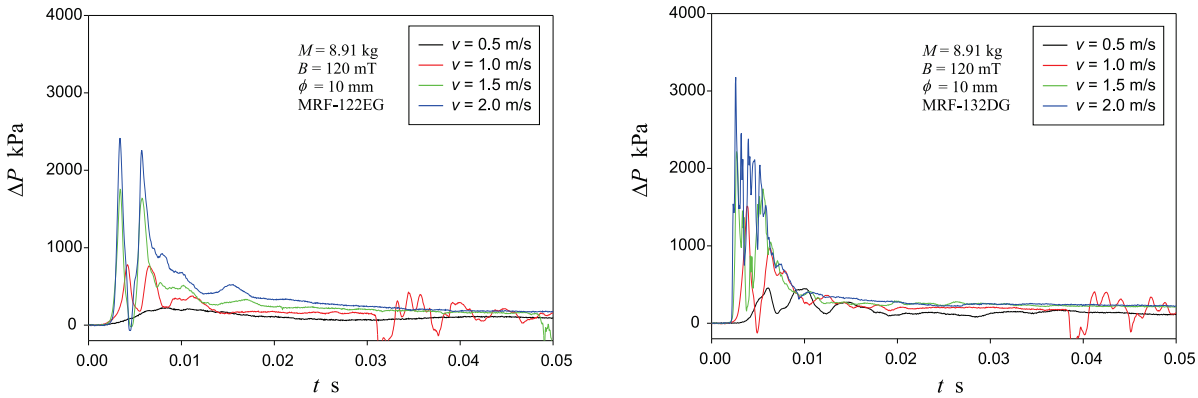

(a) MRF-122EG (b) MRF-132DG

Figure 3.44: Force vs. time of $M = 8.91$ kg of MRF-122EG (a) and MRF-132DG (b) at $B = 120$ mT

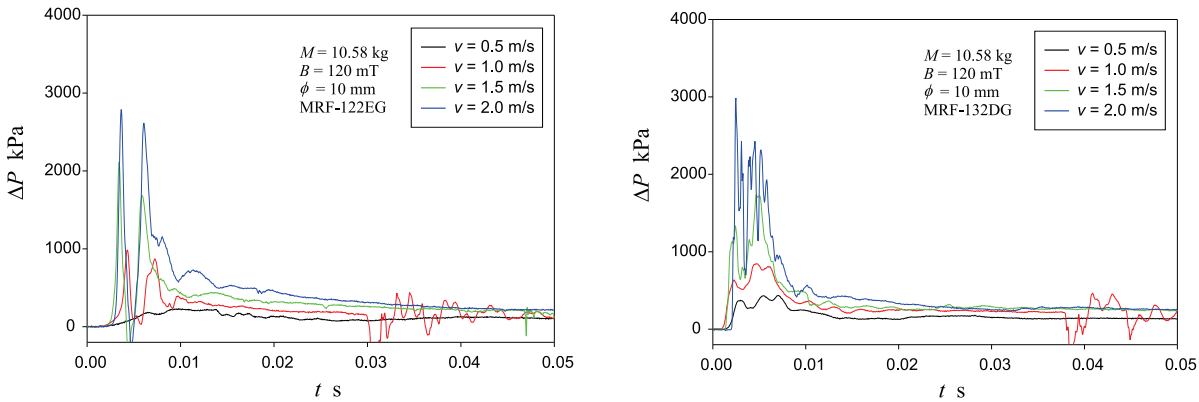

(a) MRF-122EG (b) MRF-132DG

Figure 3.45: Force vs. time of $M = 10.58$ kg of MRF-122EG (a) and MRF-132DG (b) at $B = 120$ mT

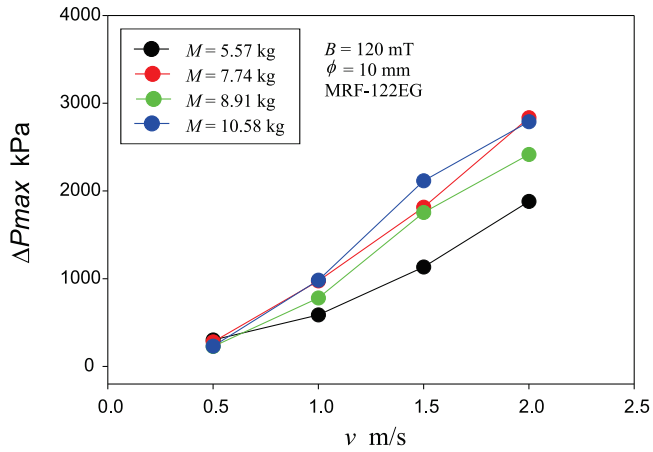

(a) MRF-122EG

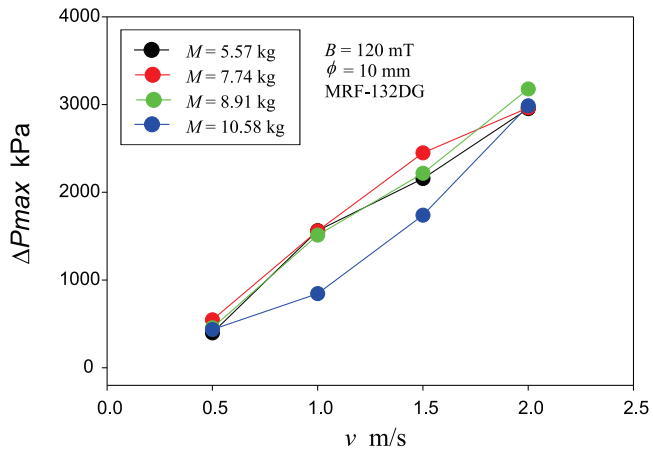

(b) MRF-132DG

Figure 3.46: Peak value of ΔP as function of v of MRF-122EG (a) and MRF-132DG (b) at B = 120 mT

Chapter 4

Ultrasonic propagation properties in MR fluid

The purpose of this chapter is to explain the ultrasonic propagation properties in MR fluid under AC and DC magnetic field. This chapter is divided into five sections. First section is the introduction which discusses about the previous studies of inner structure in magnetic and MR fluid under magnetic field. Some proposed theories and different experiment methods from previous researchers are discussed. Second section explains the experimental system and the measurement method in this study. Third section discusses the experiment results. The discussions are focused on the effects of various parameters such as temperature, elapsed time, magnetic field, magnetic field sweep rate and also hysteresis phenomenon on the change of ultrasonic propagation velocity and attenuation under DC magnetic field. Fourth section discusses the effect of frequency of AC magnetic field on the ultrasonic propagation velocity in MR fluid. Moreover, the hysteresis phenomenon for different frequency also is presented. The discussion in section third and section forth is intended to explain the relation between the change of ultrasonic propagation velocity and attenuation with the cluster formation in MR fluid under AC and DC magnetic field.

4.1 Introduction

Previous studies suggest that when an external magnetic field is applied to the magnetic and MR fluid, some of colloidal particles coagulate and form clusters. In order to analyze the inner structure in these fluids under magnetic field, some theoretical studies and experiment investigations have been conducted by several researchers.

Sano and Doi [109] proposed a simple mean field theory to analyze the formation of the agglomerates in magnetic fluid. They found that for some magnetic fluids, large agglomerates of magnetic particles are formed when a weak magnetic field is applied. They also observed that Van der Waals attraction between the particles enhances the agglomeration. Agglomeration of magnetic colloidal particles in magnetic fluid in thin film was also investigated by Taketomi et al. [110]. They derived a thermodynamical instability theory of the colloidal particles' dispersion. They found that the distribution of cluster formation in magnetic fluid is greatly influenced by

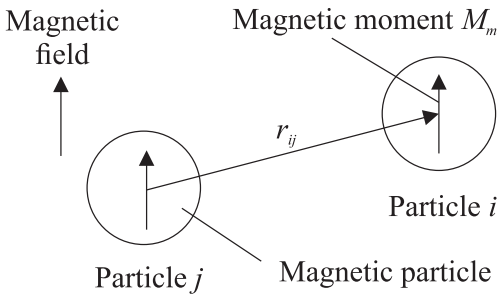

Figure 4.1: A magnetic moment between two particles in MR fluids under magnetic field [94]

the rate of the increasing magnetic field. The interval between the clusters becomes narrower with the increase of the rate of the field application.

Interaction of inner particles in MR fluid under magnetic field was presented by Lemaire et al. [111] and Bossis et al. [112]. A magnetic moment (M_m) of an isolated particle of relative magnetic permeability (μ_p) surrounded by a fluid of relative permeability (μ_f) in an external magnetic field (H) is presented by the following equation:

$$M_m = 4\pi\mu_0\mu_f\beta a^3 H \tag{4.1}$$

a is the radius of the particle, μ_0 is the permeability of vacuum and β is given by:

$$\beta = \frac{\mu_p - \mu_f}{\mu_p + 2\mu_f} \tag{4.2}$$

The interaction energy between two dipoles of moment M_m is given by [112]:

$$W = \frac{1}{4\pi\mu_0\mu_f}\left\{\frac{M_{m,i}M_{m,j}}{r^3} - \frac{3\left(M_{m,i}r\right)\left(M_{m,i}r\right)}{r^5}\right\} \tag{4.3}$$

r is the separation vector between the centers of the two particles. Figure 4.1 shows the magnetic moment between two particles in MR fluids under magnetic field [94]. The interaction energy is minimum when the two dipoles are aligned with r and maximum when they are perpendicular leading to a preferential aggregation as cluster formation aligned on the direction of the magnetic field.

The formation of aggregates of particles in MR fluid will depend on the ratio (λ) of the interaction energy to thermal energy (kT). The non-dimensional parameter λ is defined as [112]:

$$\lambda = \frac{1}{4\pi\mu_0\mu_f}\frac{M_m^2}{r^3}\frac{1}{kT} = \frac{\pi\mu_0\mu_f\beta^2 a^3 H^2}{2kT} \tag{4.4}$$

The value of λ commonly used to describe the strength of the induced magnetic interaction for two particles [113]. The higher value of λ means the interaction of two particles is stronger. The stronger interaction between two particles means that the particles in MR fluid can form a bigger cluster. From Eq. (4.4), the effect of external magnetic field (H) and temperature (T) on the cluster formation in MR fluid can be analyzed.

Some researchers also conducted theoretical approach of ultrasonic propagation properties in magnetic fluid. Parsons [114] proposed a simple linearized hydrodynamical theory for magnetic

fluids in the presence of a strong external magnetic field. He defined the ultrasonic propagation velocity (v) as

$$v = v_0 \left(1 + \Delta\right) \tag{4.5}$$

The change of sound propagation speed Δ is given by:

$$\Delta = C_0 \left(\frac{\lambda^{*2}}{8}\right) \left(\frac{\gamma_1 \omega}{\rho_0 v_0^2}\right) \left(1 - \frac{\omega^2}{\omega_C^2}\right) \left[\frac{\omega \tau_t}{\left\{\left(1 - \frac{\omega^2}{\omega_C^2}\right)^2 + \omega^2 \tau_t^2\right\}}\right] \sin^2 2\theta \tag{4.6}$$

Where C_0 is the concentration of magnetic particles, $\tau_t = \gamma_1 / m_0 H$ is the relaxation time and $\omega_C = (m_0 H / I_m)^{1/2}$ is the natural frequency for the orientation fluctuations. I_m is the moment of inertia density for the grains. $\lambda^* = \gamma_2/\gamma_1$ with $\gamma_1 = (\alpha_2 - \alpha_3)/C_0$ and $\gamma_2 = (\alpha_2 + \alpha_3)/C_0$ [114]. α_2 and α_3 are reversed in the notation of Leslie [115]. From Eq. 4.6, the sound propagation velocity is depends on the magnetic field (H) and the angle θ between the propagation direction and field direction. The change is related with the liquid and solid phase transitions of the grains in magnetic fluid under magnetic field [114].

Gotoh et al. [116] and Gotoh and Chung [117] derived expression of the attenuation from the ferrohydrodynamical equation of Tarapov et al. [118]. They analyzed theoretically and experimentally the ultrasonic propagation attenuation as a function of the magnetic field strength and the angle θ. Their results showed that qualitative agreement between the presented theory and experiment result is fairly good. Taketomi [119] also calculated ultrasonic propagation attenuation coefficient in the magnetic fluid using liquid crystal theory. They found that the value of sound attenuation coefficient under an external magnetic field varies with the angle θ between the field and ultrasonic propagation attenuation. They observed that this phenomenon was interpreted in terms of cluster formation besides the rotation of the individual particles in magnetic fluid.

Nahmad-Molinari et al. [120] applied Wood's effective medium theory to observe the predicted of sound propagation velocity (v) when no magnetic field is applied ($B = 0$ mT). The sound propagation velocity as a function of metal concentration is given by:

$$v = \sqrt{\frac{\beta_e}{\rho}} \tag{4.7}$$

where ρ and β_e are the volume averaged density and the average elastic modulus of medium respectively.

$$\rho = \Phi \rho_s + \left(1 - \Phi\right) \rho_f \tag{4.8}$$

$$\frac{1}{\beta_e} = \frac{\Phi}{\beta_s} + \left(1 - \Phi\right) \frac{1}{\beta_f} \tag{4.9}$$

Φ is the volume metal concentration and s and f stand for solid and fluid, respectively.

Several researchers also conducted simulation of inner structure in magnetic fluid [121, 122, 123] and MR fluid [124] under magnetic field. Kruse et al. [121] reported a Monte Carlo investigation of the microstructure of magnetic fluid. They observed agglomerates consisting mainly

of a small number of particles. The larger the particle radius, the agglomeration probability is higher. In addition, small particles (radius smaller than 5 nm) also take part in the cluster formation. On the application of external magnetic field, the agglomerates become elongated due to a rearrangement of the particles and orient themselves parallel to the field lines. They presented a statistical evaluation of agglomeration degree, cluster sizes, and cluster composition (sizes of clustered particles) as well as of the field-dependent change of microstructure (orientation and shape anisometry of clusters). Kantorovich et al. [122] developed a new analytical density functional model of magnetic fluid monolayers. They compared the analytical with the simulation results. The system under study consisted of soft sphere magnetic particles confined to a thin fluid layer. Using a combination of analytical density functional theory and molecular dynamics (MD) simulations, they found that the majority of aggregates in magnetic fluid are divided into two types: chains and rings. They also observed that the sizes and area fractions are strongly influenced by the geometrical constraints. Ido et al. [123] performed numerical simulations of the distribution of suspended particles in a magnetic fluid in the presence of a magnetic field. They found that magnetization in the presence of a magnetic field caused micrometer-sized magnetic particles and nonmagnetic particles to interact with each other. Ido et al. [124] also conducted simulation based on the simplified Stokesian dynamics method of microstructure formation of magnetic particles and nonmagnetic particles in MR fluid. They simulated various ordering processes and microstructure formation of both magnetic particles and non-magnetic particles in MR fluids. They found that non-magnetic particles are rearranged in the field direction when diameter of the spherical non-magnetic particles is slightly smaller than the diameter of the spherical magnetic particles.

Several experiment methods have been proposed by researchers in order to investigate inner structure in magnetic and MR fluid.

Optical visualization

Several researchers applied optical visualization technique to visualize and to observe the inner structure of magnetic and MR fluid with and without magnetic field. Cernak [125], Cernak and Macko [126] and Cernak et al. [127] investigated needle-like macro-clusters, including the full areal density and the average length of macro-clusters as well as macro-cluster length distribution as functions of the time in a magnetic field thin layer using an optical microscope. They analyzed cluster aggregation both under instantaneously and slowly applied magnetic fields. They found that some parameters describing the microscopic observations such as the number, size and mutual ordering of macro-clusters are dependent on the magnetic field history.

Sawada et al. [128] used optical method with light scattering system to investigate the influence of magnetic field intensity on the cluster formation of ferromagnetic and non-magnetic particles in magnetic fluid. They observed that the length of cluster formation in water-based magnetic fluid becomes larger when higher magnetic field ($B = 59$ mT) was applied. Jeyadevan and Nakatani [129] also used Rayleigh light scattering technique to investigate the influence of the solid fraction content and the influence of magnetic field strength on the cluster formation in ionic and water-based magnetic fluid. They applied Rayleigh light scattering technique which

has advantage for detecting objects smaller than the resolution limit of the optical column. They observed that the growth and disintegration of the cluster in both ionic and water-based magnetic fluids are different under zero and applied magnetic field. Gans et al. [130] applied a microscope to visualize the microstructure of the magnetic fluid in the absence as well as, in the presence of a magnetic field. The maximum applicable field strength was 40 kA/m. They found that the chain-like structure in magnetic fluid is formed almost instantaneously when magnetic field is applied to the magnetic fluid. They also observed that these chains are directed along the field lines of the magnetic field. Hagenbuchle and Liu [113] studied experimentally the basic of structure formation in MR fluid which consists of chain formation and chain dynamic using dynamic light scattering. They found that the motion of chains can be described by two processes: the translational diffusion of straight chains as a whole and the internal motion of chains, i.e., chain fluctuations. They claimed that the change of the translational diffusion coefficient with time directly reflects the growth of the chains. Bramantya et al. [131] applied optical microscope and CCD camera to analyze the inner structure of MR fluid. They claimed that the cluster formation in MR fluid was clearly seen. Their results showed that the rate of cluster formation in MR fluid increases with the increasing of the strength of magnetic field. However, their method has limitation to obtain the optimum thickness of gap between prepared glass in order to achieve one layer examined area.

Sedimentation measurement

López–López et al. [132] proposed a new method by measuring the change in the electromotive force induced in a sensing coil which was placed around the MR fluid. The sedimentation of the MR fluid generates a decrease in the local particle concentration inside the coil. Moreover, the magnetic permeability also decreases. Their method can be used to analyze the effect of the magnetite volume fraction on the stability of the MR fluid.

Ultrasonic propagation measurement

Several researchers have applied the ultrasonic technique to analyze clustering structures in magnetic fluid and MR fluid by measuring the ultrasonic propagation properties. Some aspects on the influence of applied time and the strength of magnetic field on ultrasonic propagation properties in magnetic fluid [133, 134, 135], in MR fluid [92, 136, 137] and comparison between these fluids [95, 138, 139] and in another phenomenon such as anisotropic [140, 141] and hysteresis [142, 143] in magnetic fluid and MR fluid were studied. The ultrasonic technique has been applied to analyze opaque fluids, such as magnetic fluid and MR fluid. Moreover, compare to the optical observation technique, the ultrasonic techniques are especially advantageous when the number of particles is high [92]. The properties of ultrasonic propagation, such as propagation velocity and attenuation, change when clustering structures formed in magnetic and MR fluids [93]. Basically, the ultrasonic propagation velocity in solid part is higher than that in liquid part. Therefore, the cluster formation in magnetic fluid and MR fluid as the effect of the application of magnetic field can be analyzed by measuring the change of ultrasonic propagation velocity.

The change of ultrasonic propagation velocity can be used to explain the inner structure in

magnetic and MR fluid in the presence of magnetic field. In the opposite, the change of ultrasonic propagation attenuation in MR fluid is rarely known. Due to this reason, a research to measure ultrasonic propagation attenuation in MR fluid under a uniform magnetic field is conducted. Experiments are performed to measure the temperature and elapsed time dependence, the effects of applying a magnetic field and hysteresis phenomenon [145].

The effect of the magnetic field sweep rate on the magnetic fluid was thoroughly investigated by several researchers [144, 146]. Józefczak et al. [146] reported that the ultrasonic propagation velocity changed as a function of magnetic field intensity, magnetic field sweep rate and the temperature of the magnetic fluid. In addition, Motozawa and Sawada [138] investigated experimentally cluster growth in MR fluid and magnetic fluid. They applied different magnetic field sweep rates. They reported that cluster growth in magnetic fluid was affected by the magnetic field sweep rate. However, the effect of the magnetic field sweep rates on cluster formation in MR fluid is still not clear. Therefore, experiments by applying different magnetic field sweep rates to different MR fluids are conducted [147].

4.2 Experimental apparatus

A block diagram of the experimental apparatus is illustrated in Fig. 4.2. The MR fluid is placed in a rectangular container inside the test cell. Two ultrasonic transducer are attached to the opposite sides of the inner rectangular container; one acted as a transmitter and the other as a receiver. The transducer made of a piezoelectric ceramic material. A piezoelectric ceramic material is a polycrystal ceramic made by compressing a high purity powder (titanium oxide, barium oxide, etc.) and firing it at a high temperature. Because the materials inside the transducer are not categorized as ferromagnetic materials, the application of magnetic field has no significant effect on the performance of transducer. Sensitivity and the operating temperature unit of the transducer are -23 dB and 5 °C – 45 °C, respectively.

One ceramic oscillator is connected to a digital oscilloscope and the other oscillator is connected to a pulse generator. The pulse generator generates burst wave and triggers signal synchronously. The ultrasonic wave is transmitted to the ceramic oscillator in the test cell. Then, the ultrasonic wave propagates between the ceramic oscillators. These transmitter-receiver operates due to the trigger signal from the I/O board. A/D board will receive the transmitter signal after being spread inside the test cell. The signal wave inside the test fluid can be shown from digital oscilloscope. From the waveform, propagation delay time and distance between the oscillators can be measured. From these values, ultrasonic propagation velocity in the test fluid inside test cell can be calculated. Data from the digital oscilloscope is transferred through a GPIB (General Purpose Interface Bus) cable to the computer. Visual programming language, called LabVIEW from National Instrument is applied to analyze the measurement data. Figure 4.3 shows the front panel of the developed LabVIEW program.

Since temperature has significant effect to the cluster formation in MR fluid, the temperature of the test fluid should be maintained constant. The temperature of the test fluid is controlled by circulating water from temperature control unit to the cylindrical container. A thermistor is used to measure temperature of the test fluid inside the test cell.

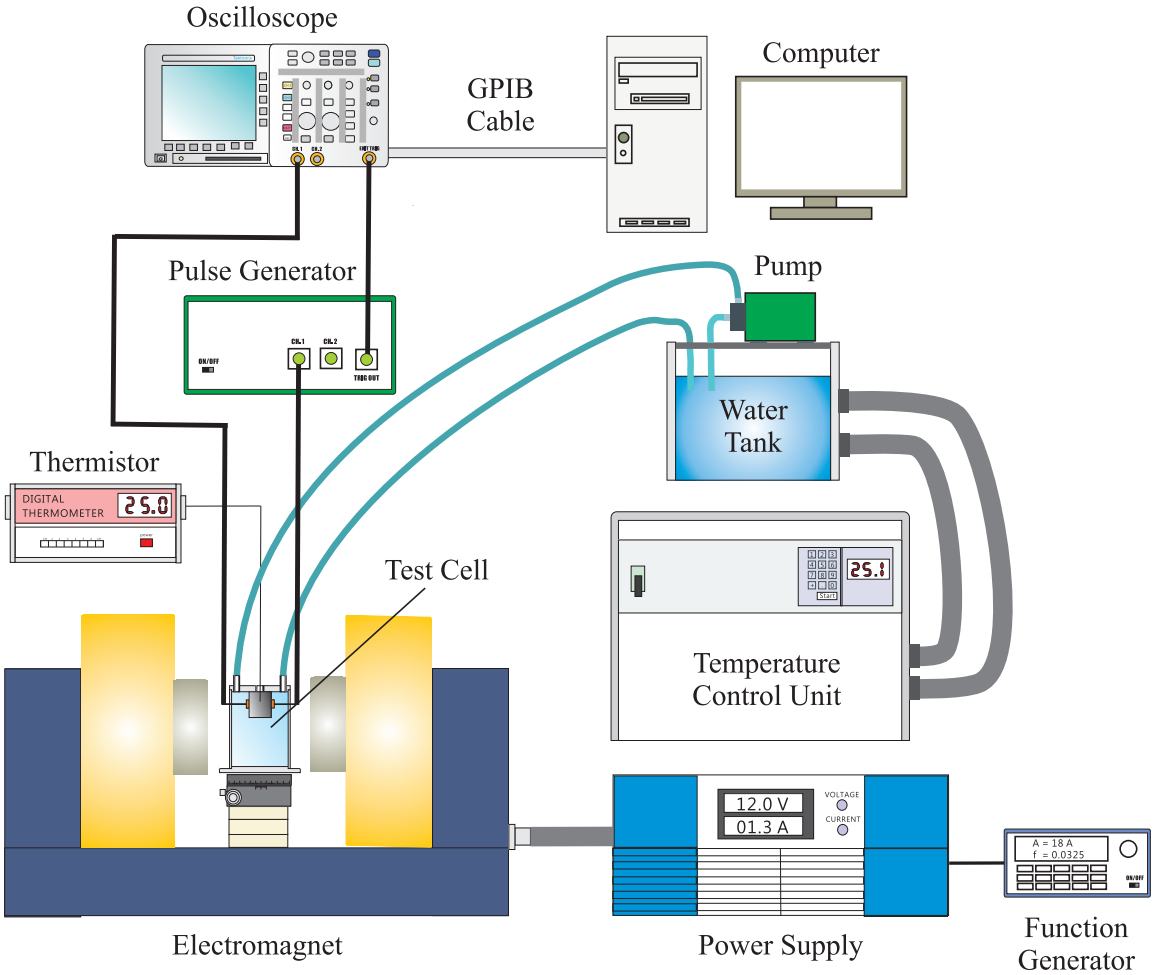

Figure 4.2: Experimental apparatus of ultrasonic propagation properties in MR fluid

DC power supply supplies electric current from 0 – 20 A. This current generates magnetic flux density from 0 to 450 mT. In this experiment, different function of magnetic field sweep rate is needed. Therefore, a function generator is applied to produce sweep rate function. General specification of the devices in this experiment is given in Table 4.1.

Table 4.1: General specification of the experimental devices

No	Name	Model	Manufacturer	Function
1	Pulse generator	n/a	Honda Electrics	Generate ultrasonic wave
2	Oscilloscope	TDS3012B	Tektronix	Visualize ultrasonic propagation wave
3	GPIB cable	DDK408JE	National Instruments	Transfer digital data from oscilloscope to computer
4	Electromagnet	n/a	n/a	Generate magnetic field
5	Power supply	PAD110-20LA	Kikusui	Supply electric current to electromagnet
6	Function generator	WF1943B	NF	Create different function of electric current in power supply
7	Temperature control unit	CTE82A	Yamato-Komatsu	Control the temperature of test fluid
8	Pump	14NSP53	Ebara	Circulate water from temperature control unit to test cell
9	Thermistor	D226	Takara	Display temperature of the test fluid

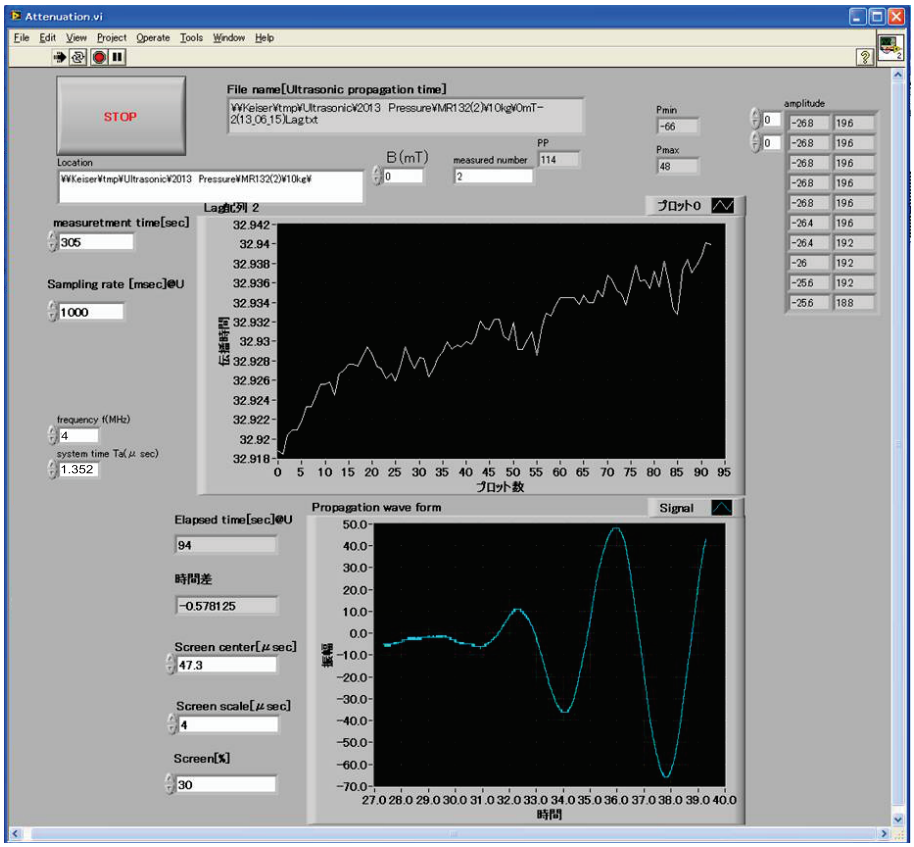

Figure 4.3: Front panel of LabVIEW program for measuring the ultrasonic propagation properties

4.2.1 Test cell

In this study, two different test cells (test cell A and B) are developed. The difference between the two test cell is the ultrasonic frequency (f) and the distance between the oscillators (L). Table 4.2 describes the difference between test cell A and B.

Details of the test cells are illustrated in Fig. 4.4. The test cell is made from transparent acrylic. The test cell consists of two containers, which are cylindrical container and rectangular container. The cylindrical container is filled with circulating water surrounded it. This circulating water is used to control the temperature of the test fluid. Test fluid or MR fluid is placed inside the rectangular container. In the container, aluminum plates are used as heat conduction to keep temperature of MR fluid satisfactory. The thickness of acrylic and aluminum plates is 2 mm.

Table 4.2: The difference between test cell A and B

Parameter	Test cell A	Test cell B
Ultrasonic frequency	2 MHz	4 MHz
Distance between two oscillators	32 mm	15 mm

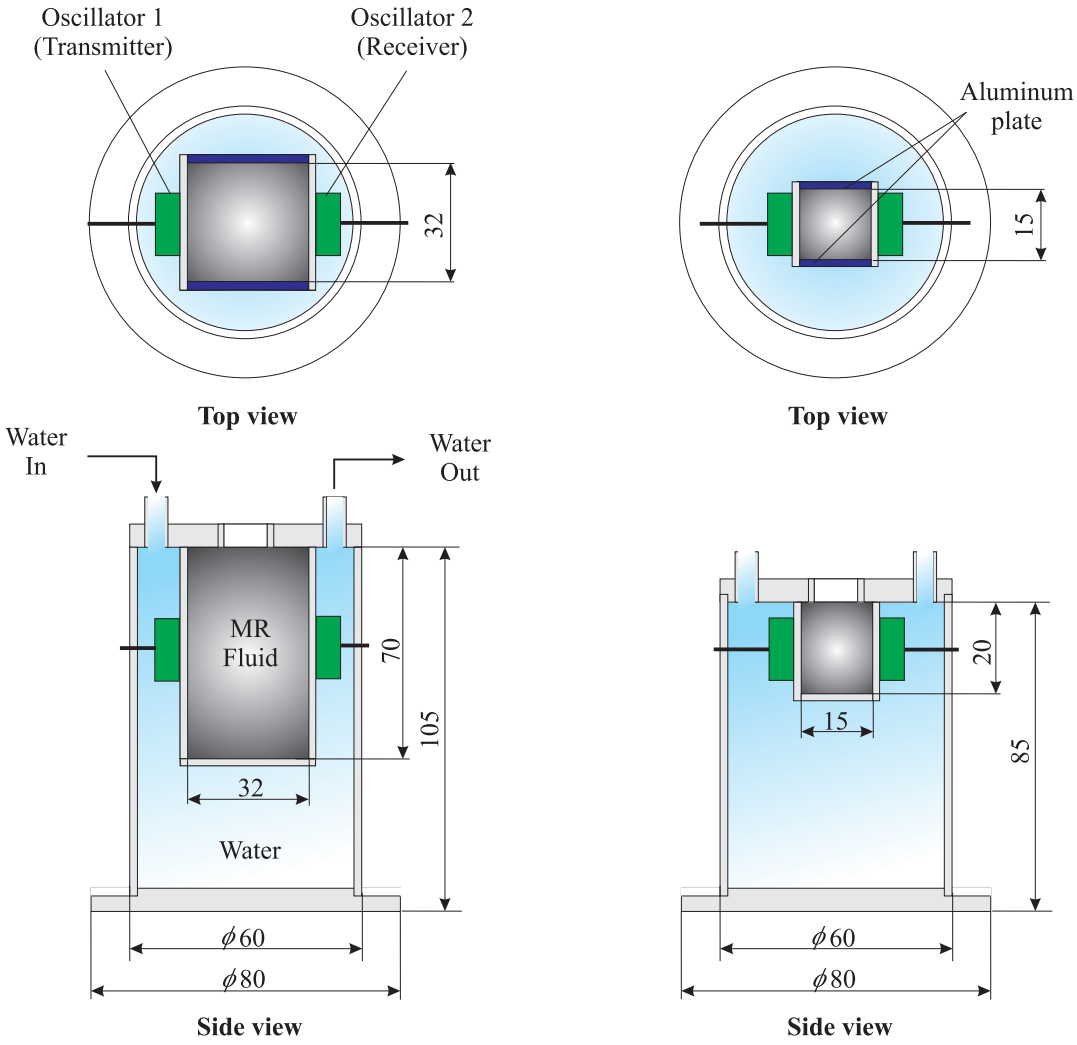

(a) Test cell A (b) Test cell B

Figure 4.4: Test cell A (f = 2 MHz) and B (f = 4 MHz)

4.2.2 Electromagnet

A set of electromagnet is used to generate magnetic field to the test fluid inside the test cell. Electric current in the electromagnet is supplied by a DC power supply. Figure 4.5 shows the picture of the power supply.

Distribution of magnetic flux density

In order to know the relation between magnetic flux density and electric current from power supply, measurement of magnetic field distribution is necessary. Figure 4.6 shows the measurement area between the pole piece of the electromagnet. The distance is between the pole is 70.0 mm. The measurements are conducted by using Gauss meter. Figure 4.7 shows the relation between magnetic flux density and electric current from power supply. The value of magnetic flux density is measured in center point of the pole piece. Power supply can supply electric current from 0 – 20 A. Maximum value of magnetic flux density that generated from electromagnet is 450 mT.

Figures 4.8 and 4.9 show the distribution of magnetic flux density along x direction and y direction. The measurements are conducted by applying three different electric currents, which are 2, 5 and 8 A. The length of rectangular container in the test cell A and test cell B along x direction are 15 mm and 32 mm, respectively. From Figs. 4.8 and 4.9, it can be observed that the distribution of magnetic field at test section area is nearly uniform.

Figure 4.5: Electromagnet (left) and power supply (right)

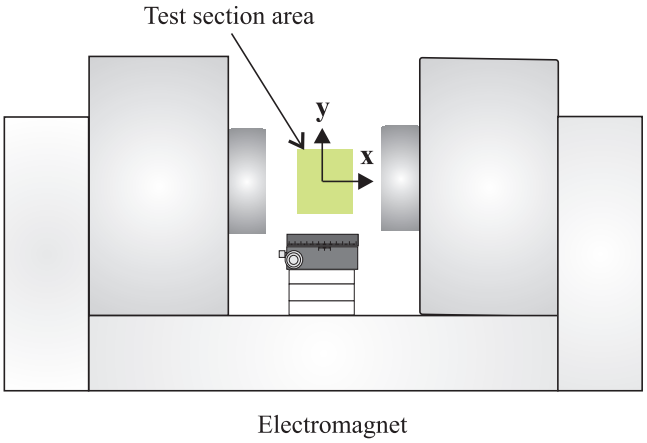

Figure 4.6: Measurement area of magnetic field distribution

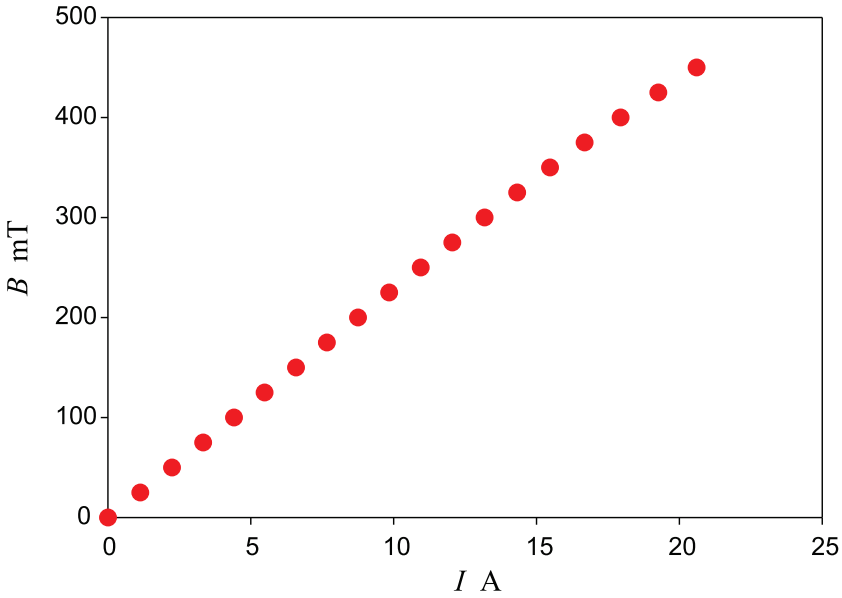

Figure 4.7: Value of DC magnetic flux density as function of electric current

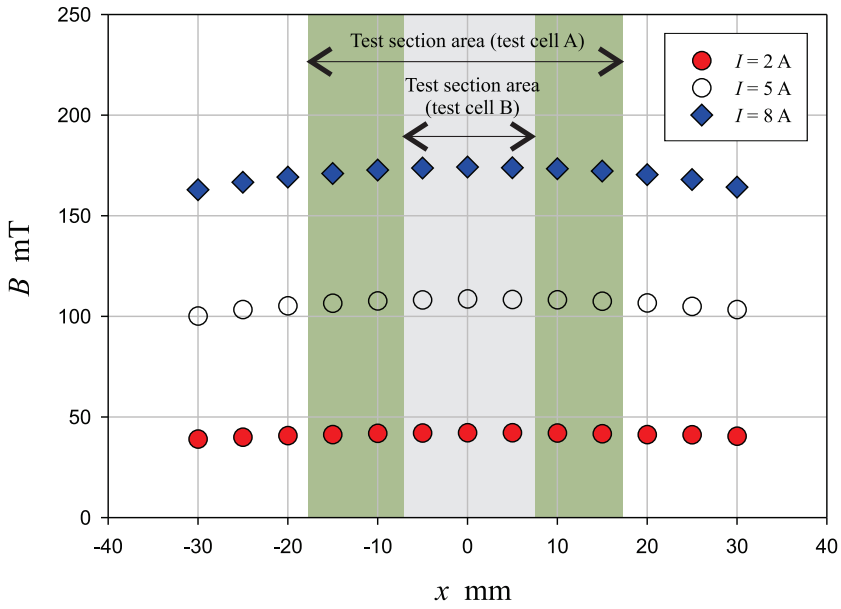

Figure 4.8: Distribution of magnetic flux density in x direction

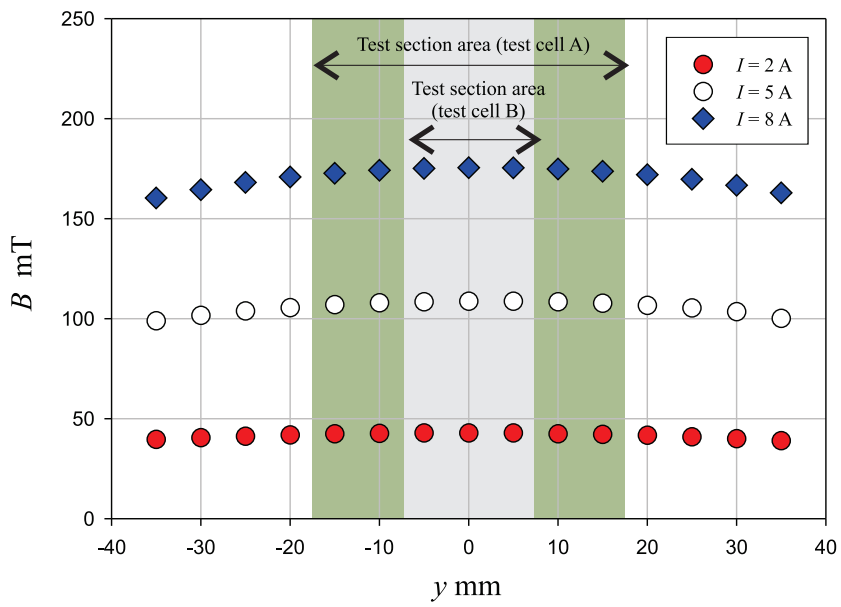

Figure 4.9: Distribution of magnetic flux density in y direction

4.3 Measurement method and experimental system

In this experiment, ultrasonic propagation properties, which consists of ultrasonic propagation velocity and ultrasonic propagation attenuation, are measured.

4.3.1 Ultrasonic propagation velocity

Ultrasonic propagation velocity is calculated based on the ultrasonic propagation time and distance between the two oscillators. Figure 4.10 illustrates ultrasonic wave propagation between two oscillators in the test cell. If L is distance between two oscillators and t is propagation time through the test fluid inside the test cell, ultrasonic propagation velocity (V) can be calculated using equation below:

$$V = \frac{L}{t} \tag{4.10}$$

Non dimensional parameter for the change value of ultrasonic propagation velocity is also developed. This value describes the difference between initial condition and condition when magnetic field is applied. If V and V_o are the ultrasonic propagation velocity with and without magnetic field, respectively, then the value of change of ultrasonic propagation velocity (Δ V/V_o) is calculated using equation below:

$$\begin{aligned} \frac{\Delta V}{V_o} &= \frac{V - V_o}{V_o} \\ &= \frac{L/t - L/t_o}{L/t_o} \\ &= \frac{t_o - t}{t} \end{aligned} \tag{4.11}$$

In assembling process of the acrylic plate and aluminum plate, some errors are likely to happen. The real value of L could be not exactly 32 mm in test cell A or 15 mm in test cell B. The real value of L can be measured by comparing the measurement results of ultrasonic propagation velocity in pure water with the other measurement results from other researcher. In this case, the measurement results are compared with experiment result from Grosso and Mader [148].

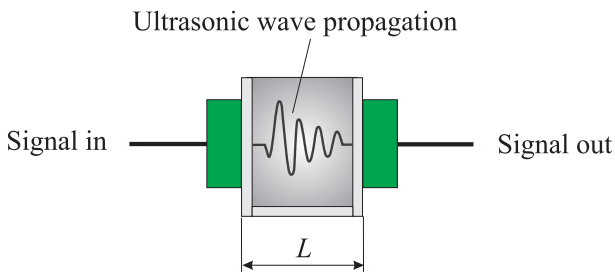

Figure 4.10: Ultrasonic wave propagation between two oscillators

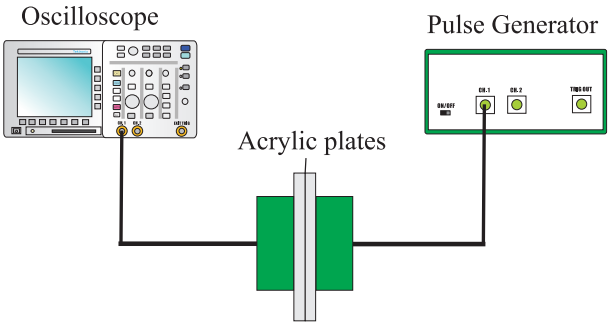

Figure 4.11: Experimental apparatus to measure T_s

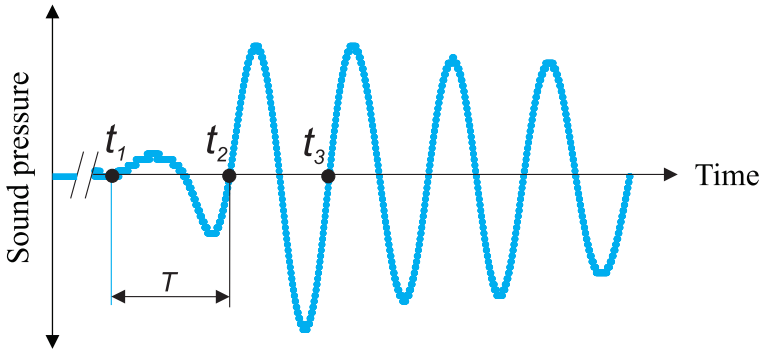

Figure 4.12: Reference points in the ultrasonic wave

In order to measure the ultrasonic propagation velocity, propagation time from the experiment system (T_s) is necessary. A simple experiments are conducted to measure the value of T_s. Figure 4.11 shows the experimental apparatus of the measurement. Two oscillators is glued to the acrylic plates. One oscillator is connected to pulse generator, while other oscillator is connected to oscilloscope.

The average value of T_s can be measured from the oscilloscope. The ultrasonic waveform that shown in the oscilloscope is illustrated in Fig. 4.12. In this measurement, three reference points in the ultrasonic wave are selected.

1. Point 1 describes the first detected signal in the oscillator.
2. Point 2 describes the traveled of one wavelength of ultrasonic wave.
3. Point 3 describes the traveled of two wavelengths of ultrasonic wave.

Tables 4.3 and 4.4 show the measurement results of the selected three reference points of test cell A and test cell B, respectively. From these measurement results, average value of T_s,

Table 4.3: Measurement result of the selected of three reference points of test cell A

No	t_1 (μs)	t_2 (μs)	t_3 (μs)	t_2-t_1(μs)	t_3-t_2(μs)
1	1.700	2.243	2.722	0.543	0.479
2	1.702	2.241	2.719	0.538	0.478
3	1.700	2.240	2.717	0.540	0.476

Table 4.4: Measurement result of the selected of three reference points of test cell B

No	t_1 (μs)	t_2 (μs)	t_3 (μs)	t_2-t_1(μs)	t_3-t_2(μs)
1	1.594	1.835	2.068	0.241	0.233
2	1.588	1.829	2.061	0.241	0.233
3	1.584	1.826	2.058	0.242	0.232

the average value of one wavelength and the measurement error can be calculated. The averages value of one wavelength (T_m) of test cell A and test cell B are calculated from the average value of t_2-t_1 and t_3-t_2 of three number of measurements using the equation as follows;

$$T_m = \sum_{i=1}^{2n} \frac{(t_2 - t_1)_i + (t_3 - t_2)_i}{2n} \tag{4.12}$$

The value of T_m of test cell A and test cell B are 0.509 μs and 0.237 μs, respectively. The ideal value of one wavelength (T_i) for the frequency 2 MHz and 4 MHz is 0.5 μs and 0.25 μs, respectively. From the measurement result and the ideal value, the value of measurement error (Er) can be calculated using equation below:

$$Er = \frac{T_i - T_m}{T_i} \times 100\ \% \tag{4.13}$$

By using the above equation, the measurement error in test cell A and B are 1.84 % and 5.23 %, respectively. The value of T_s is calculated by subtracting the average value of t_1 with the average value of T_m.

$$T_s = \bar{t_1} - T_m \tag{4.14}$$

The value of T_s in test cell A and test cell B are 1.192 μs and 1.352 μs, respectively. These values are necessary to measure the ultrasonic propagation velocity. The real value of ultrasonic propagation time in test fluid is obtained by subtracting the measurement result of ultrasonic propagation time with T_s.

In order to compare the result with Grosso and Mader's measurement results, experiments using pure water are conducted. Experiments are conducted by changing the temperature of the test fluid from 18 °C to 32 °C. Figures 4.13 and 4.14 show the measurement results. The black circle represents current measurement results, while the red line represents the measurement data from Grosso and Mader. After adjusting the distance (L), new measurement results is obtained. The approximation results is represented by white circle. In test cell A, the real distance of test cell is 32.32 mm which longer from the design (32 mm). While in test cell B, the real distance of test cell is 15.06 mm which longer from the design (15 mm). The difference could be caused by the use of adhesive glue to attach the oscillator to the acrylic plate or some error at assembling process. Figures 4.13 and 4.14 show that the approximation data confirms

with measurement data from Grosso and Mader. Therefore, the value of real distance (32.32 mm in test cell A and 15.06 mm in test cell B) is used as the parameter for calculating the ultrasonic propagation velocity.

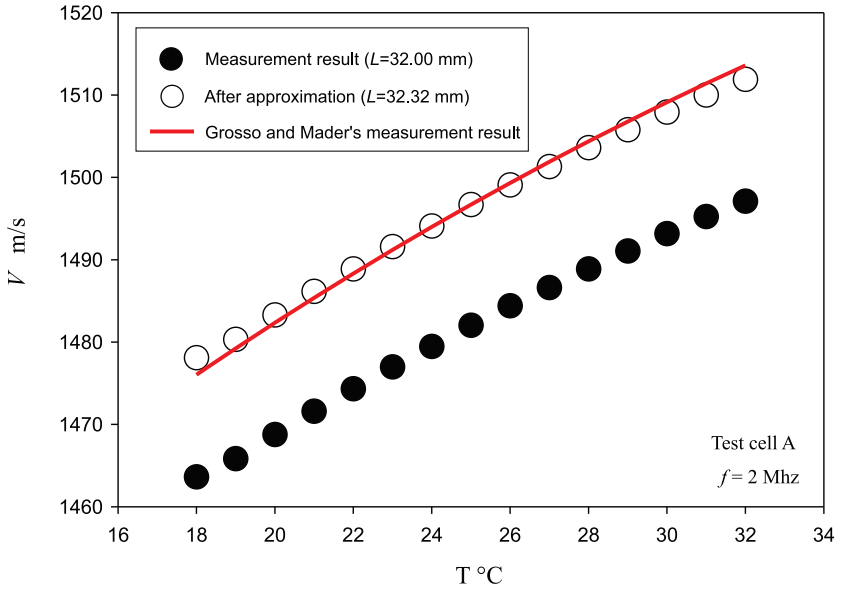

Figure 4.13: Ultrasonic propagation velocity in pure water for test cell A (f = 2 MHz)

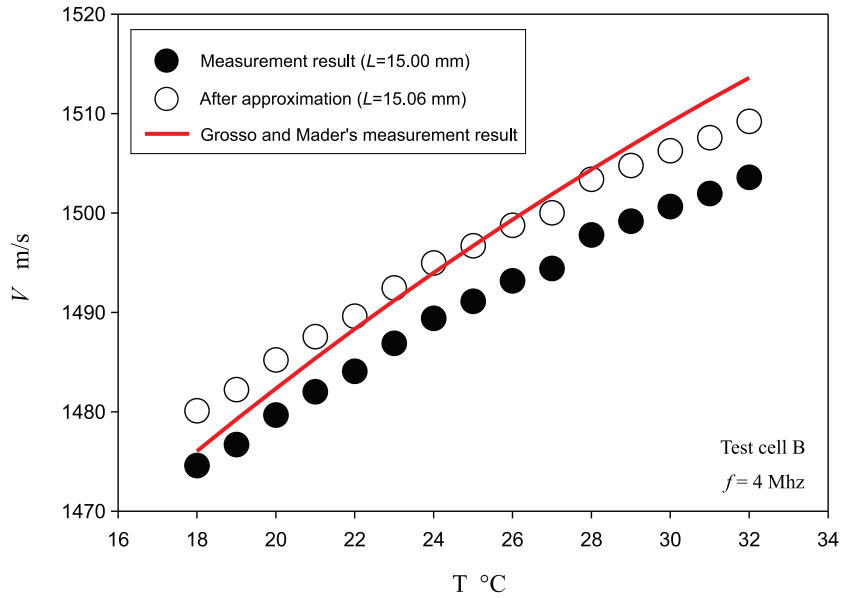

Figure 4.14: Ultrasonic propagation velocity in pure water for test cell B (f = 4 MHz)

4.3.2 Ultrasonic propagation attenuation

The value of ultrasonic propagation attenuation describes the quantity of ultrasonic wave which absorbed in the MR fluid. Ultrasonic propagation attenuation is calculated by comparing the amplitude of the receiving wave at initial value and after applying magnetic field. Amplitude of the ultrasonic wave represents the sound pressure. The amplitude decreases with the applied time. As ultrasonic wave travels or propagates across distance, the amplitude decreases. Figure 4.15 shows the graph for received ultrasonic waveform at initial condition ($B = 0$ mT) and condition when magnetic field is applied. The unit of ultrasonic propagation attenuation is decibel per meter (dB/m). The change of ultrasonic propagation attenuation or $\Delta\alpha$ is calculated using equation below:

$$\begin{aligned}\Delta\alpha &= -\frac{20}{L}\log_{10}\left(\frac{P_i}{P}\right) - \left\{-\frac{20}{L}\log_{10}\left(\frac{P_o}{P}\right)\right\} \\ &= \frac{20}{L}\log_{10}\left(\frac{P_o}{P_i}\right)\end{aligned} \tag{4.15}$$

where P is the sound pressure at the emitter, P_i and P_o are the sound pressure at the receiver with and without the applied magnetic field, respectively.

4.3.3 Experiment parameter

In this study, many experiments are conducted. Each experiment has different parameter and sometimes has different experimental setup. For example, the experiment for temperature dependence needs to change the temperature in the test fluid. On other hand, other experiments such as time dependence, magnetic field dependence and hysteresis phenomenon need constant temperature in the test fluid. The experiment parameters are summarized as follow:

1. Type of test fluid: MRF-122EG and MRF-132DG. The main difference between these MR fluids is the content of magnetic particles.
2. Magnetic flux density. Magnetic flux density can be customized from 0 to 450 mT.

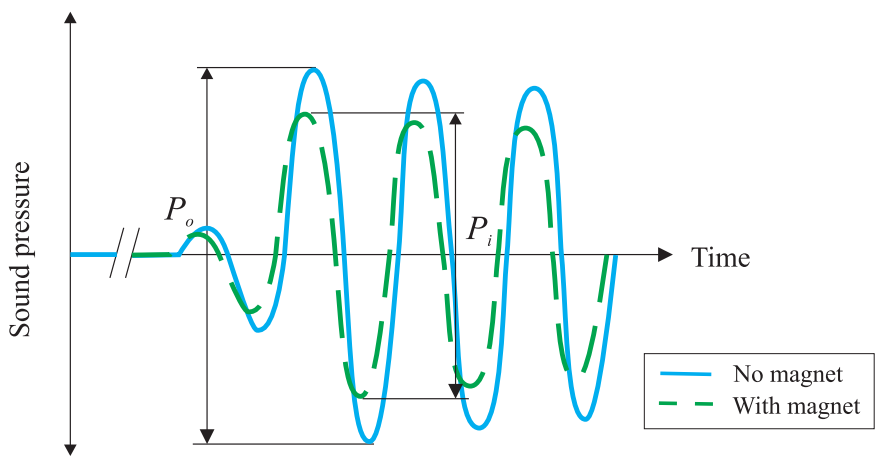

Figure 4.15: Comparison of ultrasonic wave propagation for measuring the attenuation

3. Temperature of the test fluid. For temperature dependence experiment, temperature of the test cell is customized from 20 °C to 40 °C. For other experiments, the temperature of the test fluid is kept constant at 25 °C.
4. Sweep rate of magnetic field. By applying function generator, magnetic field can be swept at different rates.

The angle θ between the directions of ultrasonic propagation and the magnetic field could be adjusted freely from 0° to 180°. At $\theta = 0°$, the direction of ultrasonic propagation is parallel to that of the magnetic field; at $\theta = 90°$, the direction of ultrasonic propagation is perpendicular to that of the magnetic field. Figures 4.16 and 4.17 illustrate the angle θ.

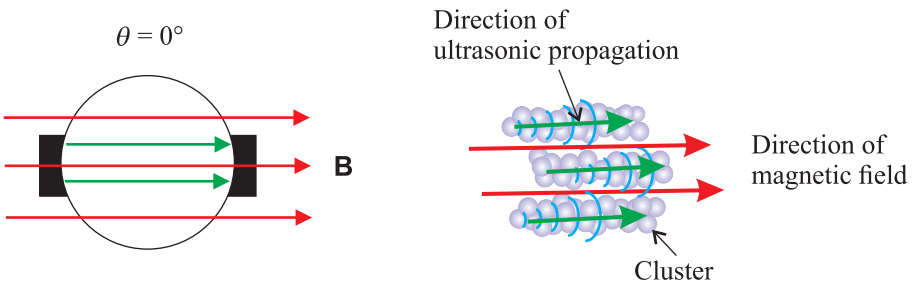

Figure 4.16: Ultrasonic propagation and magnetic field in parallel direction ($\theta = 0°$)

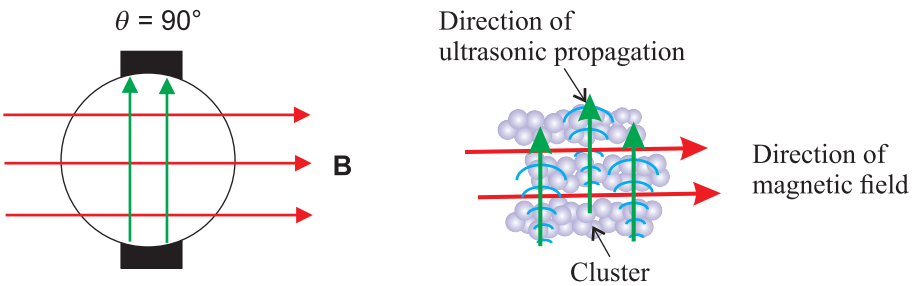

Figure 4.17: Ultrasonic propagation and magnetic field in perpendicular direction ($\theta = 90°$)

4.3.4 Repeatability of the experiment system

In order to check the repeatibility of the experiment system, experiments are conducted three times for similar conditions. The repeatibility of the experiment data for ultrasonic propagation velocity under different value of magnetic field sweep rate are shown in Figs. 4.18 $\sim$ 4.21.

Standard deviation and experimental error for the experiment data in Fig. 4.18 $\sim$ 4.21 are presented in Table 4.5. The average value of SD_x and Er_x is 0.0778 (7.78 %) and 0.0448 (4.48 %), respectively.

Table 4.5: Standard deviation and experimental error of different magnetic field sweep rates

Sweep rate	SD_x	Er_x
500 mT/min	0.110	0.064
750 mT/min	0.069	0.040
1000 mT/min	0.068	0.039
1250 mT/min	0.074	0.042
1500 mT/min	0.068	0.039

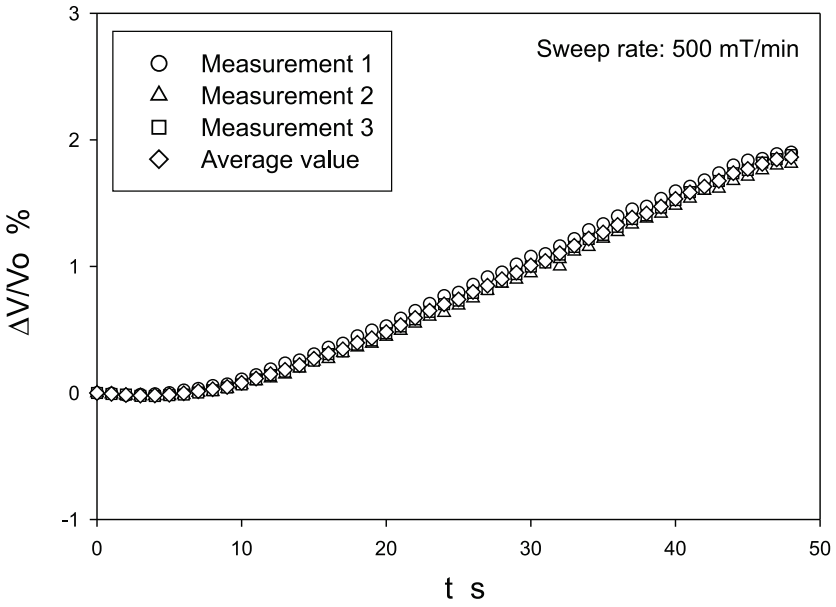

Figure 4.18: Three data of ultrasonic propagation velocity in MR fluid (MRF-132DG) under 500 mT/min of magnetic field sweep rate

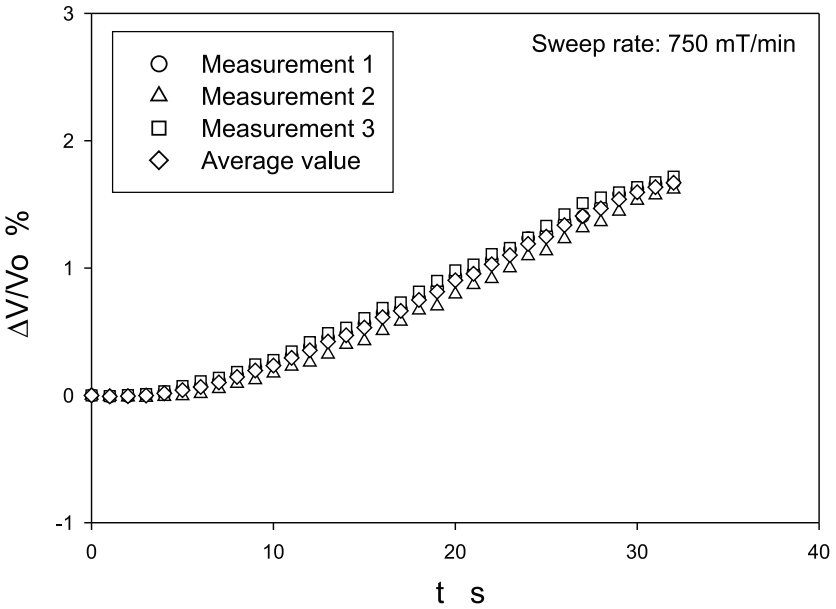

Figure 4.19: Three data of ultrasonic propagation velocity in MR fluid (MRF-132DG) under 750 mT/min of magnetic field sweep rate

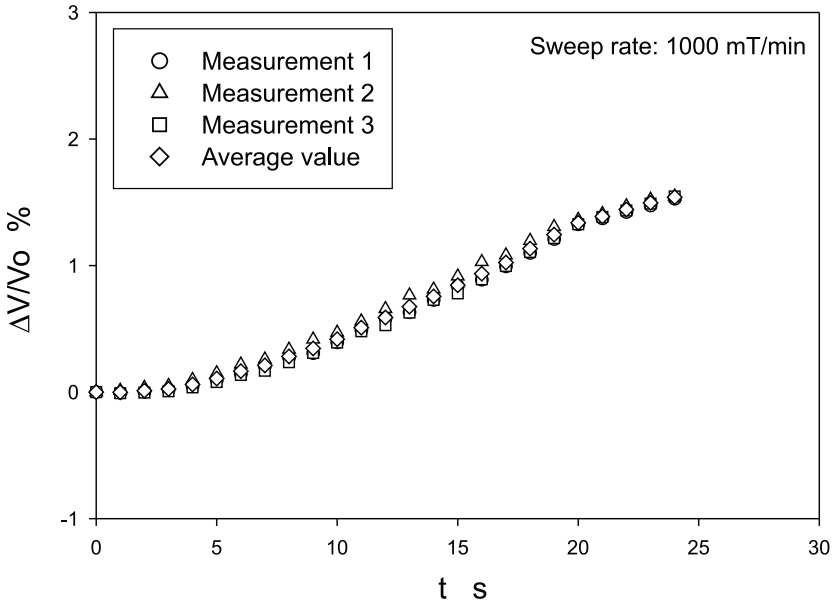

Figure 4.20: Three data of ultrasonic propagation velocity in MR fluid (MRF-132DG) under 1000 mT/min of magnetic field sweep rate

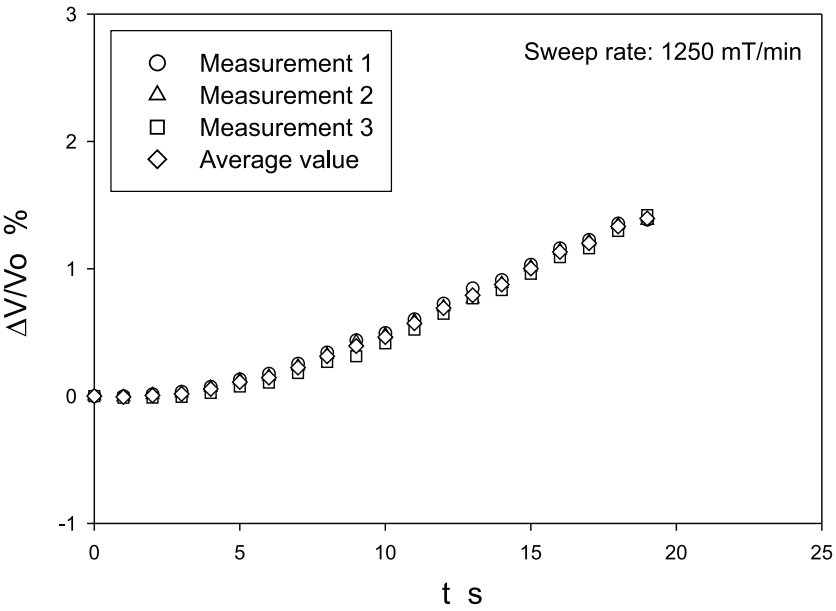

Figure 4.21: Three data of ultrasonic propagation velocity in MR fluid (MRF-132DG) under 1250 mT/min of magnetic field sweep rate

4.4 Ultrasonic propagation properties in MR fluid under DC magnetic field

Several experiments are conducted to investigate the effects of temperature, elapsed time, magnetic field and magnetic field sweep rate.

4.4.1 Effect of temperature

The effect of temperature on the clustering structure in the MR fluid is investigated by measuring the change in ultrasonic propagation velocity and attenuation. These experiment results can be seen in Figs. 4.22 and 4.23. In this experiment, the ultrasonic propagation velocity and attenuation is measured from temperatures 20 °C to 40 °C by increasing the temperature of the test cell by 2 °C every 10 min. For each measurement, a constant magnetic flux density (B) of 50 mT is applied for 10 minutes to provide sufficient time for the magnetic particles to form clustering structures.

Figure 4.22 shows the ultrasonic propagation velocity decreases with the temperature of the MR fluid. The decreasing velocity means that the cluster size becomes thinner with the increasing of temperature. Similar trend was observed in magnetic fluid by Motozawa et al. [138] and Kikura et al. [149]. They found that sound velocity in both the water-based and kerosene-based magnetic fluids decreases with the increasing temperature. According to the increasing of sound velocity in water when higher temperatures are applied, they observed that the solid characteristic is more dominant for the sound velocity of a magnetic fluid in the temperature region. In addition, from Eq. (4.4), the value of λ decreases at higher temperature (T). The decreasing of λ means the induced magnetic interaction of two particles becomes lower. The decreasing of λ also decreases the number of cluster [150]. As the results, the cluster formation in MR fluid is thinner when higher temperatures are applied.

Moreover, these effects also can be analyzed from the measurement results of ultrasonic propagation attenuation as shown in Fig. 4.23. The ultrasonic propagation attenuation increases with the temperature of the MR fluid. These results suggest that temperature has a significant effect on ultrasonic propagation velocity and attenuation. Therefore, the temperature must be keep constant for each experiment [145].

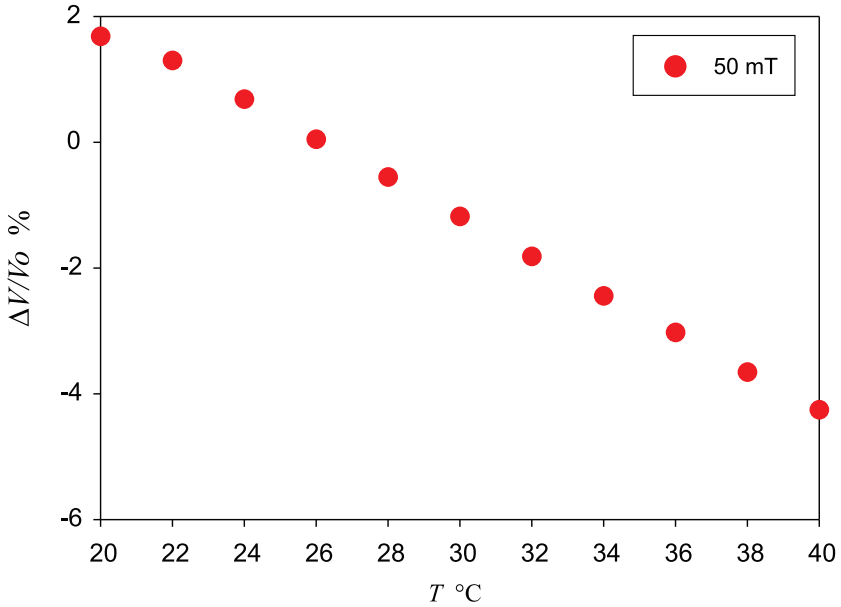

Figure 4.22: Ultrasonic propagation velocity in MR fluid as function of temperature

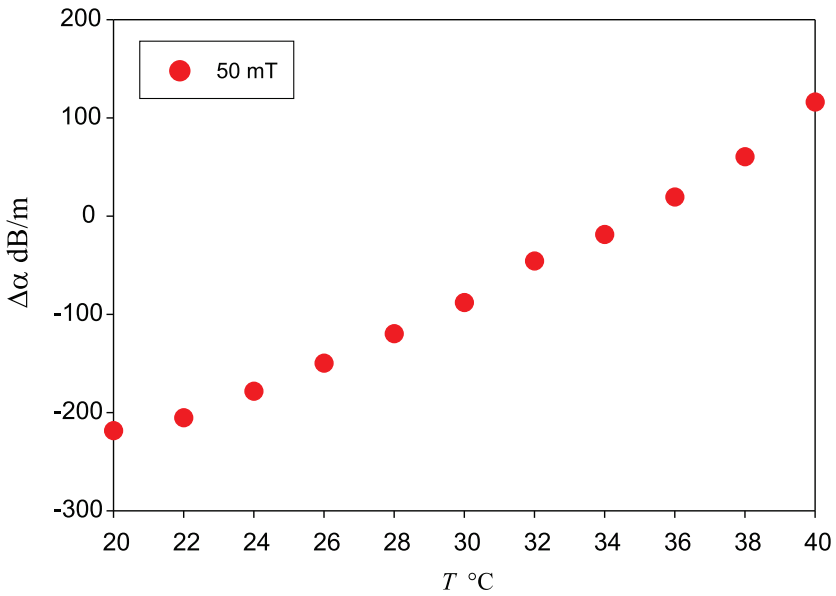

Figure 4.23: Ultrasonic propagation attenuation in MR fluid as function of temperature

4.4.2 Effect of elapsed time

Experiments are conducted to investigate the formation of clustering structures in the MR fluid when it is subjected to an instantaneous magnetic field. Figures 4.24 and 4.25 show the ultrasonic propagation velocity and attenuation in the MR fluid versus time, respectively. The obtained result in Fig. 4.24 confirms the previous study that the ultrasonic propagation velocity in MR fluid increases with the time after magnetic field is applied [95]. Moreover, from Eq. 4.6, the sound propagation velocity changes with the application of magnetic field (H).

Experiments are also conducted by measuring the ultrasonic propagation attenuation since the change of ultrasonic propagation in MR fluid when subjected to magnetic field instantaneously is relatively unknown. In this experiment, three different magnetic fields (B): 50, 100, and 200 mT are applied. These magnetic fields are applied instantaneously and remain constant for 10 min. The angle θ and the temperature of the test cell are kept constant at $\theta = 0°$ and 25 °C, respectively.

Figure 4.25 shows the change of attenuation decreases when magnetic field is applied. This change is probably caused by the formation of clustering structures. Magnetic particles in the MR fluid form clustering structures along the direction of the magnetic field. Clustering structures continue to grow until ultrasonic propagation attenuation becomes constant. This result indicates that clustering structures in the MR fluid grow for several seconds. Moreover, the order of ultrasonic propagation attenuation curve comply the magnetic flux density. For higher magnetic flux density, the ultrasonic propagation attenuation becomes lower. It is likely that in MR fluids, more clusters form as the magnetic field increases; therefore, ultrasonic propagation attenuation decreases as the magnetic flux density increases [145].

Effect of removing the magnetic field

Figures 4.26 and 4.27 show the effect of removing the magnetic field from the MR fluid. Two magnetic flux densities (B) of 100 and 200 mT are applied instantaneously and keep constant for 60 minutes; then, the magnetic field is removed, and the MR fluid is observed for 30 minutes.

Figures 4.26 and 4.27 show that ultrasonic propagation velocity and attenuation change instantaneously after the magnetic field is removed and then become constant. The curves for both magnetic flux densities tend to return to their initial values. It seems that the clustering structures in the MR fluid break instantaneously after the magnetic field is removed. However, it seems that a few cluster formations still remain while value of ultrasonic propagation velocity and attenuation for both magnetic flux densities is not exactly become 0 % and 0 dB/m, respectively. The remaining cluster formation is probably because of the residual magnetic field effect [95].

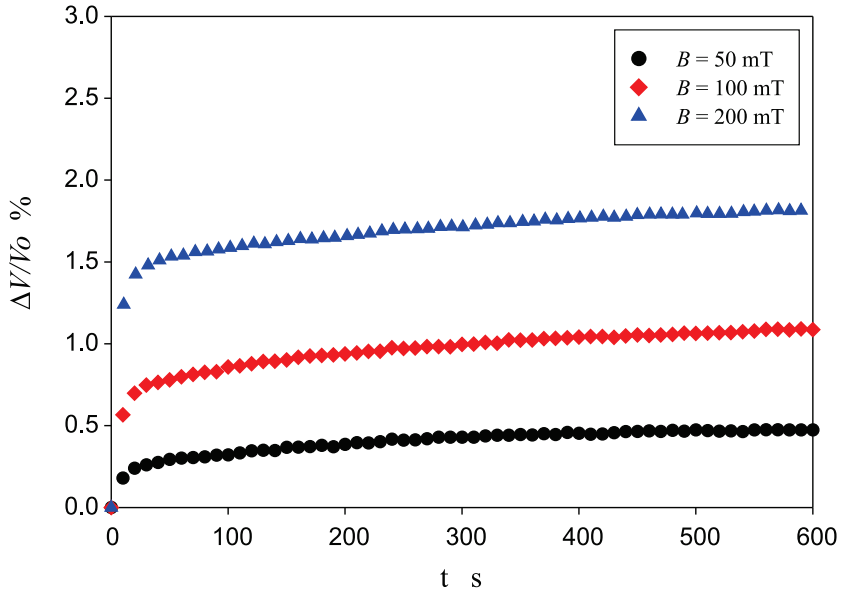

Figure 4.24: Time dependence of ultrasonic propagation velocity in MR fluid for different magnetic flux densities

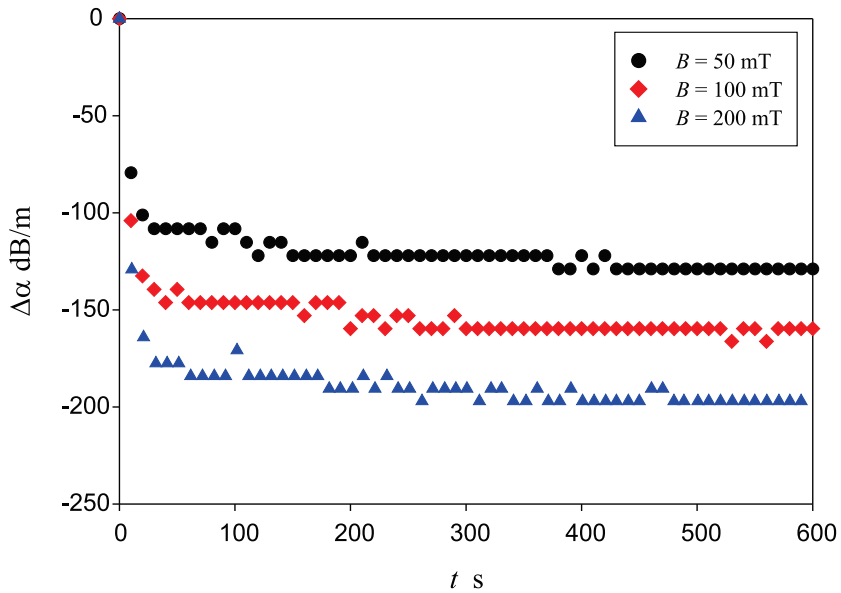

Figure 4.25: Time dependence of ultrasonic propagation attenuation in MR fluid for different magnetic flux densities

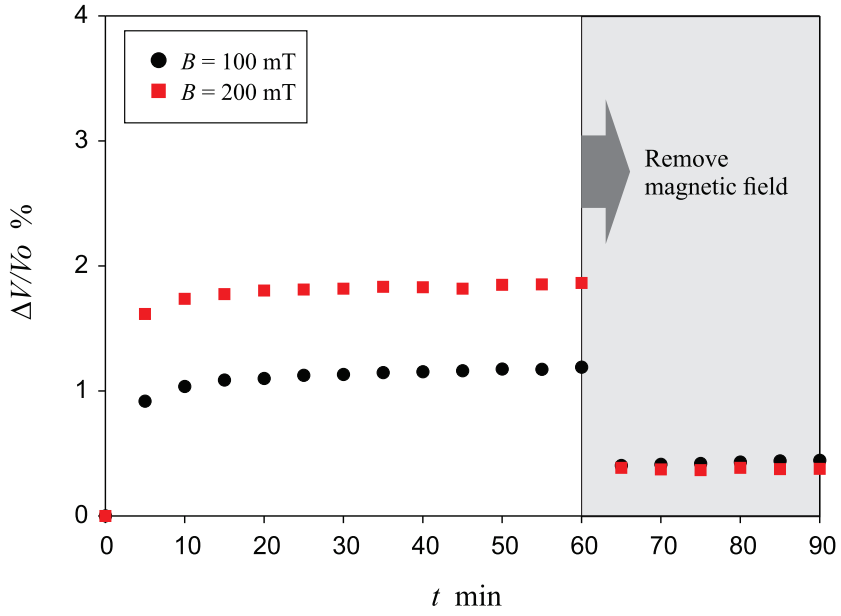

Figure 4.26: Ultrasonic propagation velocity in MR fluid before and after removing the magnetic field

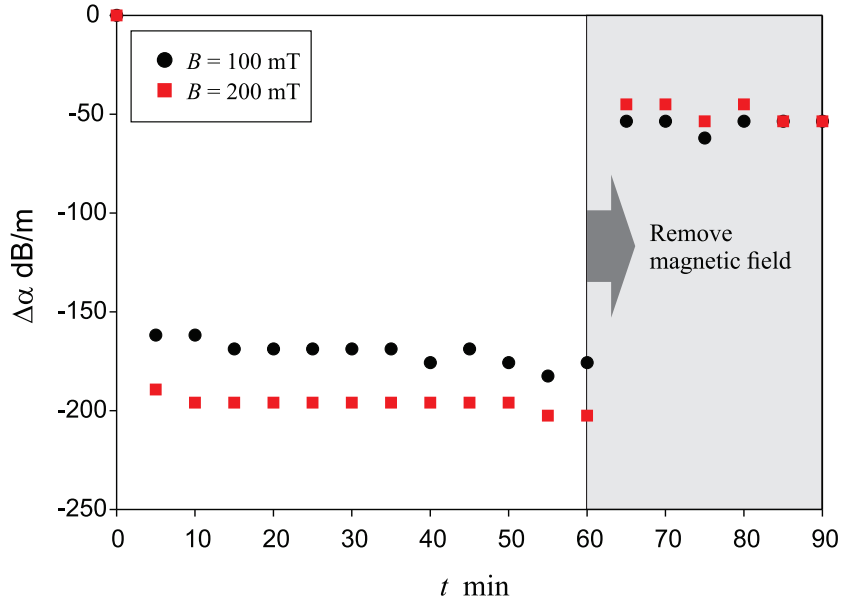

Figure 4.27: Ultrasonic propagation attenuation in MR fluid before and after removing the magnetic field

4.4.3 Effect of magnetic field

Experiments are conducted to investigate the effect of magnetic field on the clustering structures in the MR fluid. Figures 4.28 and 4.29 show the ultrasonic propagation velocity and attenuation in the MR fluid versus the magnetic flux density, respectively. The result of change of ultrasonic propagation velocity as shown in Fig. 4.28 confirms the previous study [139] that ultrasonic propagation velocity increases as the applied magnetic flux density increases. Moreover, from Eq. 4.6, parameter of magnetic field (H) has effect on the sound propagation velocity. The stronger magnetic field, the bigger cluster is formed and the sound propagation velocity becomes higher.

In other hand, effect of magnetic field on ultrasonic propagation attenuation is not well known. Therefore, experiments are also conducted by measuring the ultrasonic propagation attenuation. In this experiment, the angle θ and the temperature of the test cell are kept constant at 0° and 25 °C, respectively. The experiments are conducted by increasing the magnetic flux density by 50 mT at two different intervals: 1 and 5 min. For both intervals, ultrasonic propagation attenuation decreases as the applied magnetic flux density increases. This change seems to be caused by the formation of clustering structures: as the magnetic flux density increases, more clusters formed. This result indicates that the magnetic flux density has a strong effect on ultrasonic propagation attenuation in MR fluids [145]. In addition, from Eq. (4.4), the value of λ increases at higher external magnetic field (H). The increasing of λ means the induced magnetic interaction of two particles becomes stronger. As the results, the cluster formation in MR fluid is bigger when higher magnetic fields are applied.

Figures 4.28 and 4.29 also show the effect of applying the magnetic field for different time intervals on ultrasonic propagation velocity and attenuation, respectively. The interval is defined as the time between two measurements. For example, a 1-min interval indicates that the magnetic flux density is increased after 1 min. Ultrasonic propagation velocity for the 5-min interval is slightly lower than that for the 1-min interval. The trend of this result is similar with the previous studies [136, 137]. In other hand, ultrasonic propagation attenuation for the 5-min interval is slightly higher than that for the 1-min interval. From these results, at 5-min interval, it seems that some magnetic particles have sufficient time to separate from clustering structures because of sedimentation when the MR fluid is applied low magnetic flux density.

4.4.4 Hysteresis

Hysteresis is observed in ultrasonic propagation velocity and attenuation in the MR fluid when the magnetic flux density is increased from 0 mT to a certain value and then is decreased to the initial value. Figures 4.30 and 4.31 show the ultrasonic propagation velocity and attenuation in the MR fluid versus the applied magnetic flux density, respectively. The experiment is conducted by increasing the magnetic flux density in increments of 50 mT from 0 to 400 mT and then decreasing it by the same amount to 0 mT.

The obtained result of hysteresis of ultrasonic propagation velocity as shown in Fig. 4.30 has similar trend with the previous studies [139, 136, 137]. The change of ultrasonic propagation velocity increased during the increasing process of magnetic field. Thus, hysteresis on MR fluid

tends to return to the initial value ($B = 0$ mT).

Figure 4.31 shows the ultrasonic propagation attenuation decreases as the magnetic field intensity increases from 0 to 400 mT. Then, the ultrasonic propagation attenuation increases, and the curves return to their initial values as the magnetic flux density decreases from 400 mT to 0 mT. This result confirms that clustering structures in MR fluid quickly dissolve after the magnetic field is reduced to zero [145].

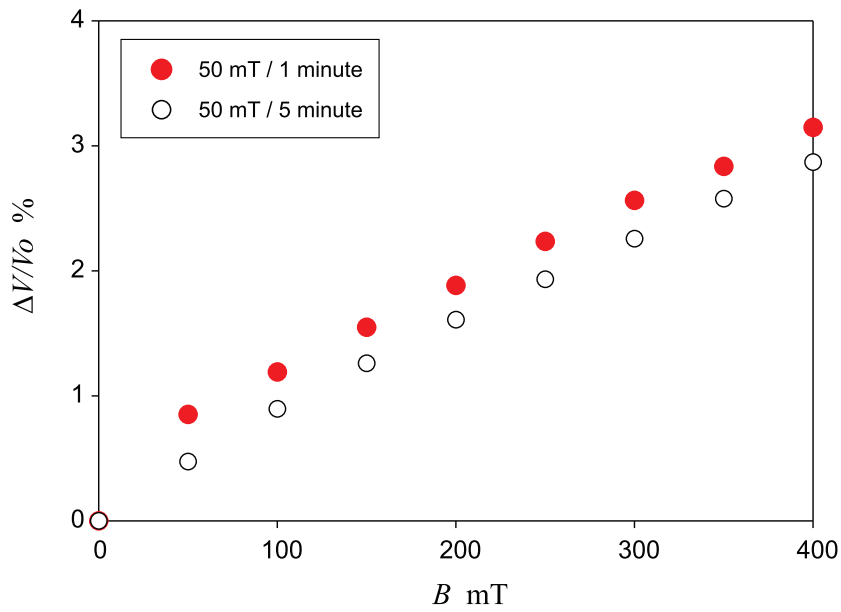

Figure 4.28: Magnetic field dependence of ultrasonic propagation velocity in MR fluid

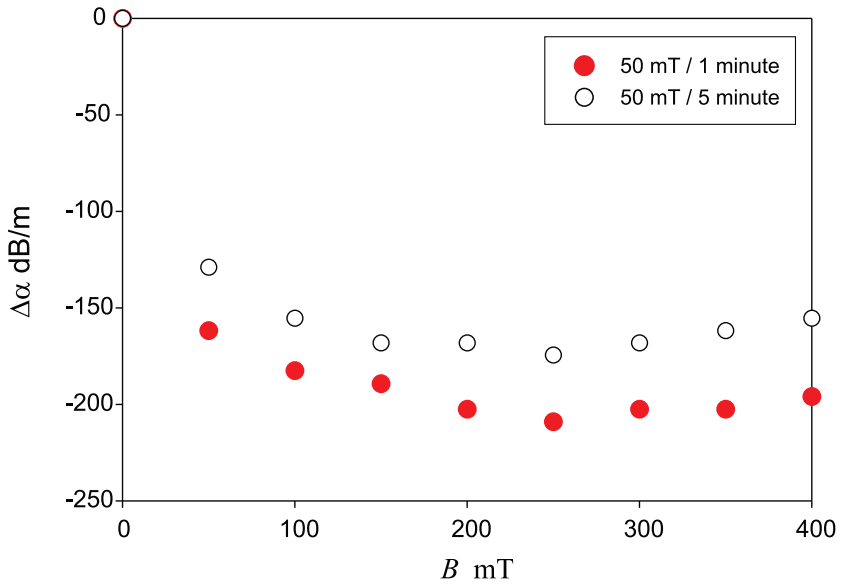

Figure 4.29: Magnetic field dependence of ultrasonic propagation attenuation in MR fluid

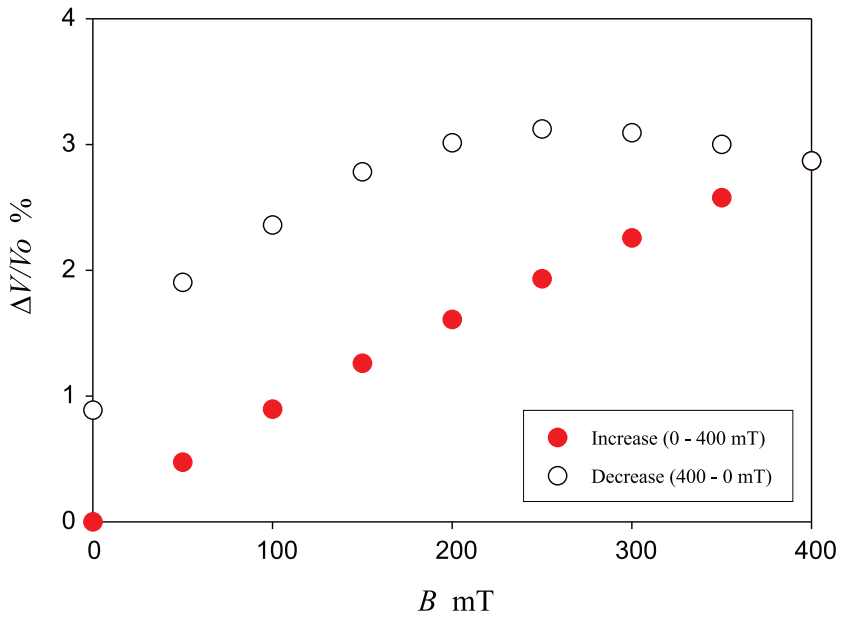

Figure 4.30: Hysteresis of ultrasonic propagation velocity in MR fluid

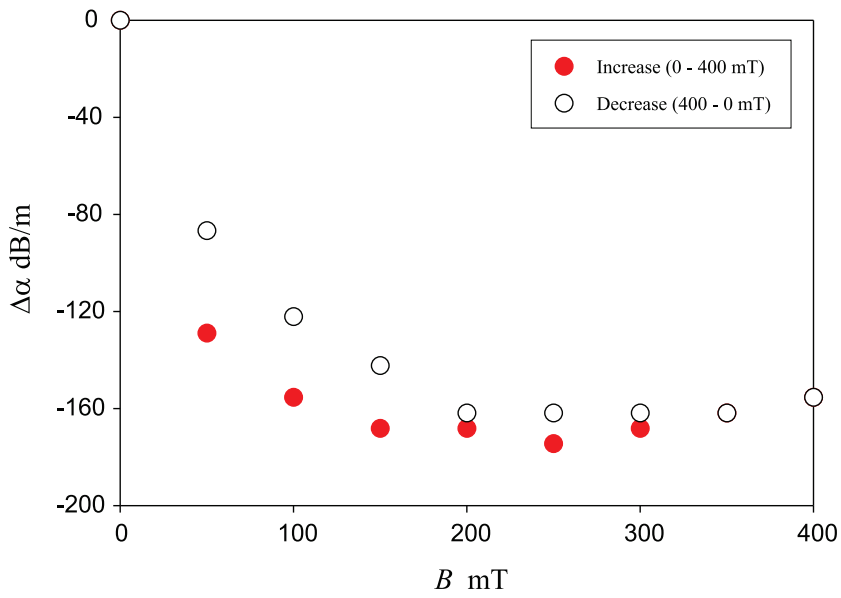

Figure 4.31: Hysteresis of ultrasonic propagation attenuation in MR fluid

4.4.5 Effect of magnetic field sweep rate

Experiments are conducted to investigate the effect of magnetic field sweep rate on the cluster formation in MR fluid. For different sweep rates, the change of ultrasonic propagation velocity is measured. The magnetic flux densities of the electromagnet are adjusted by changing the current in the power supply. A function generator is used to control the power supply so that different magnetic field sweep rates could be produced (Fig. 4.2). Different magnetic field sweep rates, from 6 to 80 mT/min are applied for various lengths of time and the magnetic flux density is increased from 0 to 400 mT (Fig. 4.32). The magnetic field sweep rates and the length of time are given in Table 4.6.

Figure 4.33 shows the change of ultrasonic propagation velocity versus time for different magnetic field sweep rates. The change of ultrasonic propagation velocity increases when higher magnetic field is applied. As ultrasonic propagation velocity increases, the cluster becomes thicker. This result clarifies the previous reports [95, 138] that the cluster formed in the MR fluid becomes thicker when a higher magnetic field is applied. The maximum value of the change in ultrasonic propagation velocity, $(\Delta V/V_0)_{\mathrm{max}}$, is very similar throughout the magnetic field sweep rate range from 6 to 40 mT/min. This also agrees with the finding of the previous study [138] that ultrasonic propagation velocity in MR fluid increases in a similar manner at each sweep rate. However, the value of $(\Delta V/V_0)_{\mathrm{max}}$ decreased when a higher magnetic field sweep rate is applied, as shown at 50 and 80 mT/min. The decrease of the value of $(\Delta V/V_0)_{\mathrm{max}}$ indicates that the cluster size becomes thinner when the magnetic field is applied at higher sweep rates. Magnetic particles in MR fluid do not have sufficient time to form clusters of bigger size at high magnetic field sweep rates. This result suggests that magnetic field sweep rate affects the size of the cluster in MR fluid.

Figure 4.34 shows the change of ultrasonic propagation velocity versus magnetic flux density. The change of ultrasonic propagation velocity increases at an approximately similar rate for the magnetic field sweep rates ranging from 6 to 40 mT/min. It indicates cluster grows at a similar rate in that range. However, the change of ultrasonic propagation velocity increases at slower rate for the higher magnetic field sweep rates (50 and 80 mT/min). It indicates in that range, the cluster grows slower in the fluid that is being subjected to higher magnetic field and swept faster. This result indicates that the magnetic field sweep rate affects the cluster formation in MR fluid.

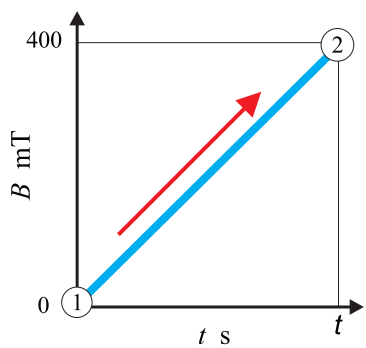

Figure 4.32: Sweep rate setting

Table 4.6: Magnetic field sweep rate and application times

Sweep rate mT/min	6	8	10	15	30	40	50	80
Application Time s	4000	3000	2400	1600	800	600	480	300

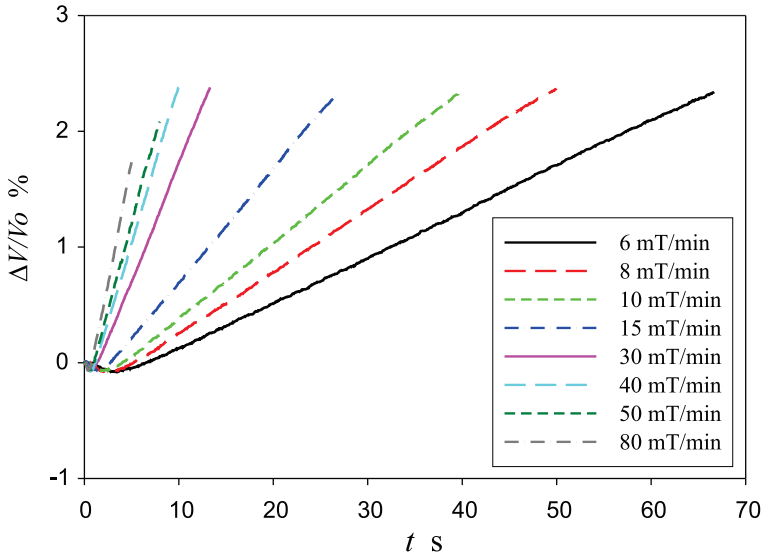

Figure 4.33: The change of ultrasonic propagation velocity in MR fluid with time

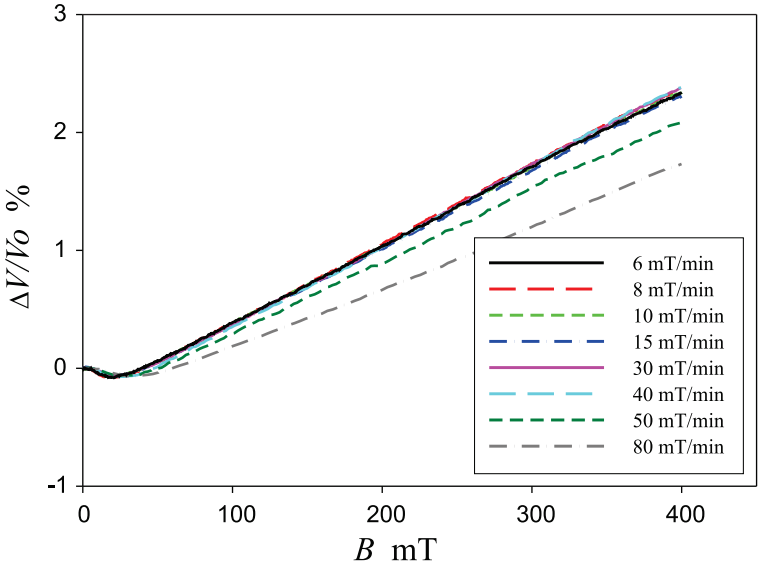

Figure 4.34: The change of ultrasonic propagation velocity in MR fluid with magnetic flux density

Effect of volume fraction of MR fluids under magnetic field sweep rate

In this experiment, two types of MR fluids, MRF-122EG and MRF-132DG from Lord Corporation, are used. The main difference between these MR fluids is the volume fraction of magnetic particles, which is 22 % for MRF-122EG and 32 % for MRF-132DG. The difference between these MR fluids is presented in Table 2.5 in chapter 2. For all the experiments, the temperature of the test cell is maintained at 25 °C, and magnetic field sweep rates of 500, 750, 1000, 1250, 1500 and 2000 mT/min are applied. Table 4.7 presents the magnetic field sweep rates and the length of time.

Figures 4.35 and 4.36 show the values of $\Delta V/V_0$ for MRF-122EG and MRF-132DG, respectively, at various sweep rates. At different sweep rates, the value of $\Delta V/V_0$ increases with an increase in the magnetic field. It is well known that this change is due to the formation of clustering structures; when the magnetic field increases, more clusters are formed [95].

Figures 4.35 and 4.36 show the influence of the volume fractions of the MR fluid on $\Delta V/V_0$ is significant. At a lower volume fraction (MRF-122EG), the value of $\Delta V/V_0$ is lower than that for the higher volume fraction, and the cluster size is proportional to the volume fraction. As a result, the value of $\Delta V/V_0$ increases when the volume fraction of the MR fluid increases. In other words, the size of the cluster increases for higher volume fractions. Moreover, at lower volume fraction (MRF-122EG), the value of $\Delta V/V_0$ decreases when lower magnetic flux densities are applied for different sweep rates (Fig. 4.35). The value of $\Delta V/V_0$ tends to increase when higher magnetic flux densities are applied. At low magnetic flux density and at low fraction of MR fluid, the decreasing $\Delta V/V_0$ means that the cluster formation is quite small. The small cluster makes the portion of liquid part in ultrasonic propagation area increases. In other words, the increasing of liquid area makes the decreasing of ultrasonic propagation velocity. The similar trend was observed by previous researcher [143] that curve of ultrasonic propagation velocity in small volume fraction of MR fluid (MRF-122CG) move downward due to the increasing of interval time of applied magnetic field. The decreasing of value of $\Delta V/V_0$ is not shown in higher volume fraction (MRF-132DG). It means that the cluster formation in MRF-132DG is formed bigger. The bigger cluster makes the portion of solid part in the propagation area increases. The increasing solid part means the increasing of ultrasonic propagation velocity. These results suggest that the volume fraction and sweep rate affect the cluster formation in MR fluids.

Figure 4.37 shows the maximum values of $\Delta V/V_0$ for the two types of MR fluids at various sweep rates. The maximum value of $\Delta V/V_0$ decreases at higher applied sweep rates. It appears that the magnetic particles in the MR fluids do not have sufficient time to form clusters of greater size at high sweep rates. Therefore, the maximum size of the cluster decreases at higher sweep rates. This result indicates that the sweep rate affects the maximum size of the clusters in MR fluids [147].

Table 4.7: Magnetic field sweep rate and application times (high sweep rate)

Sweep rate mT/min	500	750	1000	1250	1500	2000
Application Time s	48	32	24	19.2	16	12

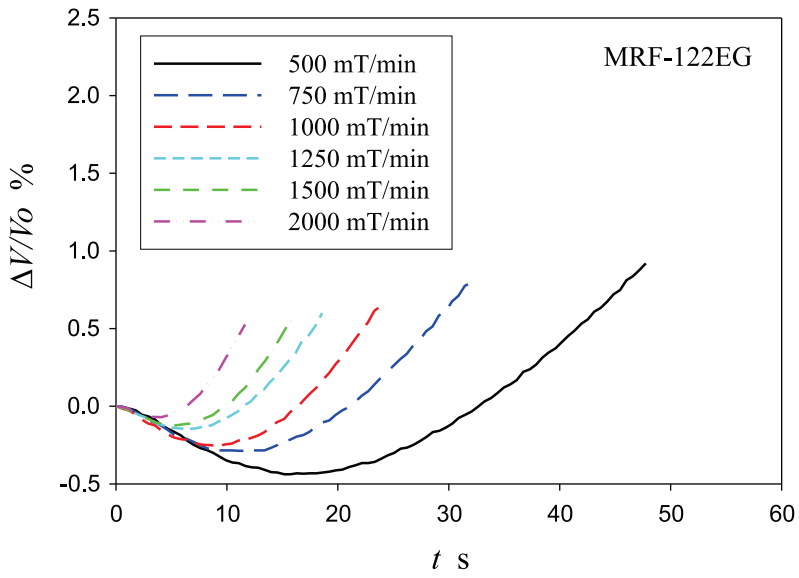

Figure 4.35: Change of ultrasonic propagation velocity in MRF-122ED

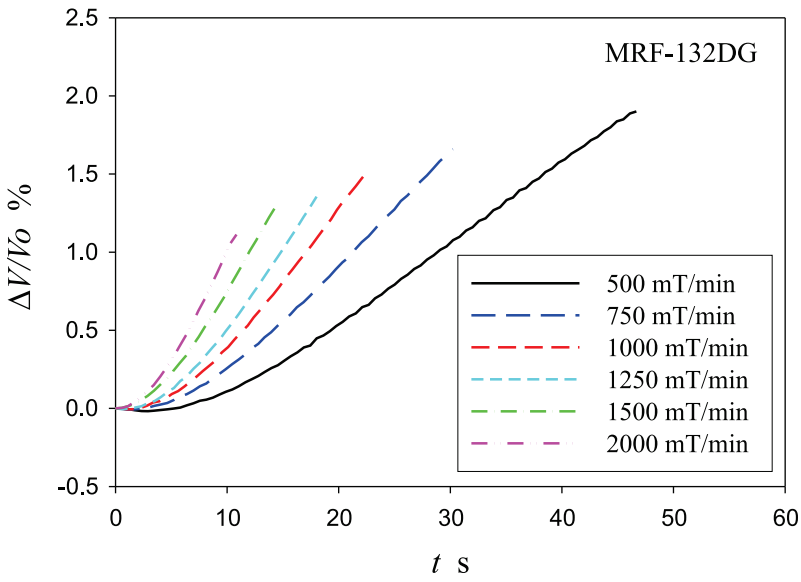

Figure 4.36: Change of ultrasonic propagation velocity in MRF-132DG

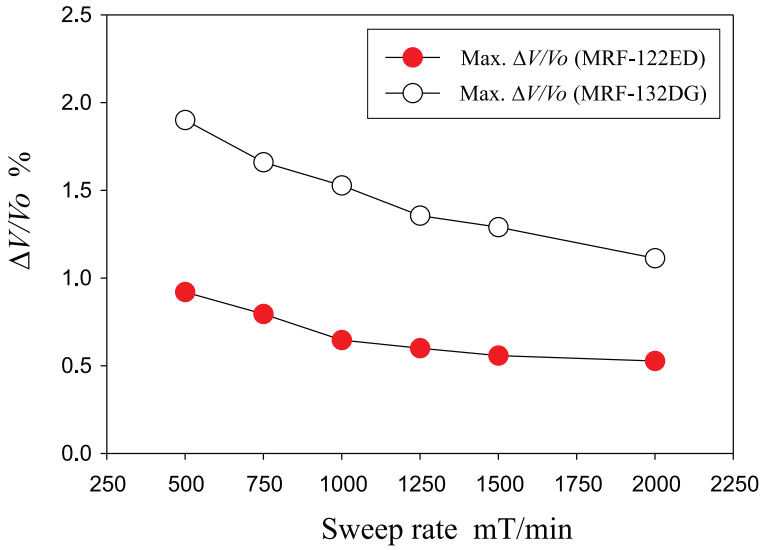

Figure 4.37: Maximum value of change of ultrasonic propagation velocity in MRF-122ED and MRF-132DG as function of magnetic field sweep rates

4.5 Ultrasonic propagation properties in MR fluid under AC magnetic field

From the previous discussions, it is well known that DC magnetic field has strong effect on the cluster formation in MR fluids. However, cluster formation in MR fluids under AC magnetic field is relatively unknown. There are a few publication on the behavior of cluster formation in magnetic and MR fluids. Takahashi et al. [151] investigated the behavior of magnetic particles in magnetic and MR fluid under AC magnetic fluid by using dark-field microscopy. Experiments were conducted by applying different frequency of AC magnetic field (f = 0.1, 0.5 and 1.0 Hz) on magnetic and MR fluid. They found that cluster size in magnetic fluid becomes thinner when higher frequency of AC magnetic field was applied. However, these effects was not found in the MR fluid. Cluster size in MR fluid is nearly similar under different frequency of magnetic field. In this study, experiments are conducted to analyze the cluster formation in MR fluid under AC magnetic field by measuring the ultrasonic propagation velocity.

4.5.1 Experimental apparatus

The experimental apparatus is almost similar with experimental apparatus illustrated in Fig. 4.2. There are only two different items with previous experimental apparatus;

1. First, new power supply is used. Compare to the previous power supply, the new power supply can generate both AC and DC current. Even though the maximum strength of the DC current is lower then the previous power supply.
2. Second, function generator is not used. Several different setting of wave form in new power supply can be set easily, without applying a function generator.

Figure 4.38 shows the photograph of the power supply. Specification of the power supply is presented in Table 4.8.

Figure 4.38: AC power supply

Table 4.8: Detail specification of power supply

Model	BP 4610
Operation mode	Constant voltage (CV) or constant current (CC)
Max. output voltage (CV)	± 115 V
Max. output voltage (CC)	± 10 A
Manufacturer	NF Corporation

Magnetic field distribution

Similar procedure to the one shown in Fig. 4.6 is used to measure the distribution of magnetic field in new magnetic field. The value of DC and AC magnetic flux density as function of current is presented in Figs. 4.39 and 4.40, respectively. The value of magnetic flux density is measured in the center point of the pole piece. The maximum value of magnetic flux density that is generated by new power supply ($\sim$ 200 mT) is lower than that value at previous power supply ($\sim$ 450 mT). Maximum value of magnetic flux density which generated by new power supply is ± 210 mT.

In the center point of the pole piece, the value of AC magnetic flux density as the function of time for different current (0 – 10 A) at $f = 1$ Hz is measured. In the power supply, sine wave is selected as the output waveform. The measurement result is presented in Fig. 4.41.

In order to know the limitation of the power supply, the overload range in the relation between current and its frequency is investigated. Investigation is conducted by changing the composition the value of current and its frequency. The overload area in Fig. 4.42 represents the over capacity of the power supply.

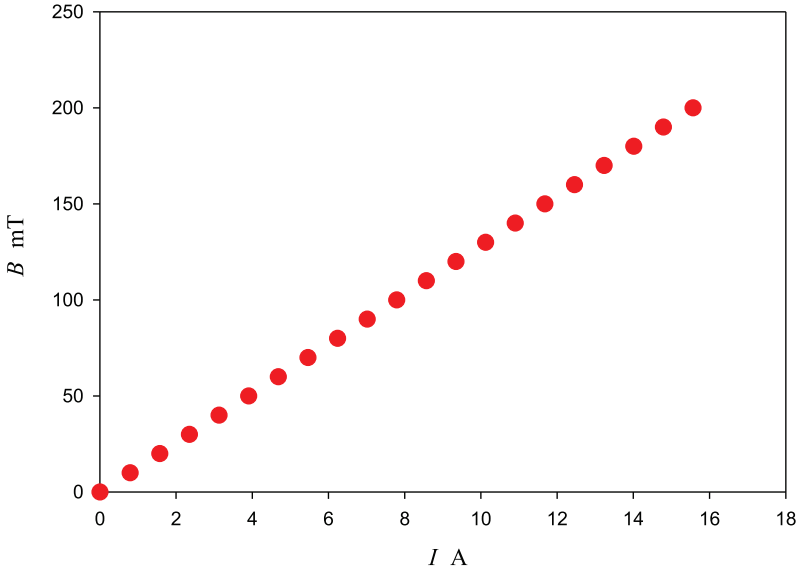

Figure 4.39: Value of DC magnetic flux density as function of electric current

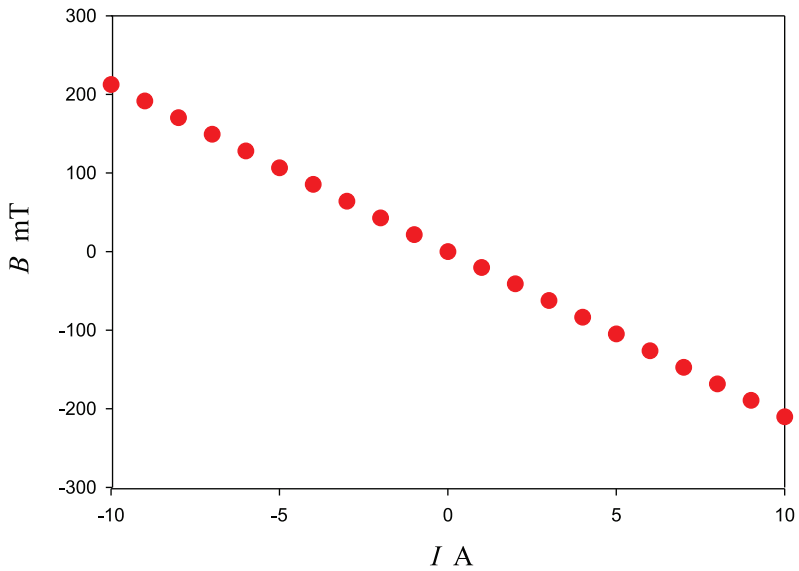

Figure 4.40: Value of AC magnetic flux density as function of electric current

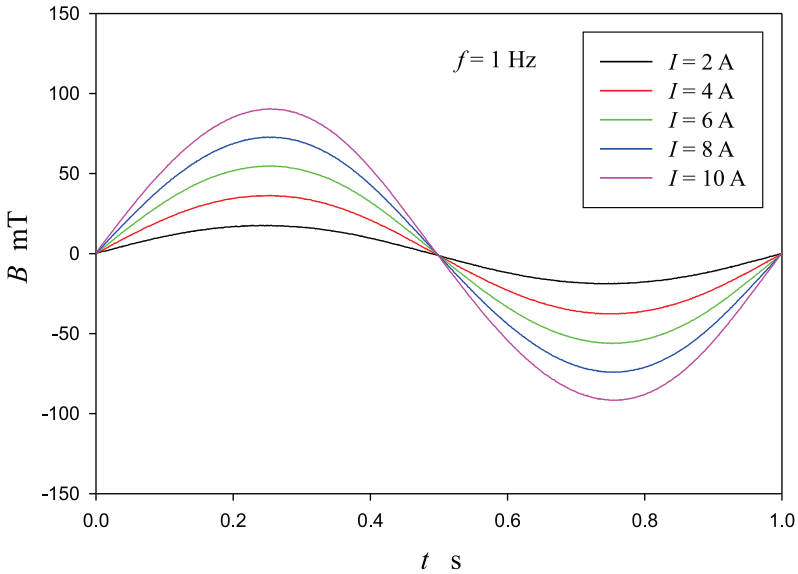

Figure 4.41: Value of AC magnetic flux density at $f = 1$ Hz for various current (2–10 A)

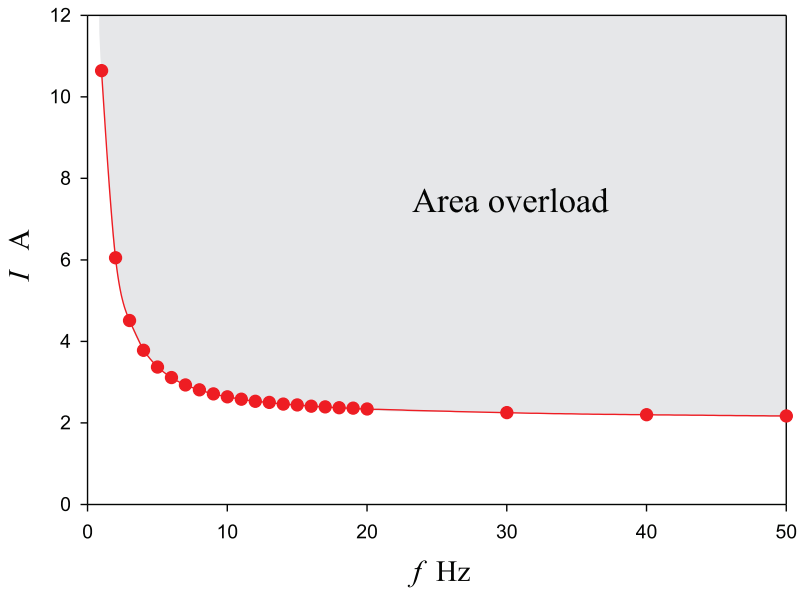

Figure 4.42: Workable area of AC magnetic flux density

4.5.2 Experiment parameter

The parameters in this study consist of:

1. Type of test fluid: MRF-132DG.
2. Frequency of ultrasonic wave: 4 MHz.
3. AC current (0 – 10 A).
4. Temperature of the test fluid is kept constant at 25 °C.
5. Angle θ between direction of ultrasonic propagation and direction of magnetic field is kept constant at 0°.

4.5.3 Effect of elapsed time

This experiment is conducted to investigate the formation of clustering structures in the MR fluid when it is subjected to an instantaneous of AC magnetic field. Figure 4.43 shows the ultrasonic propagation velocity in the MR fluid versus time. In this experiment, four different AC currents: 2.5, 5, 7.5 and 10 A, are applied. These magnetic fields are applied instantaneously and remain constant for 10 min, then, the magnetic fields are removed, and the MR fluid is observed for $\sim$ 7 min.

Figure 4.43 shows ultrasonic propagation velocity changes immediately after the magnetic field is applied and becomes constant after several seconds. The trend of this result is similar to when it is subjected to DC magnetic field. The order of ultrasonic propagation velocity curve complies the AC current. For higher current, the ultrasonic propagation velocity becomes higher. It is likely that in MR fluids, more clusters form as the current increases; therefore, ultrasonic propagation velocity increases as the current increases.

Figure 4.43 shows ultrasonic propagation velocity decreases instantaneously after the magnetic field is removed and then becomes constant. The trend of the result is similar to when it is subjected to DC magnetic field. The curves for all currents tend to return to their initial values. It seems that the clustering structures in the MR fluid break instantaneously after the magnetic field is removed.

4.5.4 Effect of magnetic field

The experiment is conducted to investigate the effect of AC magnetic field on the clustering structures in the MR fluid. Figure 4.44 shows the ultrasonic propagation velocity in the MR fluid versus AC current. The experiment is conducted by increasing the current from 0 to 6 A for different frequencies (1 – 2 Hz). For various frequency, ultrasonic propagation velocity in the MR fluid increases as the applied current increases. This trend is similar with the DC current application. The increasing ultrasonic propagation velocity means the cluster size becomes bigger under higher magnetic field. In addition, from Eq. (4.4), the value of λ increases at higher external magnetic field (H). The increasing of λ means the induced magnetic interaction of two particles becomes stronger. As the results, the cluster size becomes bigger when higher magnetic fields are applied.

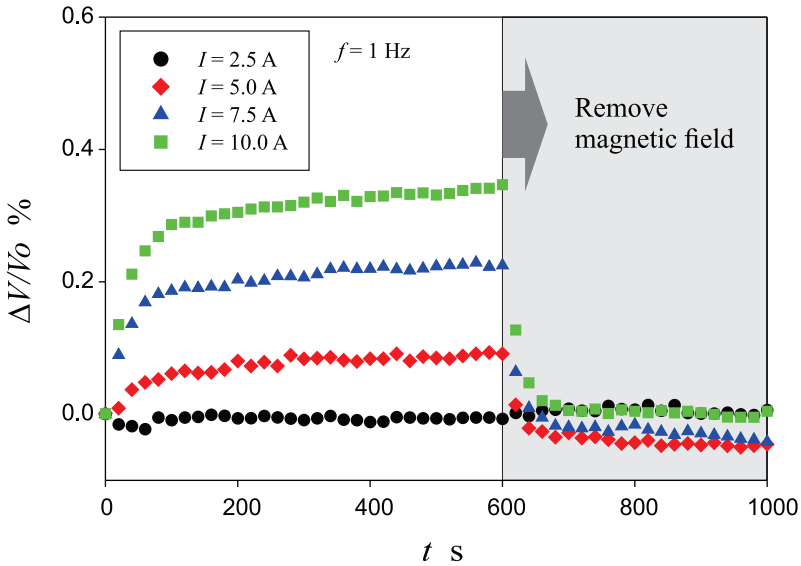

Figure 4.43: Time dependence of ultrasonic propagation velocity in MR fluid for different AC current (2.5 – 10 A)

Figure 4.44 shows the ultrasonic propagation velocity is higher at lower frequency. The size of cluster formation in MR fluid seems to be smaller when higher frequency of AC current is applied. These results indicate that frequency of AC current has significant effect on the cluster formation in MR fluid. These results is different with the previous study [151]. Takahashi et al. [151] observed that cluster size in MR fluid was not affected by frequency of AC magnetic field. This difference could be caused by the different of the applied magnetic flux density. Takahashi et al. applied 11 mT of magnetic flux density while in the current study, higher magnetic flux density is applied (B = ∼130 mT).

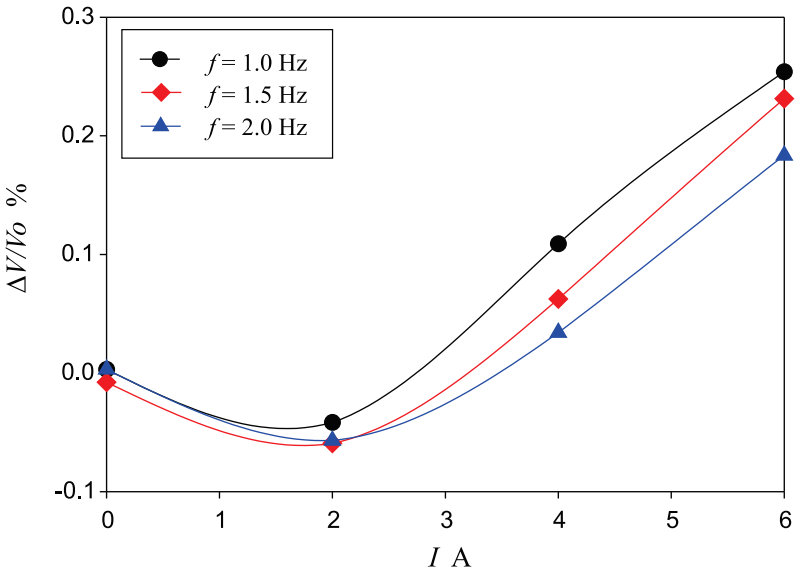

Figure 4.44: Magnetic field dependence of ultrasonic propagation velocity in MR fluid for different frequency (1 – 2 Hz)

4.5.5 Hysteresis

Similar with the DC current, hysteresis phenomenon also can be found in ultrasonic propagation velocity in the MR fluid under AC current. Figure 4.45 shows the ultrasonic propagation velocity in the MR fluid versus the current for different frequencies (f = 1 – 2 Hz). The experiment is conducted by increasing the AC current in increments of 2 A from 0 to 6 A and then decreasing it by the same amount to 0 mT.

Figure 4.45 shows the ultrasonic propagation velocity increases as the current increases from 0 to 6 A. Then, ultrasonic propagation velocity decreases, and the curves return to their initial values as the current decreases from 6 A to 0 A. These results confirm the previous results that cluster structures in the MR fluid quickly dissolve after the magnetic field is reduced to zero. Moreover, the curve of hysteresis at smaller frequency (f = 1 Hz) is higher than that value at higher frequency (f = 1.5 and 2 Hz). This result also confirms the previous results that size of cluster becomes smaller when higher frequencies of AC magnetic field are applied.

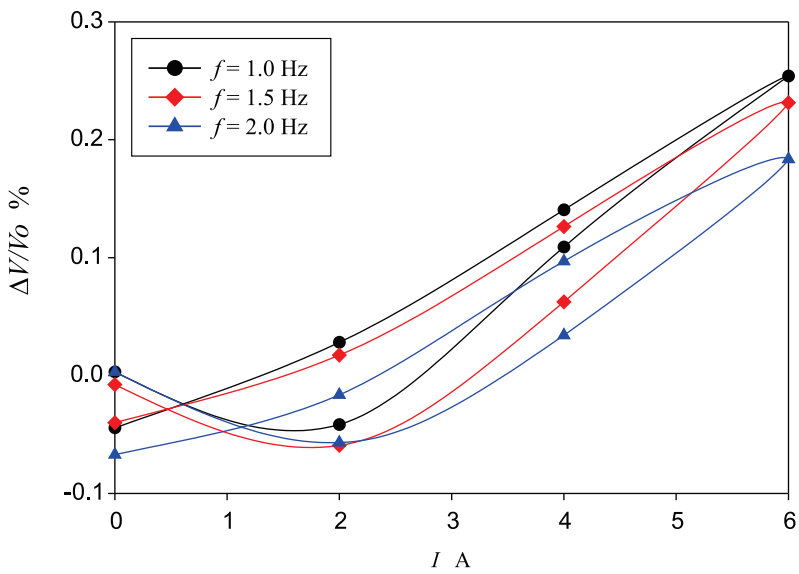

Figure 4.45: Hysteresis of ultrasonic propagation velocity in MR fluid for different frequency (1 – 2 Hz)

Chapter 5

Ultrasonic propagation properties in MR fluid under pressure

The purpose of this chapter is to explain the ultrasonic propagation properties in MR fluid under pressure. From the discussion in the previous chapter (chapter 4), the change of ultrasonic propagation properties, ultrasonic propagation velocity and attenuation, can be used to explain the cluster formation in MR fluid under magnetic field. Therefore, in this study, measurements of ultrasonic propagation velocity in MR fluid under pressure are conducted.

This chapter is divided into three sections. First section is the introduction which discusses the previous studies about the behavior of MR fluid in compression mode. Second section explain the experimental system in this study which consist of experimental apparatus, experiment parameter and experiment procedure. Third chapter discuss about the experiment results. The experiments are conducted by applying different magnetic flux densities and different pressures. The discussion focuses on the effect of pressure and magnetic flux density on the ultrasonic propagation properties in MR fluid. Moreover, discussions are intended to explain the relation between the changes of ultrasonic propagation velocities with the cluster formation in MR fluid under pressure.

5.1 Introduction

Several researchers [96, 97, 152] conducted experimental investigation of behavior of MR fluid in compression mode. The compression to the MR fluid was conducted by subjecting a load through a cylinder. The load was moved from the initial position to a certain gap. The effect of magnetic flux density, gap size and speed in the performance and behavior of MR fluid were analyzed from the measurement results of stress–strain relationship [96] and the normal force [97, 152].

Mazlan et al. [96, 153, 154] conducted experimental investigation of two different MR fluids which are water-based and hydrocarbon-based MR fluids in compression mode under various applied currents. They constructed a compression test (Fig. 5.1) where the MR fluid was sandwiched between two flat surfaces. The compression test was operated by decreasing the size of the gap at a constant rate (0.5 mm/min). They found that high values of compressive

stress occur where the compressive strain is high, and that even higher values are obtained when the magnetic flux density is high. Furthermore, they also found that the magnitude of the compressive stress, for a given compressive strain, depends on the initial gap size. From the relationship between compressive stress and compressive strain for two different initial gap sizes, they observed that for the larger initial gap size there are larger compressive stress values.

Farjoud et al. [97, 155, 156] focused on modeling and testing MR fluids in squeeze mode. They squeezed the MR fluids for different initial gap sizes, different magnetic flux densities with speeds 0.003 and 0.015 inch/s. Based on the MR fluid squeeze test results, they found that MR fluid can deliver a large range of force in squeeze mode. They also found that the amount of the force achieved depends on the type of the MR fluid, magnetic field density and gap size. Moreover, they observed that liquid carrier in MR fluid leaves the gap in greater portion than the magnetic particles when the load is pressed to the MR fluid. In other words, magnetic particles stick on the gap, at the place where magnetic field is applied. They described that phenomenon as the clumping effect.

Guo et al. [152] studied experimentally the compression properties of MR fluids under the non-uniform field. They conducted experiments by compressing the MR fluid from the initial gap (0.625 mm) at constant velocity (2 – 10 μm/s). The commercial plate-plate magneto-rheometer (Physica MCR 301; Anton Paar, Austria) was used to test the compression behaviors of MR fluids. They measured the normal force by applying a sensor built into air bearing, and it could be recorded from -50 to 50 N. They found that normal forces increase with the decreasing of the gap distance, and two regions were found through the normal force versus gap distance curves: elastic deformation and plastic flow. They also observed that high normal forces could be obtained in the case of high magnetic field, high compression velocity, low initial gap distance, high volume fraction, and high medium viscosity.

Tao [36] examined the micro-structure of the MR fluid before and after compression-assisted aggregation. In one process, he did not compress the fluid and let the resin solidify. In another process, he compressed the MR fluid with a pressure of 1.2 MPa and let the resin solidify under pressure. They let the sample solidify and cut the sample and conducted scanning electron microscope analysis. For the first sample (without the compression), he found that the MR fluid micro-structure was dominated by single chains. In the other sample, he found that the MR fluid micro-structure changed into thick columns after the compression. They observed that when MR fluid is compressed, chains get shorter and bent. When the chains are bent, the attraction between the chains becomes stronger and pulls these chains quickly together. Meanwhile, as many particles are pushed by the plates, the ends of the columns are much thicker than their middle. The illustration of compression-assisted-aggregation process is presented in Fig. 5.2.

In this study, experiments in which various magnetic fields and various pressures are conducted to investigate the effect of pressure on cluster formation in MR fluid. The gap of the MR fluid is nearly constant during the measurement. The ultrasonic propagation velocity in the MR fluid is measured and the influence of high pressure on the change of ultrasonic propagation velocity is clarified. From the results of change of ultrasonic propagation velocity, cluster formation in MR fluid under pressure is analyzed.

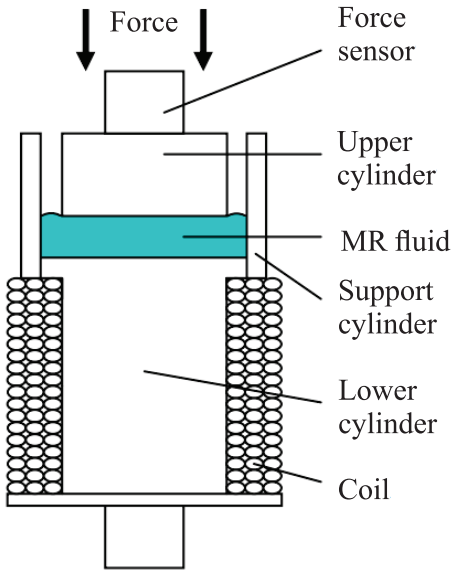

Figure 5.1: Schematic drawing of compression test of Mazlan et al. [153]

5.2 Experimental system

5.2.1 Experimental apparatus

The experimental apparatus is almost similar to the one as illustrated in Fig. 4.2. Nevertheless, the different design of test cell is applied in the current apparatus. In the new test cell, the pressure is applied to the MR fluid by subjecting some loads through a piston (Fig. 5.3). The detail of the test cell can be seen in Fig. 5.4. The frequency of the oscillator is 2 MHz. The diameter of the piston is 15.5 mm. A rubber is attached in the piston to avoid the leaking during subjecting the pressure. An air tunnel is created to remove the air when the piston is inserted to the test cell and to provide a similar volume of MR fluid for each experiments. MR fluid is placed inside the inner container. The shape of inner container in the test cell is circle (or a cylindrical container) to ensure the uniform pressure distribution. The cylinder is made from acrylic, while the piston is made from aluminum, which is non-magnetic material. The magnetic field is applied in perpendicular direction with the pressure direction. The gap size of the MR fluid after the applying pressure is assumed constant.

5.2.2 Experimental parameter

In this study, two different experiments, which are time dependence and hysteresis, are conducted. The experiment parameters are as follows:

1. Type of test fluid: MRF-132DG. The properties of MR fluid can be seen in Table 2.5.
2. Magnetic flux density, $B = 0 - 400$ mT.
3. Load masses, $M = 0 - 15$ kg. These masses correspond to the pressures, $P = 0 - 0.78$ MPa.
4. Temperature of the test fluid, $T = 25$ °C. Temperature of the test cell is kept constant for all experiments.

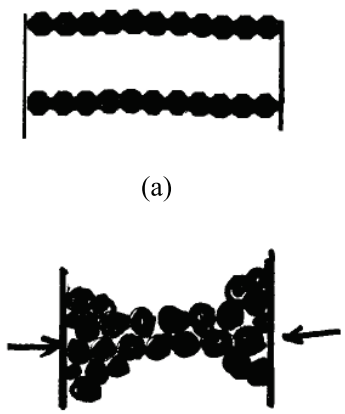

Figure 5.2: Formation of the robust MR micro-structure during compression-assisted aggregation. Chains before the compression (a) and the compression forces the chains to aggregate into thick columns with robust ends (b) [36]

.

5. Angle $\theta = 0°$. It means that the direction of ultrasonic propagation is parallel with the direction of magnetic field.

5.2.3 Experimental procedure

The procedures of each experiment are as follows:

1. The MR fluid is stirred using stirring machine for 20 min. The stirring process is conducted to minimize the effect of sedimentation. The stirring process of MR fluids is presented in Fig. 2.18.
2. Experiment is started by setting the temperature of the test cell constant at 25 °C.
3. Pressure is applied at similar time with the magnetic field. Therefore, the effect of pressure and magnetic field on cluster formation in MR fluid can be analyzed.
4. Experiments are conducted three times for similar condition to get the proper result.

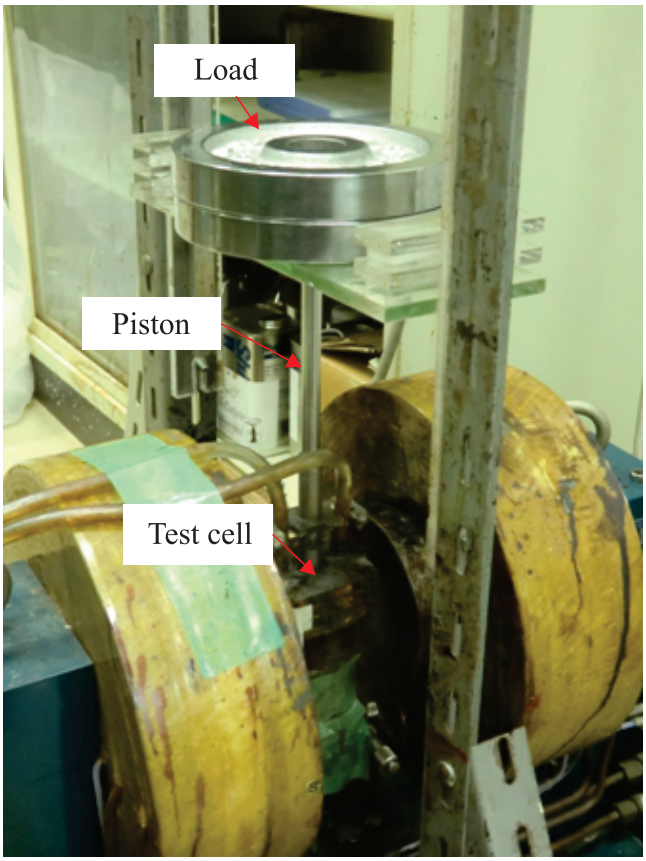

Figure 5.3: Subjecting load to the test cell through a piston

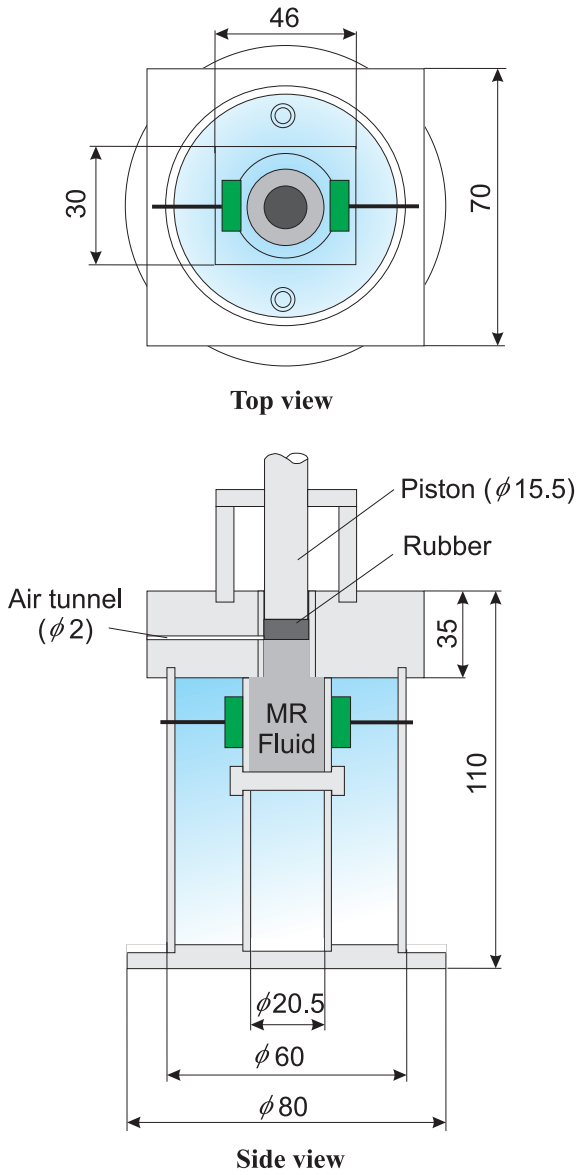

Figure 5.4: Test cell for investigating cluster formation in MR fluid under pressure ($f = 2$ MHz)

5.3 Result and discussion

The experiments are performed for time dependency and hysteresis. The effect of pressure on the inner structure of MR fluid is analyzed based on the value of change of ultrasonic propagation velocity. The change of ultrasonic propagation velocity describes the difference between initial condition and condition when magnetic field and pressure is applied. If V and V_o are the ultrasonic propagation velocity with and without magnetic field and pressure, respectively, then the value of change of ultrasonic propagation velocity ($\Delta V/V_o$) is calculated using equation below;

$$\frac{\Delta V}{V_o} = \frac{V - V_o}{V_o} \tag{5.1}$$

5.3.1 Time dependency

Time dependent experiment is conducted to investigate the formation of clustering structures in the MR fluid when it is subjected to an instantaneous magnetic field and pressure. The magnetic field and the pressure are remained constant for 5 min. This experiment is performed by applying four different magnetic flux densities (B): 100, 200, 300 and 400 mT and four different load masses (M): 2.5, 5, 7.5 and 10 kg. These masses correspond to the pressures, P: 0.13, 0.26, 0.39 and 0.52 MPa, respectively.

Figures 5.5 $\sim$ 5.8 show the ultrasonic propagation velocity in the MR fluid versus time at B = 100, 200, 300 and 400 mT, respectively, under different pressures. Ultrasonic propagation velocity changes immediately after the magnetic field and pressure are applied and become constant after several seconds. This change is probably caused by the formation of clustering structures. Magnetic particles in the MR fluid form clustering structures along the direction of the magnetic field; therefore, ultrasonic propagation velocity increases when magnetic field and pressure are applied. Clustering structures continue to grow until ultrasonic propagation velocity becomes constant.

From Figs. 5.5 and 5.6, it can be observed that at low magnetic flux densities (100 and 200 mT), the effect of pressure can be seen clearly. The change of ultrasonic propagation velocity at P = 0.52 MPa is much lower than that at lower pressures (P = 0 – 0.39 MPa). This result suggest that the size of the cluster formation at higher pressure (P = 0.52 MPa) is thinner than that at lower pressures (P = 0 – 0.39 MPa). The trend of the results is different compare to the Tao's results [36]. The different is caused by the difference setup in the experiment. In Tao's experiment, the direction of magnetic field is parallel with the compression direction. In addition, the gap of MR fluid becomes lower under the compression. Therefore, the size of clusters in MR fluid is much thicker when the gap is shorter. On the other hand, in the current experiment presented in this study, the direction of magnetic field is perpendicular in respect to the given pressure direction. Moreover, the gap of MR fluid is nearly constant during the subjecting pressure. When the cluster of MR fluid formed along the direction of magnetic field

and the given pressure is perpendicular with the direction of cluster, the size of the cluster become thinner when higher pressure is applied.

However, from Figs. 5.7 and 5.8, it can be observed that at high magnetic flux densities (300 and 400 mT), the effect of pressure is not seen clearly. The value of change of ultrasonic propagation velocity is nearly similar at different loads. These results indicate that the effect of pressure on the size of cluster formation becomes not significant at high magnetic flux density. In other words, the size of the cluster is nearly similar under different pressures.

Figure 5.9 shows the change of ultrasonic propagation velocity in MR fluid as function of magnetic flux density for different load. It shows that pressure affect the cluster size at low magnetic flux densities (B = 100 and 200 mT). Then, the effect becomes not significant at higher magnetic flux densities (B = 300 and 400 mT). These results confirm the previous results (in Chapter 3) that magnetic field has significant effect on the performance of MR fluid to handle pressure that caused by shock loading. The higher magnetic flux densities produces bigger cluster. The bigger clusters are stronger to handle the amount of pressures that caused by the shock loading (at low impact velocity, v = 0.5 m/s). However, at higher impact velocity (v = 2.0 m/s), magnetic flux density has no remarkable effect on the performance of MR fluid to handle the pressure that caused by shock loading. It seems because the pressure that caused by shock loading at high impact velocity is very high. For example pressure that caused from shock loading of M = 10.58 kg, B = 120 mT, v = 2 m/s in MRF-132DG is about 5 MPa. Therefore, clusters are not strong enough to handle the amount of high pressure (5 MPa).

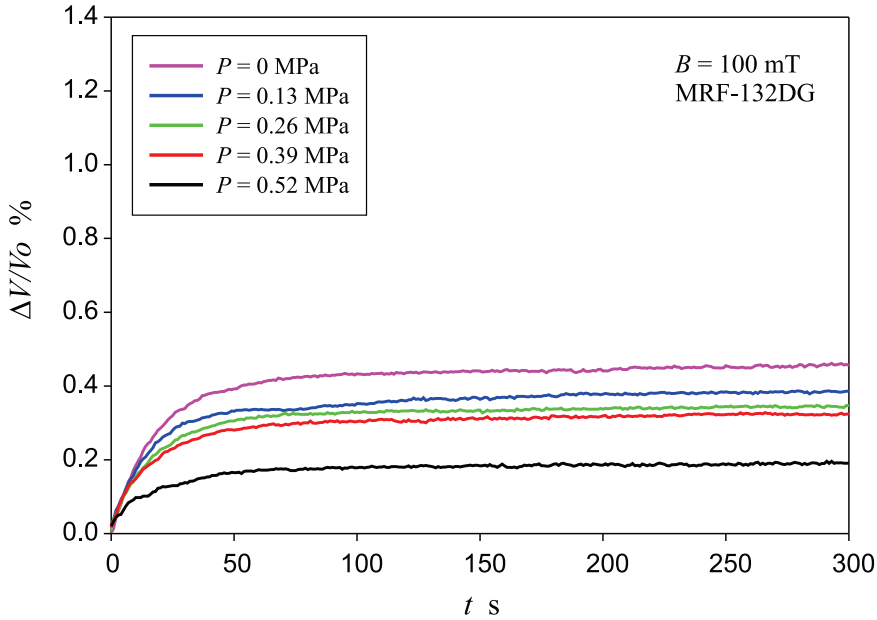

Figure 5.5: Time dependence of ultrasonic propagation velocity in MR fluid at $B = 100$ mT under different pressures

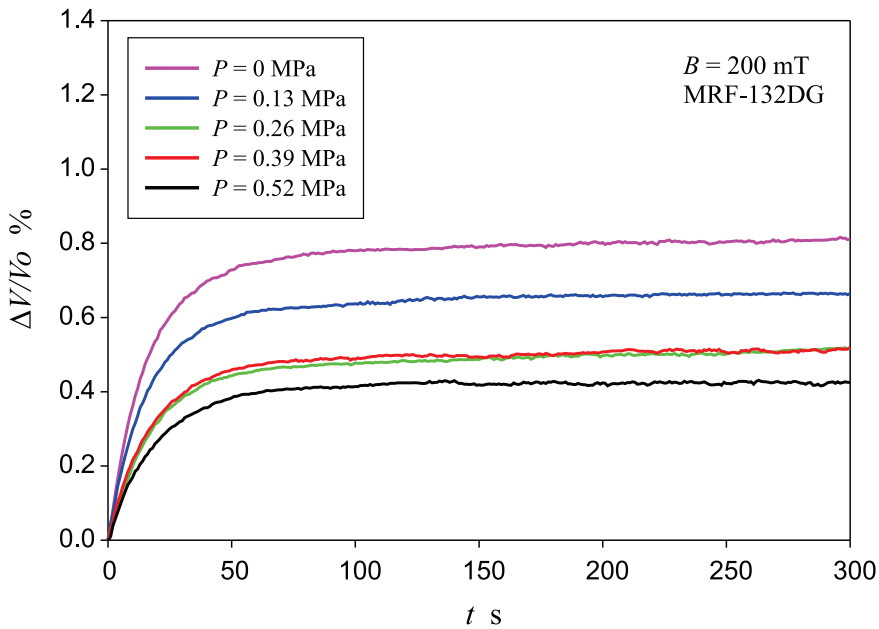

Figure 5.6: Time dependence of ultrasonic propagation velocity in MR fluid at $B = 200$ mT under different pressures

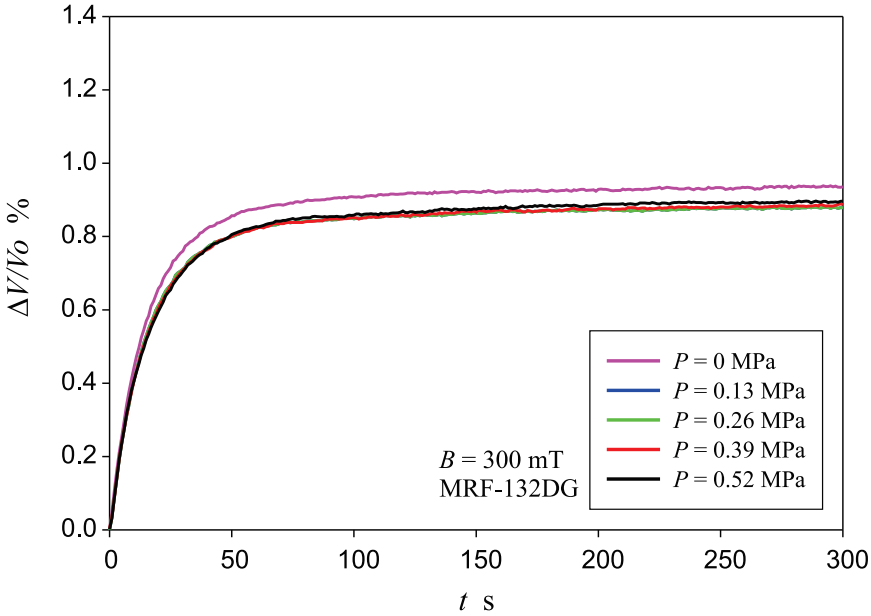

Figure 5.7: Time dependence of ultrasonic propagation velocity in MR fluid at $B = 300$ mT under different pressures

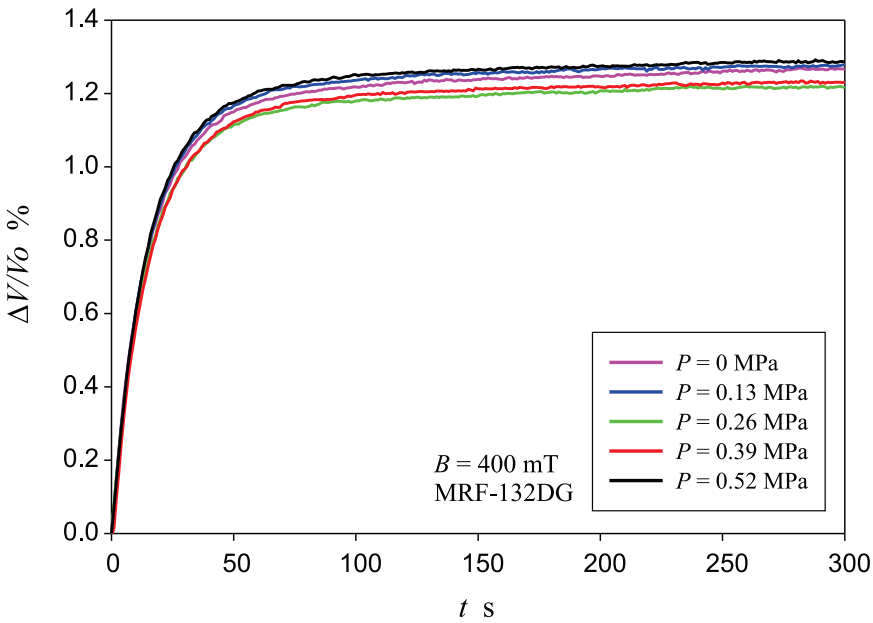

Figure 5.8: Time dependence of ultrasonic propagation velocity in MR fluid at $B = 400$ mT under different pressures

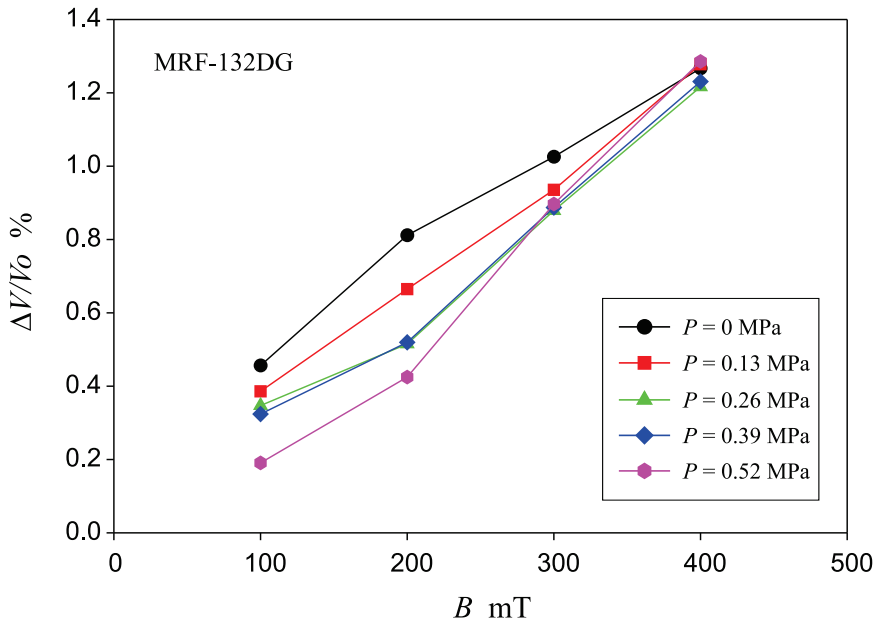

Figure 5.9: Ultrasonic propagation velocity in MR fluid as function of magnetic flux density at $t = 5$ minutes under different pressures

5.3.2 Hysteresis

Hysteresis phenomenon is also observed in ultrasonic propagation velocity in the MR fluid when the magnetic field is increased from 0 mT to a certain value and then is decreased to the initial value under constant of pressure. Figure 5.10 shows the ultrasonic propagation velocity versus the applied magnetic flux density under different pressures (P = 0, 0.26, 0.52 and 0.78 MPa). The experiment is conducted by increasing the magnetic field intensity in increments of 100 mT from 0 to 400 mT and then decreasing it by the same amount to 0 mT every 2 min. By varying the amount of pressure, the effect of the pressure in the hysteresis phenomenon can be analyzed.

Figure 5.10 shows the similar trend with the results in the previous chapter (chapter 4). For different pressure, the ultrasonic propagation velocity tends to increase as the magnetic field intensity increases from 0 to 400 mT. Then, the ultrasonic propagation velocity decreases, and the curves tends to return to their initial values as the magnetic field intensity decreases from 400 mT to 0 mT. At higher pressure, all the value of change of ultrasonic propagation velocity in the hysteresis curve is slightly lower than that at smaller pressure. These results confirm the previous results in the time dependence experiment, that cluster in MR fluid becomes thinner when higher pressure is applied.

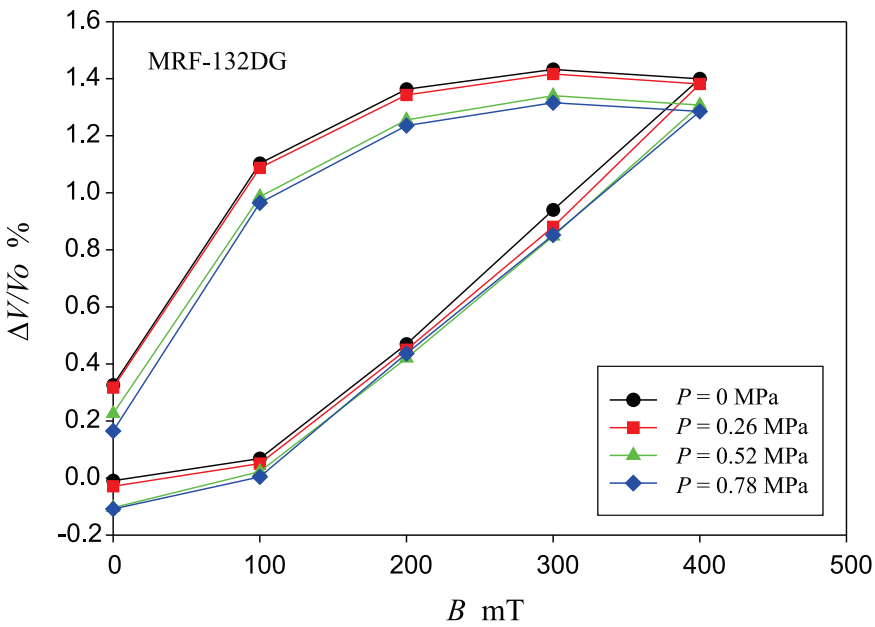

Figure 5.10: Hysteresis of ultrasonic propagation velocity in MR fluid under different pressures

Chapter 6

Conclusions and future research

In this chapter, based on the experimental result and discussion in the previous chapters, conclusion of the study is described. In addition, some future works are presented.

6.1 Conclusions

Conclusions in this study are divided into three parts, which are the investigation of behavior of MR fluid under shock loading, the investigation of ultrasonic propagation properties in MR fluid under DC and AC magnetic fluid and the investigation of ultrasonic propagation properties in MR fluid under pressure. The conclusions are match with the objectives of the research which are summarized as follow;

1. Study the behavior of MR fluids under shock loading.
2. Investigate the effect of magnetic field, volume fraction of MR fluid and orifice inner diameter in terms of the behavior of MR fluid to handle the shock loading.
3. Investigate the cluster formation in MR fluid under DC and AC magnetic field by measuring the ultrasonic propagation properties.
4. Investigate the cluster formation in MR fluid under pressure by measuring the ultrasonic propagation velocities.

6.1.1 Behavior of MR fluid under shock loading

In order to investigate the behavior of MR fluid under shock loading, experimental apparatus is successfully developed and fabricated. Based on the experiment results, which consist of relation of piston displacement, piston velocity, damping force and pressure difference, various effects (magnetic field, orifice inner diameter and volume fraction of MR fluids), in term of the behavior of MR fluid to handle shock loading are analyzed.

Effect of magnetic field

- In the relation of piston velocity to piston displacement, piston velocity increases abruptly in the initial stage. There is no influence of magnetic field on the initial increase of the

velocity because the force caused by shock loading is much greater than the viscous force of the MR fluid, which produced by the magnetic field. The piston velocity reduces after reaching the peak velocity. An almost constant velocity region appears for every magnetic flux density. The gravitational force of the drop mass and the viscous force are balanced in this area. Subsequently, the velocity decreases suddenly according to the magnetic flux density.

- For different impact velocities, after the peak value of piston velocity, the order of the velocity value follows the value of magnetic flux density. As the density of the magnetic flux increases, the velocity decreases. This implies that the magnetic field affects the reduction in the piston velocity after the shock loading.

- Piston travels at shorter distance when higher magnetic flux densities (B = 80 and 120 mT) are applied. This result agrees with the expected increase in apparent yield stress when higher magnetic flux density is applied. However, the effect of magnetic field on the movement resistance of MR fluid under shock loading reduces at higher impact velocities.

- At low impact velocity (v = 0.5 m/s), the value of F_{max} increases at higher magnetic flux density. The increasing damping force means that for higher magnetic flux density, MR fluid has more resistant under shock loading. However, at higher impact velocity (v = 2.0 m/s), the peak value of damping force is relatively similar for different magnetic flux densities. These results imply that magnetic field has no remarkable effect on the resistance force of MR fluid under shock loading at high impact velocity.

- At low impact velocity, the value of ΔP_{max} tends to increases with the increasing of magnetic flux density. The increasing of the value of ΔP_{max} means that the higher magnetic flux density is more effective to restrict the flow of MR fluid under shock loading. However, at high impact velocity, the value of ΔP_{max} is relatively similar for different magnetic flux densities. This result confirms that at high impact velocity, the magnetic field has no remarkable effect to restrict the flow of MR fluid under shock loading.

Effect of orifice inner diameter

- In the relation of piston velocity to piston displacement, piston velocities reduce after reaching the peak velocity (Vp_{max}) for different orifice inner diameter. The value of Vp_{max} and Vp after the peak value at bigger orifice inner diameter (ϕ 10 mm) is higher than that at smaller orifice inner diameter (ϕ 8.7 and ϕ 5 mm). The order of the decreasing in Vp_{max} value follows the size of orifice inner diameter for different magnetic flux density (B = 0 and 120 mT). When the orifice inner diameter decreases, the velocity decreases. In other words, the peak velocity depends on the orifice size. This difference is caused by the flow resistance through the orifice. These results imply that the orifice inner diameter affects the reduction in the piston velocity.

- The travel length of the piston becomes shorter with smaller orifice inner diameter when the intensity of the applied magnetic field is the same. These results indicate the strong

effect of orifice inner diameter towards the displacement and velocity of the piston just after MR fluid is subjected to shock loading.

- The peak value of damping force (F_{max}) increases at smaller orifice inner diameter. The value of F_{max} of ϕ 5 mm is much higher than that value of ϕ 8.6 mm and ϕ 10 mm for different drop masses. The order of the increasing value of F_{max} follow the value of drop masses. The increasing value of F_{max} means that the smaller of orifice inner diameter is more effective to resist the impact force caused by shock loading. These results indicate that orifice inner diameter has remarkable effects on the resistance force of MR fluid under shock loading.

- The peak value of pressure difference (ΔP_{max}) tend to increases with the decreasing of orifice inner diameter. The value of ΔP_{max} of ϕ 5 mm is higher than that value of ϕ 8.6 mm and ϕ 10 mm for different drop masses. The increasing value of ΔP_{max} means that the smaller of orifice inner diameter is more effective to restrict the flow of MR fluid under shock loading. These results indicate that orifice inner diameter has remarkable effects to restrict the flow of MR fluid under shock loading.

Effect of volume fraction of MR fluids

- In the relation of piston velocity to piston displacement, the value of Vp_{max} at smaller volume fraction (MRF-122EG) is higher than the value at MRF-132DG for different impact velocities. It indicates that the bigger volume fraction of MR fluid is more effective to reduce the piston velocity after reaching the peak velocity.

- At $B = 0$ mT, the value of Dp_{max} in MRF-132DG is lower than that value in MRF-122EG due to the viscosity of MRF-122EG is smaller than MRF-132DG. As a result, the piston stroke is farther for smaller viscosity. At higher magnetic flux density (120 mT), cluster formation in MRF-132DG is thicker than its value in MRF-122EG. The thicker of cluster formation increases the viscosity of MR fluid. At higher viscosity, MR fluid becomes harder to flow in the orifice area. As a result, the piston travels in a shorter distance at higher volume fraction. These results indicate that volume fraction of MR fluid affects the reduction of the piston travel length.

- The value of F_{max} of MRF-132DG is slightly higher than that value in MRF-122EG. The increasing value of F_{max} means that higher volume fraction of MR fluid (MRF-132DG) is more resistant under shock loading. These results imply that volume fraction of MR fluid has significant effect on the resistance force of MR fluid under shock loading.

- The value of ΔP_{max} tend to increase at higher impact velocity for different MR fluids. At light drop mass ($M = 5.57$ kg), it shows that the value of ΔP_{max} of MRF-132DG is slightly higher than that value in MRF-122EG. However, at heavier drop mass ($M = 7.24 \sim 10.91$ kg), the value of ΔP_{max} is nearly similar for different MR fluids. These results imply that under heavy drop mass ($M = 7.24 \sim 10.91$ kg), the effect of volume fraction of MR fluid becomes less significant to restrict the flow of MR fluid under shock loading.

6.1.2 Ultrasonic propagation properties of MR fluid under DC and AC magnetic field

In order to analyze cluster formation in MR fluid under DC and AC magnetic field, ultrasonic propagation properties which consist of ultrasonic propagation velocity and attenuation in MR fluid are measured. Based on the experiment results, various effects (temperature, elapsed time, magnetic field and magnetic field sweep rate), hysteresis phenomenon and behavior of cluster formation in MR fluid under AC magnetic field are analyzed.

Effect of temperature

- Ultrasonic propagation velocity and attenuation change with the increasing of temperature the MR fluid. This result suggests that temperature has a significant effect on ultrasonic propagation velocity and attenuation. Therefore, the temperature must be keep constant for each experiment

Effect of elapsed time

- Ultrasonic propagation velocity in MR fluid increases with time after magnetic field is applied. On the other hand, ultrasonic propagation attenuation decreases with the time after magnetic field is applied. These changes are probably caused by the formation of clustering structures. Magnetic particles in the MR fluid form clustering structures along the direction of the magnetic field. Clustering structures continue to grow until ultrasonic propagation attenuation becomes constant.

- The order of ultrasonic propagation attenuation curve complies the magnetic flux density. For higher magnetic flux density, the ultrasonic propagation attenuation becomes lower. It is likely that in MR fluids, more clusters are formed as the magnetic field increases; therefore, ultrasonic propagation attenuation decreases as the magnetic flux density increases.

Effect of magnetic field

- Ultrasonic propagation attenuation decreases as the applied magnetic flux density increases. This change seems to be caused by the formation of clustering structures: as the magnetic flux density increases, more clusters formed. This result indicates that the density of the applied magnetic field has a strong effect on ultrasonic propagation attenuation in MR fluids

- Time interval of applying magnetic field affects the value of ultrasonic propagation attenuation. Ultrasonic propagation attenuation for the 5-min interval is slightly higher than that for the 1-min interval. From these results, at 5-min interval, it seems that some magnetic particles have sufficient time to separate from clustering structures because of sedimentation when the MR fluid is applied low magnetic flux density.

Hysteresis

- Hysteresis is observed in ultrasonic propagation velocity and attenuation in the MR fluid when the magnetic flux density is increased from 0 mT to a certain value (B = 400 mT) and then is decreased to the initial value.
- The change of ultrasonic propagation velocity increased during the increasing process of magnetic field. Thus, hysteresis on MR fluid tends to return to the initial value (B = 0 mT). In other hand, ultrasonic propagation attenuation decreases as the magnetic field intensity increases from 0 to 400 mT. Then, the ultrasonic propagation attenuation increases, and the curves return to their initial values as the magnetic flux density decreases from 400 mT to 0 mT. These results confirm that clustering structures in the MR fluid quickly dissolve after the magnetic field is reduced to zero

Effect of magnetic field sweep rate

- Ultrasonic propagation velocity increased when a higher magnetic field is applied. As the ultrasonic propagation velocity increases, the cluster becomes thicker. The maximum value of the change in ultrasonic propagation velocity ($(\Delta V/V_0)_{\mathrm{max}}$) is very similar throughout the magnetic field sweep rate range from 6 to 40 mT/min. This results suggest that at that range of sweep rate, ultrasonic propagation velocity is not affected by magnetic field sweep rates.
- The value of $(\Delta V/V_0)_{\mathrm{max}}$ decreased when a higher magnetic field sweep rate is applied, as shown at 50 and 80 mT/min. The decrease of the value of $(\Delta V/V_0)_{\mathrm{max}}$ indicates that the size of the cluster becomes thinner when the magnetic field is applied at higher sweep rates. Magnetic particles in MR fluid do not have sufficient time to form clusters of bigger size at high magnetic field sweep rates. This result suggests that high sweep rate affects the size of the cluster in MR fluid.
- The influence of the volume fractions of the MR fluid on ultrasonic propagation velocity is significant. At a lower volume fraction (MRF-122EG), ultrasonic propagation velocity is lower than that for the higher volume fraction, and the cluster size is proportional to the volume fraction. As a result, the ultrasonic propagation velocity increases when the volume fraction of the MR fluid increases. In other words, the size of the cluster increases for higher volume fractions. This result suggests that the volume fraction and sweep rate affect the formation of the clustering structures in MR fluids.

Ultrasonic propagation properties of MR fluid under AC magnetic field

Cluster formation in MR fluid under AC magnetic field is analyzed in term of elapsed time dependence, magnetic field dependence and hysteresis phenomenon.

- The ultrasonic propagation velocity changes immediately after the AC magnetic field is applied and becomes constant after several seconds. The trend of this result is similar to when it is subjected to DC magnetic field. The order of ultrasonic propagation velocity

curve comply the AC current. For higher current, the ultrasonic propagation velocity becomes higher. It is likely that in MR fluids, more clusters form as the current increases; therefore, ultrasonic propagation velocity increases as the current increases.

- The ultrasonic propagation velocity decreases instantaneously after the magnetic field is removed and then becomes constant. The trend of the result is similar to when it is subjected to DC magnetic field. The curves for all currents tend to return to their initial values. It seems that the clustering structures in the MR fluid break instantaneously after the magnetic field is removed.

- For various frequency, ultrasonic propagation velocity in the MR fluid increases as the applied current increases. The ultrasonic propagation velocity is higher at lower frequency. The size of the cluster formation in MR fluid is smaller when higher frequency of AC current is applied. These results indicate that the frequency of AC current has significant effect on the cluster formation in MR fluid.

- Hysteresis phenomenon also can be found in ultrasonic propagation velocity in the MR fluid under AC current. The ultrasonic propagation velocity increases as the current increases from 0 to 6 A. Then, ultrasonic propagation velocity decreases, and the curves tends to return to their initial values as the current decreases from 6 A to 0 A. These results confirm the previous result that that cluster structures in the MR fluid quickly dissolve after the magnetic field is reduced to zero. Moreover, the curve of hysteresis at smaller frequency ($f = 1$ Hz) is higher than that value at higher frequency ($f = 1.5$ and 2 Hz). These results also confirm the previous results that size of cluster is smaller when higher frequencies of AC current are applied.

6.1.3 Ultrasonic propagation properties of MR fluid when subjected to pressure

The effect of pressure on the cluster formation in MR fluid is analyzed based on the value of change of ultrasonic propagation velocity. The change of ultrasonic propagation velocity describes the difference between initial condition and condition when magnetic field and pressure are applied. The conducted experiments consist of time dependency and hysteresis.

- Ultrasonic propagation velocity changes immediately after the magnetic field and pressure are applied, and become constant after several seconds. Magnetic particles in the MR fluid form clustering structures along the direction of the magnetic field; therefore, ultrasonic propagation velocities increases when magnetic field and pressure are applied. Clustering structures continue to grow until ultrasonic propagation velocity becomes constant.

- At low magnetic flux densities ($B = 100$ and 200 mT), the effect of pressure can be seen clearly. The change of ultrasonic propagation velocity at $P = 0.52$ MPa is much lower than that at lighter load ($P = 0 - 0.39$ MPa). As smaller the value of ultrasonic propagation velocity, the size of the cluster formation at higher pressure ($P = 0.52$ MPa) is thinner than that at lower pressures ($P = 0 - 0.39$ MPa). When the cluster of MR fluid formed along

the direction of magnetic field and the given pressure is perpendicular with the direction of cluster, the size of the cluster becomes thinner when higher pressure is applied.

- At high magnetic flux densities (B = 300 and 400 mT), the effect of pressure can not seen clearly. The value of change of ultrasonic propagation velocity is nearly similar at different loads. These results indicate that the effect of pressure on the size of cluster formation becomes not significant at high magnetic flux density. In other words, the size of the cluster is nearly similar under different pressures (P = 0 – 0.52 MPa).

- At low magnetic flux density (B = 100 and 200 mT), the change of ultrasonic propagation velocity is nearly similar under high pressures (P = 0.26, 0.39 kg and 0.52 MPa). At that range of magnetic flux densities, the cluster in MR fluid is not strong enough to hold the pressure. When higher magnetic flux densities are applied (B = 300 and 400 mT), the effect of pressure becomes not significant on the cluster formation in MR fluid since the change of ultrasonic propagation velocity is slightly similar under different pressures. These results confirm the previous results that magnetic field has significant effect on the performance of MR fluid to handle pressure that caused by shock loading. The higher magnetic flux densities produces bigger cluster. The bigger clusters are stronger to handle the amount of pressures that caused by the shock loading (at low impact velocity, v = 0.5 m/s).

6.2 Future research

In order to study more detail about the behavior of MR fluid under shock loading and the effect of pressure on the cluster formation in MR fluid, several investigations are recommended and necessary to be conducted. The following items are the future researches which are the extensions of the current study.

6.2.1 Behavior of MR fluid when subjected to shock loading

- Modeling of MR fluid flow under shock loading is necessary to be developed. Numerical and simulation studies will provide more detail understanding about the behavior of MR fluid under shock loading.

- Controlling the current correspond to the given shock loading is necessary to be added in the system. Therefore, MR fluid can perform actively in handling the shock loading.

6.2.2 Cluster formation in MR fluid under AC magnetic field

- The effect of AC magnetic field on the temperature of the test fluid is necessary to be investigated.

- The range of workable frequency from the power supply need to be increased. Currently, the range of workable frequency of AC magnetic field is very low because the coil re-

sistance in the present electromagnet is quite high. Therefore, by changing the smaller electromagnet coil, bigger range of AC magnetic field can be achieved.

6.2.3 Cluster formation in MR fluid under pressure

- In the current research, the value of the given pressure to the MR fluid is calculated from the masses of the loads. Pressure losses which can be caused by the use of rubber in the piston is neglected. In order to measure the real value of the given pressure to the MR fluid, new test cell with pressure transducer is necessary to be designed and fabricated. The position of the pressure transducer in the test cell is illustrated in Fig 6.1.

- Two sets of oscillators are necessary to use in new test cell to investigate more detail about the distribution of cluster formation in MR fluid under pressure. Figure 6.1 illustrates the two sets of oscillators in the test cell. One set is attached in the middle and another set is attached in the side area, which near to the pressure application.

- In order to accommodate the high pressures, it is necessary to design and fabricate the stronger inner container in test cell. The acrylic material in the current test cell will be changed with the aluminum material. Therefore, high pressures can be applied to the new test cell.

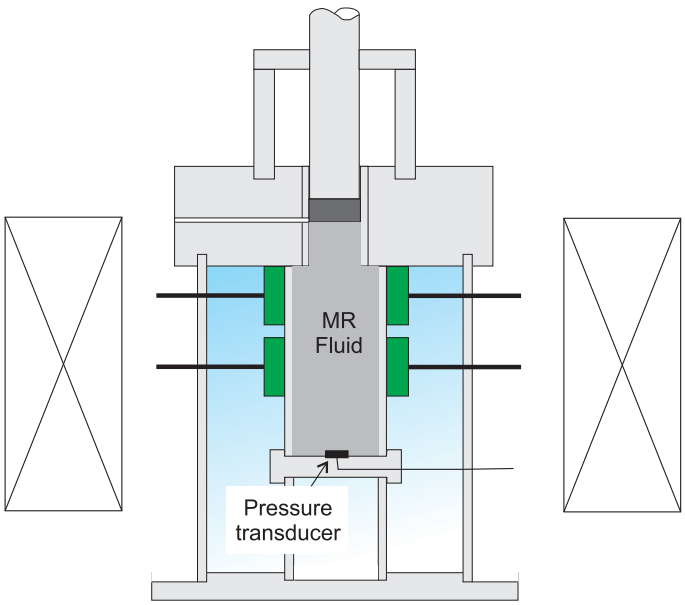

Figure 6.1: New test cell with two sets of oscillators and pressure transducer

Bibliography

[1] P. P. Phule, Magnetorheological (MR) fluids: Principles and applications, *Smart Mater. Bulletin* (2001), pp. 7–10.

[2] W. M. Winslow, Method and means for translating electrical impulses into mechanical force, *US Patent* (1947) 2417850.

[3] J. N. Foulc, P. Atten and N. Felici, Macroscopic model of interaction between particles in an electrorheological fluid, *J. Electrostat.*, **33** (1994), pp. 103–112.

[4] G. L. Gulley and R. Tao, Structures of an electrorheological fluid, *Phys. Rev. E*, **56** (1997), pp. 4328–4336.

[5] W. Wen, X. Huang and P. Sheng, Electrorheological fluids: structures and mechanism, *Soft. Matter.*, **4** (2007), pp. 200–210.

[6] W. S. Yen and P. J. Achorn, A study of the dynamic behavior of an electrorheological fluid, *J. Rheol.*, **35** (1991), pp. 1375–1384.

[7] H. See, Advances in electro-rheological fluids: materials, modelling and applications, *J. Ind. Eng. Chem.*, **10** (2004), pp. 1132–1145.

[8] J. E. Stangroom, Electrorheological fluids, *Phys. Technol.*, **14** (1983), pp. 290–296.

[9] G. L. Gulley and R. Tao, Static shear stress of electrorheological fluids, *Phys. Rev. E*, **48** (1993), pp. 2744–2751.

[10] J. Furusho, G. Zhang and M. Sakaguchi, Vibration suppression control of robot arms using a homogeneous-type electrorheological fluid, *IEEE Int. Conf. Robot.*, **4** (1997), pp. 3441–3448.

[11] H. Block and J. P. Kelly, Electo-rheology, *J. Phys. D: Appl. Phys.*, **21** (1988), pp. 1661–1677.

[12] G. M. Kamath, M. K. Hurt and N. M. Wereley, Analysis and testing of Bingham plastic behavior in semi-active electrorheological fluid dampers, *Smart Mater. Struct.*, **5** (1996), pp. 576–590.

[13] A. Inoue and S. Maniwa, Electrorheological effect of liquid cryatalline polymers, *J. Appl. Polym. Scie.*, **55** (1995),pp. 113–118.

[14] J. Rabinow, The magnetic fluid clutch, *IEEE Trans.*, **67** (1948), pp. 1308.

[15] J. C. Ulicny and A. M. Mance, Evaluation of electroless nickel surface treatment for iron powder used in MR fluids, *Mat. Sci. Eng. A*, **369** (2004), pp. 309–313.

[16] S. Genc and P. P. Phule, Rheological properties of magnetorheological fluids, *Smart Mat. Struct.*, **11**, pp. 140–146.

[17] J. D. Carlson and M. R. Jolly, MR fluid, foam and elastomer devices,*Mechatronics*, **10** (2000), pp. 555–569.

[18] M. R. Jolly, J. W. Bender and J. D. Carlson, Properties and applications of commercial magnetorheological fluids, *J. Intel. Mat. Syst. Str.*, **10** (1999), pp. 5–13.

[19] D. L. Hartsock, R. F. Novak, and G. J. Chaundy, ER fluid requirements for automotive devices, *J. Rheol.*, **35** (1991), pp. 1305–1325.

[20] E. W. Williams, S. G. Rigby, J. L. Sproston and Stanway, Electrorheological fluids applied to an automotive engine mount, *J. Non-Newton. Fluid*, **47** (1993), pp. 221–238.

[21] J. L. Sproston, R. Stanway, W. W. Williams and S. Rigby, The electrorheological automotive engine mount, *J. Electrostat.*, **32** (1994), pp. 253–259.

[22] M. Gurka, D. Adams, L. Johnston and R. Petricevic, New electrorheological fluids characteristics and implementation in industrial and mobile applications, *J. Phys: Conf. Series*, **149** (2009), 012008 (5pp).

[23] T. Kikuchi, J. Furusho and K. Oda, Development of isokinetic exercise machine using ER brake, *IEEE Int. Conf. Robot.*, **1** (2003), pp. 214–219.

[24] J. Madeja, Z. Kesy and A. Kesy, Application of electrorheological fluid in a hydrodynamic clutch, *Smart Mater. Struct.*, **20** (2011), 105005 (9pp).

[25] H. Shinno and H. Hashizume, Nanometer positioning of a linear motor-driven ultraprecision aerostatic table system with electrorheological fluid dampers, *CIRP Ann–Manuf. Techn.*, **48** (1999), pp. 289–292.

[26] T. Aoyama and I. Inasaki, Application of electrorheological fluid Ddmpers to machine tool elements, *CIRP Ann–Manuf. Techn.*, **46** (1997), pp. 309–312.

[27] T. Kuriyagawa, M. Saeki and K. Syoji, Electrorheological fluid-assisted ultra-precision polishing for small three-dimensional parts, *Precis. Eng.*, **26** (2002), pp. 370–380.

[28] W. B. Kim, S. J. Lee, Y. J. Kim and E. S. Lee, The electromechanical principle of electrorheological fluid-assisted polishing, *Int. J. Mach. Tool. Manu.*, **43** (2003), pp. 81–88.

[29] W. B. Kim, B. K. Min and S. J. Lee, Development of a padless ultraprecision polishing method using electrorheological fluid, *J. Mater. Process. Tech.*, **155-156** (2004), pp. 1293–1299.

[30] T. Noritsugu, Y. Tsuji and K. Ito, Improvement of control performance of pneumatic rubber artificial muscle manipulator by using electroreological fluid damper, *IEEE Syst. Man. Cybern.*, **4** (1999), pp. 788–793.

[31] J. Furusho, M. Sakaguchi, N. Takesue and K. Koyanagi, Development of ER brake and its application to passive force display, *J. Intel. Mat. Syst. Str.*, **13** (2002), pp. 425–429.

[32] D. G. Caldwell, Characteristics and adaptive control of pneumatic muscle actuators for a robotic elbow, *IEEE Int. Conf. Robot.*, **4** (1994), pp. 3558–3563.

[33] C. Mavroidis, Development of advanced actuators using shape memory alloys and electrorheological fluids, *Res. Nondestruct. Eval.*, **14** (2002), pp. 1–32.

[34] J. Furusho and M. Sakaguchi, New actuators using ER fluid and their applications to force display devices in virtual reality and medical treatments, *Int. J. Mod. Phys. B*, **13** (1999), pp. 2151–2159.

[35] Y. M. Han, P. S. Kang, K. G. Sung and S. B. Choi, Force feedback control of a medical haptic master using an electrorheological fluid, *J. Intel. Mat. Syst. Str.*, **18** (2007), pp. 1149–1154.

[36] R. Tao, Super-strong magnetorheological fluids, *J. Phys.: Condens. Matter*, **13** (2001), pp. 979–999.

[37] S. W. Charles, The preparation of magnetic fluids, Stefan Odenbach (Ed.): LNP, **594** Springer-Verlag Berlin Heidelberg (2002), pp. 3–18.

[38] S. Odenbach, Ferrofluids-magnetically controlled suspensions, *Colloids Surfaces A: Physicochem. Eng. Aspects*, **217** (2003), pp. 171–178.

[39] C. Scherer and A. M. Figueiredo Neto, Ferrofluids: Properties and applications, *Braz. J. Phyis*, **35** (2005), pp. 718–727.

[40] S. Taketomi, Aggregation of magnetic fluids under an external field: Micelle formation: A Review, *Jordan. J. Phyis*, **4** (2011), pp. 1–37.

[41] S. Odenbach, Recent progress in magnetic fluid research, *J. Phys.: Condens. Matter.*, **16** (2004), pp. R1135–R1150.

[42] D. E. Simon and M. Ahmadian, Vehicle evaluation of the performance of magnetorheological dampers for heavy truck suspensions, *J. Vib. Acoust.*, **123** (2001), pp. 365–375.

[43] G. Z. Yao, F. F. Yap, G. Chen, W. H. Li and S. H Yeo, MR damper and its application for semi-active control of vehicle suspension system, *Mechatronics*, **12** (2002), pp. 967–973.

[44] S. Sassi, K. Cherif, L. Mezghani, M. Thomas and A. Kotrane, An innovative magnetorheological damper for automotive suspension: from design to experimental characterization, *Smart Mater. Struct.*, **15** (2005), pp. 811–822.

[45] S. P. Kelso, Experimental characterization of commercially practical magnetorheological fluid damper technology, *Proc. SPIE*, **4332** (2001), pp. 292–299.

[46] D. E. Barber and J. D. Carlson, Performance characteristics of prototype MR engine mounts containing glycol MR fluids, *J. Intel. Mat. Syst. Str.*, **21** (2010), pp. 1509–1516.

[47] G. J. Hiemenz, W. Hu and N. M. Wereley, Semi-active magnetorheological helicopter crew seat suspension for vibration isolation, *J. Aircraft*, **45** (2008), pp. 945–953.

[48] Y. Chen, V. Wickramasinghe and D. G. Zimcik, Development of adaptive helicopter seat for aircrew vibration reduction, *J. Intel. Mat. Syst. Str.*, **22** (2011), pp. 489–502.

[49] V. A. Neelakantan and G. N. Washington, Modeling and reduction of centrifuging in magnetorheological (MR) Transmission clutches for automotive applications, *J. Intel. Mat. Syst. Str.*, **16** (2005), pp. 703–711.

[50] U. Lee, D. Kim, N. Hur and D. Jeon, Design Analysis and experimental evaluation of an MR fluid clutch, *J. Intel. Mat. Syst. Str.*, **10** (1999), pp. 701–707.

[51] J. D. Carlson, D. M. Catanzarite and K. A. St. Clair, Commercial magnetorheological fluid devices, *Int. J. Mod. Phys. B*, **10** (1996), pp. 2857.–2865.

[52] A. G. Olabi and A. Grunwald, Design and application of magneto-rheological fluid, *Mater. Design*, **28** (2007), pp. 2658–2664.

[53] K. Karakoc, E. J. Park and A. Suleman, Design considerations for an automotive magnetorheological brake, *Mechatronics*, **18** (2008), pp. 434–447.

[54] J. Huang, J. Q. Zhang, Y. Yang and Y. Q. Wei, Analysis and design of a cylindrical magneto-rheological fluid brake, *J. Mater. Process Tech.*, **129** (2002), pp. 559–562.

[55] W. H. Li and H. Du, Design and experimental evaluation of a magnetorheological brake, *Int. J. Adv. Manuf. Tech.*, **21** (2003), pp. 508–515.

[56] S. J. Dyke, B. F. Spencer Jr, M. K. Sain and J. D. Carlson, An experimental study of MR dampers for seismic protection, *Smart Mater. Struct.*, **7** (1998), pp. 693–703.

[57] G. Yang, B.F. Spencer Jr., J.D. Carlson and M.K. Sain, Large-scale MR fluid dampers: modeling and dynamic performance considerations, *Eng. Struct.*, **24** (2002), pp. 309–323.

[58] A. S. Shafer and M. R. Kermani, On the feasibility and suitability of MR fluid clutches in human-friendly manipulators, *IEEE–ASME T. Mech.*, **16** (2011), pp. 1073–1082.

[59] J. Blake and H. B. Gurocak, Haptic glove with MR brakes for virtual reality, *IEEE–ASME T. Mech.*, **14** (2009), pp. 606–615.

[60] T. Kikuchi, K. Oda and J. Furusho, Leg-robot for demonstration of spastic movements of brain-injured patients with compact, *Adv. Robotics*, **24** (2010), pp. 671–686.

[61] J. Furusho, T. Kikuchi, M. Tokuda, T. Kakehashi, K. Ikeda, S. Morimoto, Y. Hashimoto, H. Tomiyama, A. Nakagawa and Y. Akazawa, Development of shear type compact MR brake for the intelligent ankle-foot orthosis and its control; research and development in NEDO for practical application of human support robot, *Proc. Int. Conf. Rehabilitation Robotics*, **1** (2007), pp. 89–94.

[62] M. Motozawa, Y. Iizuka and T. Sawada, Experimental measurements of ultrasonic propagation velocity and attenuation in a magnetic fluid, *J. Phys.: Condens. Matter*, **20** (2008), 204117 (5pp).

[63] A. Einstein, Investigations of the theory of brownian movement, *Dover.* (1956).

[64] S. Rhurm and S. Odenbach, Particle size distribution as key parameter for the flow behavior of ferrofluids, *Phys. Fluids*, **15** (2003), 1658 (7pp).

[65] K. Raj and R. Moskowitz, Commercial applicaiton of ferrofluids, *J. Magn. Magn. Mater.*, **85** (1990), pp. 233–245.

[66] K. Raj, B. Moskowitz and R. Casciari, Advances in ferrofluid technology, *J. Magn. Magn. Mater.*, **149** (1995), pp. 174–180.

[67] K. Shimada, S. Shuchi, A. Shibayama, S. Kamiyama and A. Satoh, Effect of a magnetic cluster on the magnetic pressure of a magnetic compound fluid, *Fluid Dyn. Res.*, **34** (2004), pp. 21–32.

[68] K. Shimada and H. Oka, Magnetic characteristics of magnetic compound fluid (MCF) under DC and AC magnetic fields, *J. Magn. Magn. Mater.*, **290-291** (2005), pp. 804–807.

[69] K. Shimada, S. Shuchi, H. Kanno, Y. Wu and S. Kamiyama, Magnetic cluster and its applications, *J. Magn. Magn. Mater.*, **289** (2005), pp. 9–12.

[70] K. Shimada, Y. Akagami, S. Kamiyama, T. Fujita, T. Miyazaki and A. Shibayama, New microscopic polishing with magnetic compound fluid (MCF), *J. Intel. Mat. Syst. Str.*, **13** (2002), pp. 405–408.

[71] R. Patel, Mechanism of chain formation in nanofluid based MR fluids, *J. Magn. Magn. Mater.*, **323** (2011), pp. 1360–1363.

[72] K. Ozaki and T. Fujiwara, An experimental study of high-speed single stage magnetic fluid seals, *J. Magn. Magn. Mater.*, **65** (1987), pp. 382–384.

[73] K. Nakatsuka, Trends of magnetic fluid applications in Japan, *J. Magn. Magn. Mater.*, **122** (1993), pp. 387–394.

[74] T. A. Osman, G. S. Nada, Z. S. Safar, Static and dynamic characteristics of magnetized journal bearings lubricated with ferrofluid, *Tribol. Int.*, **34** (2001), pp. 369–380.

[75] K. Nakatsuka and H. Yokoyama, Damper application of magnetic fluid for a vibration isolating table, *J. Magn. Magn. Mater.*, **65** (1987), pp. 359–362.

[76] K. Morita, Magnetic fluid bearing, *US Patent* No. 5032751, 1991.

[77] T. H. C. Childs and H. J. Yoon, Magnetic fluid grinding cell design, *CIRP Ann–Manuf. Techn.*, **41** (1992), pp. 343–346.

[78] N. Umehara and S. Kalpakjian, Magnetic fluid grinding a new technique for finishing advanced ceramics, *CIRP Ann–Manuf. Techn.*, **43** (1994), pp. 185–188.

[79] Y. Tani, K. Kawata, K. Nakayama, Development of high-efficient fine finishing process using magnetic fluid, *CIRP Ann–Manuf. Techn.*, **33** (1984), pp. 217–220.

[80] N. Umehara, MAGIC polishing, *J. Magn. Magn. Mater.*, **252** (2002), pp. 341–343.

[81] A. Jordan, R. Scholz, P. Wust, H. Fakhling and R. Felix, Magnetic fluid hyperthermia (MFH): Cancer treatment with AC magnetic field induced excitation of biocompatible superparamagnetic nanoparticles, *J. Magn. Magn. Mater.*, **201** (1999), pp. 413–419.

[82] C. Alexiou, W. Arnold, R. J. Klein, F. G. Parak, P. Hulin, C. Bergemann, W. Erhardt, S. Wagenpfeil, and A. S. Lubbe, Locoregional cancer treatment with magnetic drug targeting, *Cancer Res.*, **60** (2000), pp. 6641–6648.

[83] C. C. Berry and A. S. G. Curtis, Functionalisation of magnetic nanoparticles for applications in biomedicine, *J. Phys. D: Appl. Phys.*, **36** (2003), pp. R198–R206

[84] Q. A. Pankhurst, J. Connolly, S. K. Jones and J. Dobson, Applications of magnetic nanoparticles in biomedicine, *J. Phys. D: Appl. Phys.* **36** (2003), pp. R167–R181.

[85] M. R. Jolly, J. W. Bender, and J. D. Carlson, Properties and applications of commercial magnetorheological fluids, *SPIE 5th Annual Int. Symp. Smart Struct. Mater.*, San Diego, CA, March (1998).

[86] G. Bossis, S. Lacis, A. Meunier and O. Volkova, Magnetorheological fluids, *J. Magn. Magn. Mater.*, **252** (2002), pp. 224–228.

[87] T. Siretanu and N. Stoia, Damping optimization of passive and semi-active vehicle suspension by numerical simulation, *Proc. Rom. Acad. Ser. A*, **4** (2003), pp. 1–7.

[88] W. H. Li, G. Z. Yai, G. Chen, S. H. Yeo and F. F. Yap, Testing and steady state modeling of a linear MR damper under sinusoidal loading, *Smart Mater. Struct.*, **9** (2000), pp. 95–102.

[89] W. W. Chooi and S. O. Oyadiji, Design, modeling and testing of magnetorheological (MR) dampers using analytical flow solutions, *Comput. struct.*, **86** (2008), pp. 473–482.

[90] A. K. El Wahed, J. L. Sproston and G. K. Schleyer, Electrorheological and magnetorheological fluids in blast resistant design applications, *Mater. Design*, **23** (2002), pp. 391–404.

[91] M. Ahmadian and J. A. Norris, Experimental analysis of magnetorheological dampers when subjected to impact and shock loading, *Commun. Nonlinear Sci. Numer. Simul.*, **13** (2008), pp. 1978–1985.

[92] J. Rodriguez-Lopez, L. E. Sewura and F. M. E. Freijo, Ultrasonic velocity and amplitude characterization of magnetorheological fluids under magnetic fields, *J. Magn. Magn. Mater.*, **324** (2012), pp. 222–230.

[93] M. Motozawa and T. Sawada, Velocity and attenuation of ultrasonic propagation in magnetic fluids under a uniform magnetic field, *Int. J. App. Electromagnet. Mech.*, **28** (2008), pp. 143–148.

[94] T. Ukai and T. Maekawa, Patterns formed by paramagnetic particles in a horizontal layer of a magnetorheological fluid subjected to a dc magnetic field, *Phys. Rev.*, **69** (2004), 032501 (4pp).

[95] M. A. Bramantya, M. Motozawa and T. Sawada, Ultrasonic propagation velocity in magnetic and magnetorheological fluids due to an external magnetic field, *J. Phys.: Condens. Matter*, **22** (2010), 324102 (5pp).

[96] S. A. Mazlan, N. B. Ekreem and A. G. Olabi, The performance of magnetorheological fluid in squeeze mode, *Smart Mater. Struct.*, **16** (2007), pp. 678–1682.

[97] A. Farjoud, R. Cavey, M. Ahmadian and M. Craft, Magneto-rheological fluid behavior in squeeze mode, *Smart Mater. Struct.*, **18** (2009), 095001 (7pp).

[98] H. Yoshioka, J. C. Ramallo, and B. F. Spencer Jr., "Smart" base isolation strategies employing magnetorheological dampers, *J. Eng. Mech-ASCE*, **128** (2002), pp. 540–551.

[99] J. C. Ramallo, E. A. Johnson, and B. F. Spencer, "Smart" base isolation systems, *J. Eng. Mech-ASCE*, **128** (2002), pp. 1088-1099.

[100] X. Wang and F. Gordaninejad, Flow analysis and modeling of field-contrallable, electro- and Magneto-rheological fluid dampers, *J. Appl. Mech.*, **74** (2007), pp. 13–22.

[101] W. W. Chooi and S. O. Oyadiji, Mathematical modeling, analysis and design of magnetorheological (MR) dampers, *J. Vib. Acoust.*, **131** (2009), 061002 (10pp).

[102] W. W. Chooi and S. O. Oyadiji, Experimental testing and validation of a magnetorheological (MR)damper model, *J. Vib. Acoust.*, **131** (2009), 061003 (10pp).

[103] U. Dogruer, F. Goridaninejad and C. A. Evrensel, A new magneto-rheological fluid damper for high-mobility multi-purpose wheeled vehicle (HMMWW), *J. Intel. Mat. Syst. Str.*, **19** (2008), pp. 641–650.

[104] B. F. Spencer, J. D. Carlson, M. K. Sain and G. Yang, On the current status of magnetorheological dampers: seismic protection of full-scale structures, *Proc. Amer. Control Conf.*, **1** (1997), pp. 458–462.

[105] M. Ahmadian and J. A. Norris, Rheological controllability of double-ended MR dampers subjected to impact loading, *Proc. SPIE*, **5386** (2004), pp. 185–194.

[106] Lord Corporation website, http://www.lord.com

[107] B. N. Taylor and C. E. Kuyatt, Guidelines for evaluating and expressing the uncertainty of NIST measurement results, *NIST Tech. Note*, **1297** (1994), pp. 1–24.

[108] J. M. Bland and D. G. Altman, Statistical methods for assessing agreement between two methods of clinical measurement, *Int. J. Nurs. Stud.*, **47** (2010), pp. 931–936.

[109] K. Sano and M. Doi, Theory of agglomeration of ferromagnetic particles in magnetic fluids, *J. Phys. Soc. Jpn.* **52** (1983), pp. 2810–2815.

[110] S. Taketomi, H. Takahashi, N. Inaba and H. Miyajima, Experimental and Theoretical investigations on agglomeration of magnetic colloidal particles in magnetic fluids, *J. Phys. Soc. Jpn.*, **60** (1991), pp. 1689–1707.

[111] E. Lemaire, A. Meunier, G. Bossis, J. Liu, D. Felt, P. Bashtovoi and N. Matoussevitch, Influence of the particle size on the rheology of magnetorheological fluids, *J. Rheol.*, **39** (1995), pp. 1011–1020.

[112] G. Bossis, O. Volkova, S. Lacis and A. Meunier, Magnetorheology: fluids, structures and rheology, Stefan Odenbach (Ed.): LNP, **594** Springer-Verlag Berlin Heidelberg (2002), pp. 202–230.

[113] M. Hagenbuchle and J. Liu, Chain formation and chain dynamic in a dilute magnetorheological fluid, *Appl. Optics*, **36** (1997), pp. 7664–7671.

[114] J. D. Parsons, Sound velocity in a magnetic fluid, *J. Phys. D: Appl. Phys.*, **8** (1975), pp. 1219–1226.

[115] F. M. Leslie, Some constitutive equations for liquid crystals, *Arch. Ratl. Mech. Anal*, **28** (1968), pp. 265–283.

[116] K. Gotoh, W. E. Isler and D. Y. Chung, Theory of ultrasonic attenuation in magnetic fluids, *IEEE Trans.*, **16** (1980), pp. 211–213.

[117] K. Gotoh and D. Y. Chung, Ultrasonic attenuation in magnetic fluids, *J. Phys. Soc. Jpn.*, **53** (1984), pp. 2521–2528.

[118] I. Ye. Tarapov, N. F. Patsegon and A. I. Phedonenko, Some physical and mechanical phenomena in magnetizable fluids, *J. Magn. Magn. Mater.*, **39** (1983), pp. 51–55.

[119] S. Taketomi, The anisotropy of the sound attenuation in magnetic fluid under an external magnetic field, *J. Phys. Soc. Jpn.*, **55** (1986), pp. 838–844.

[120] Y. Nahmad-Molinari, C. A. Arancibia-Bulnes and J. C. Ruiz-Suarez, Sound in a Magnetorheological Slurry, *Phys. Rev. Lett.*, **82** (1999), pp. 727–730.

[121] T. Kruse, A. Sanoudaki and R. Pelster, Monte Carlo simulations of polydisperse ferrofluids: Cluster formation and field-dependent microstructure, *Phys. Rev. B*, **68** (2003), 054208 (12pp).

[122] S. Kantorovich, J. J. Cerda and C. Holm, Microstructure analysis of monodisperse ferrofluid monolayers: theory and simulation, *Phys. Chem. Chem. Phys.*, **10** (2008), pp. 1883–1895.

[123] Y. Ido, T. Yamaguchi and Y. Kiuchi, Distribution of micrometer-size particles in magnetic uids in the presence of steady uniform magnetic field, *J. Magn. Magn. Mater.*, **323** (2011), pp. 1283–1287.

[124] Y. Ido, T. Inagaki and T. Yamaguchi, Numerical simulation of microstructure formation of suspended particles in magnetorheological fluids, *J. Phys. Condens. Matter.*, **22** (2010), 324103 (7pp).

[125] J. Cernak, Aggregation of needle-like macro-clusters in thin layers of magnetic fluid, *J. Magn. Magn. Mater.*, **132** (1994), pp. 258–269.

[126] J. Cernak and P. Macko, The time dependence of particle aggregation in magnetic fluid layers, *J. Magn. Magn. Mater.*, **123** (1993), pp. 107–116.

[127] J. Cernak, G. Helgesen and A. T. Skjeltorp, Aggregation dynamics of nonmagnetic particles in a ferrofluid, *Phys. Rev. E*, **70** (1994), 0315404 (8pp).

[128] T. Sawada, H. Kikura, G. Yamanaka, M. Matsuzaki, M. Aritomi and I. Nakatani, Visualization of clustering on non-magnetic and ferromagnetic particles in magnetic fluids, *Proc. SPIE*, **3783** (1999), pp. 389–396.

[129] B. Jeyadevan and I. Nakatani, Characterization of field-induced needle-like structures in ionic and water-based magnetic fuids, *J. Magn. Magn. Mater.*, **201** (1999), pp. 62–65.

[130] B. J. de Gans, N. J. Duin, D. van den Ende and J. Mellema, The influence of particle size on the magnetorheological properties of an inverse ferrofluid, *J. Chem. Phys.*, **113** (2000), pp. 2032–2042.

[131] M. A Bramantya, H. Takuma, J. Kuroiwa and T. Sawada, A study on the inner structure of magnetorheological fluids by image processing, *J. Jpn. Soc. Appl. Elec. Mech.*, **19** (2011), pp. 228–233.

[132] M. T. López-López, J. de Vicente, G. Bossis, F. Gonzáales-Caballero and J. D. G. Durán, Preparation of stable magnetorheological fluids based on extremely bimodal ironmagnetite suspensions, *J. Mater. Res.*, **20** (2005), pp. 874–881.

[133] D. Y. Chung, H. Z. Hung and J. X. Lin, Ultrasonic properties of magnetic fluids, *J. Magn. Magn. Mater.*, **39** (1983), pp. 111–112.

[134] A. Skumiel, T. Hornowski and A. Józefczak, Investigation of magnetic fluids by ultrasonic and magnetic methods, *Ultrasonics*, **38** (2000), pp. 864–867.

[135] A. Józefczak, The time dependence of the changes of ultrasonic wave velocity in ferrofluid under parallel magnetic field, *J. Magn. Magn. Mater.*, **256** (2003), pp. 267–270.

[136] M. A. Bramantya, H. Takuma, M. Faiz and T. Sawada, Ultrasonic propagation velocity in magneto rheological fluid under a uniform magnetic fields, *J. Jpn. Soc. Appl. Elec. Mech*, **17** (2009), pp. 433–436.

[137] M. A. Bramantya, H. Takuma and T. Sawada, Ultrasonic study of a magnetorheological fluid under uniform magnetic fields, *J. Jpn. Soc. Appl. Electromagn. Mech*, **17** (2009), pp. 279–284.

[138] M. Motozawa, T. Sawada and Y. Matsumoto, Properties of ultrasonic propagation in functional fluids under magnetic fields, *Int. J. Mod. Phys. B*, **21** (2007), pp. 4914–4921.

[139] M. A. Bramantya, M. Motozawa, H. Takuma, M. Faiz and T. Sawada, Experimental analysis of clustering structures in magnetic and MR fluids using ultrasound, *J. Phys.: Conf. Series*, **149** (2009), 012040 (4pp).

[140] D. Y. Chung and W. E. Isler, Ultrasonic velocity anisotropy in ferrofluids under the influence of a magnetic field, *J. Appl. Phys.*, **49** (1978), pp. 1809–1811.

[141] K. Shah and R. V. Upadhyay, Experimental investigation of ultrasonic velocity anisotropy in magnetic fluids: Influence of grain-grain interaction, *PRAMANA-J. Phys.*, **77** (2011), pp. 345–355.

[142] A. Józefczak, M.Łabowski and A. Skumiel, Hysteresis of changes of ultrasonic wave absorption coefficient in a magnetic fluid caused by the magnetic field, *J. Magn. Magn. Mater.*, **252** (2002), pp. 356–359.

[143] M. A. Bramantya, H. Takuma and T. Sawada, Hysteresis phenomena of ultrasonic velocity change in magnetorheological fluids, *Int. J. Appl. Elec. Mech.*, **33** (2010), pp. 1365–1372.

[144] C. Y. Wen, J. Z. Lin, M. Y. Chen, L. Q. Chen and T. K. Liang, Effects of sweep rates of external magnetic fields on the labyrinthine instabilities of miscible magnetic fluids, *J. Magn. Magn. Mater.*, **323** (2011), pp. 1258–1262.

[145] A. Isnikurniawan, J. Kuroiwa, S. Abell and T. Sawada, Ultrasonic propagation attenuation in an MR fluid under an external magentic field, *J. Jpn. Soc. Appl. Elec. Mech.*, **20** (2012), pp. 434–439.

[146] A. Józefczak, A. Skumiel and M.Łabowski, Effects of the sweep rate of the magnetic field on the changes of ultrasonic wave velocity in magnetic fluid, *J. Magn. Magn. Mater.*, **258–259** (2003), pp. 474–476.

[147] A. Isnikurniawan, J. Kuroiwa, S. Abell and T. Sawada, Investigation of cluster growth in MR fluids using ultrasonic wave propagation, *J.Phys.: Conf. Ser.*, **412** (2013), 012019 (5pp).

[148] V. A. D. Grosso and C. W. Mader, Speed of sound in pure water, *J. Acoust. Soc. Am.*, **52** (1972), pp. 1442–1446.

[149] H. Kikura, Y. Takeda and F. Durst, Velocity profile measurement of the Taylor vortex flow of a magnetic fluid using the ultrasonic Doppler method, *Exp. Fluid*, **26** (1999), pp. 208–214.

[150] H. Morimoto and T. Maekawa, Cluster structures and cluster-cluster aggregations in a two-dimensional ferromagnetic colloidal system, *J. Phys. A: Math. Gen.*, **33** (2000), pp. 247–258.

[151] H. Takahashi, T. Hayashida, H. Kikura, M. Aritomi and K. Okada, A fundamental study on behaviors of magnetic particles in magnetic fluid and magnetorheological fluid under alternating magnetic fluid, *Proc. JSME Fluid Eng. Div.*, Kawagoe, Japan, (2006), 215 (4pp) (in Japanese).

[152] C. Guo, X. Gong, S. Xuan, L. Qin and Q. Yan, Compression behaviors of magnetorheological fluids under nonuniform magnetic field, *Rheol. Acta*, **52** (2013), pp. 165–176.

[153] S. A. Mazlan, N. B. Ekreem and A. G. Olabi, Apparent stress-strain relationships in experimental equipment where magnetorheological fluids operate under compression mode, *J. Phys. D: Appl. Phys.*, **41** (2008), 095002 (6pp).

[154] S. A. Mazlan, A. Issa, H. A. Chowdhury and A. G. Olabi, Magnetic circuit design for the squeeze mode experiments on magnetorheological fluids, *Mater. Design*, **30** (2009), pp. 1985–1993.

[155] A. Farjoud, M. Ahmadian and R. Cavey, Rheometer characterization of MR fluids in squeeze mode, *Proc. SPIE*, **7288** (2009), 72880R (14pp).

[156] A. Farjoud, M. Ahmadian and R. Cavey, Non-dimensional modeling and experimental evaluation of a MR squeeze mode rheometer, *J. Phys.: Conf. Series*, **149** (2009), 012048 (4pp).

Supplementary Materials

Article on periodicals (related to the thesis)

1. A. Isnikurniawan, Y. Moroka, H. Ohba and T. Sawada, Experimental investigation into the effect of a magnetic field on magnetorheological fluids under an impact load, *Materials Science Forum*, **721** (2012), pp. 179–184.

2. A. Isnikurniawan, J. Kuroiwa, S. Abell and T. Sawada, Ultrasonic propagation attenuation in an MR fluid under an external magnetic field, *Journal of the Japan Society of Applied Electromagnetics and Mechanics*, **20**, No. 2 (2012), pp. 434–439.

3. Y. Moroka, A. Isnikurniawan, H. Ohba and T. Sawada, Effect of a uniform magnetic field on magnetorheological fluid under an impact load, *International Journal of Applied Electromagnetics and Mechanics*, **39**, No. 1–4 (2012), pp. 569–573.

4. A. Isnikurniawan, Y. Fujita, S. Tanimoto and T. Sawada, Investigation of ultrasonic properties of MR fluid under various sweep rates of magnetic field, *Magnetohydrodynamics*, Accepted for publication.

5. Y. Fujita, A. Isnikurniawan, S. Tanimoto and T. Sawada Ultrasonic characteristics of a magnetic fluid under compressive force, *Magnetohydrodynamics*, Accepted for publication.

Article on international conference proceedings (reviewed full-length articles)

1. A. Isnikurniawan*, J. Kuroiwa, S. Abell and T. Sawada, Investigation of cluster growth in MR fluids using ultrasonic wave propagation, *Journal of Physics: Conference Series*, **412** (2013), 012019 (5pp).

Presentations at international conferences

1. A. Isnikurniawan*, Y. Moroka, H. Ohba and T. Sawada, Experimental investigation into the effect of a magnetic field on magnetorheological fluids under an impact load, 7th Japanese-Mediterranean and Central European Workshop on Applied Electromagnetic Engineering for Magnetic, Superconducting and Nano Materials, Budapest, Hungary, 6–9 July 2011.

2. Y. Moroka*, A. Isnikurniawan, H. Ohba and T. Sawada, Effect of a uniform magnetic field on magnetorheological fluid under an impact load, 15th International Symposium on Applied Electromagnetics and Mechanics, Napoli, Italy, 6–9 September 2011.

3. A. Isnikurniawan*, J. Kuroiwa, S. Abell and T. Sawada, Ultrasonic propagation attenuation in an MR fluid under an external magnetic field, 20th Magnetodynamics Conference, Kaohsiung, Taiwan, 14–16 November 2011.

4. H. Ohba*, A. Isnikurniawan, Y. Moroka, H. Kaneko and T. Sawada, Effect of the orifice inner-diameter on damping characteristic of MR fluid under shock loading, 20th Magnetodynamics Conference, Kaohsiung, Taiwan, 14–16 November 2011.

5. A. Isnikurniawan*, J. Kuroiwa, S. Abell and T. Sawada, Investigation of cluster growth in MR fluids using ultrasonic wave propagation, 13th International Conference on Electrorheological Fluids and Magnetorheological Suspensions, Ankara, Turkey, 2–6 July 2012.

6. A. Isnikurniawan*, H. Ohba, H. Kaneko and T. Sawada, Experimental investigation of resistance force of MR fluid when subjected to a shock loading, The Asia-Pacific Symposium on Applied Electromagnetics and Mechanics 2012, Ho Chi Minh City, Vietnam, 25–27 July 2012.

7. A. Isnikurniawan*, Y. Fujita, S. Tanimoto and T. Sawada, Investigation of ultrasonic properties of MR Fluid under various sweep rates of magnetic field, 13th International Conference on Magnetic Fluids, New Delhi, India, 7–11 January 2013.

8. Y. Fujita*, A. Isnikurniawan, S. Tanimoto and T. Sawada, Ultrasonic characteristics of a magnetic fluid under compressive force, 13th International Conference on Magnetic Fluids, New Delhi, India, 7–11 January 2013.

9. A. Isnikurniawan, Y. Fujita, S. Tanimoto* and T. Sawada, Investigation of inner structure in magnetic fluid under compression using ultrasonic measurement, 8th Japanese-Mediterranean Workshop on Applied Electromagnetic Engineering for Magnetic, Superconducting, Multifunctional and Nanomaterials, Athens, Greece, 23–26 June 2013.

10. A. Isnikurniawan, H. Ohba, H. Kaneko, R. Yoshizawa* and T. Sawada, Effect of chamfered orifice inlet on magnetorheological fluid subjected to shock loading, 16th International Symposium on Applied Electromagnetics and Mechanics, Quebec, Canada, 31 July–2 August 2013.

11. Y. Fujita*, A. Isnikurniawan, S. Tanimoto and T. Sawada, Ultrasonic propagation characteristics of a magnetic fluid under AC magnetic fields, 16th International Symposium on Applied Electromagnetics and Mechanics, Quebec, Canada, 31 July–2 August 2013.

Presentations at domestic meetings

1. A. Isnikurniawan*, J. Kuroiwa, Y. Suzuki and T. Sawada, Experimental measurements of ultrasonic propagation attenuation in MR fluids under a uniform magnetic field, Annual Seminar of JSME Kanto Branch, Yokohama, Japan, 18–19 March 2011.

2. A. Isnikurniawan*, H. Ohba, Y. Moroka and T. Sawada, Behavior of MR fluids under a uniform magnetic field subjected to an impact load, 23rd Symposium on Electromagnetics and Dynamics, Nagoya, Japan, 18–20 May 2011.

3. A. Isnikurniawan*, J. Kuroiwa and T. Sawada, Effect of magnetic field on ultrasonic propagation attenuation in MR fluids, Japan Symposium on Visualization, Toyama, Japan, 26–27 September 2011.

4. A. Isnikurniawan*, Y. Moroka, H. Ohba, H. Kaneko and T. Sawada, Damping characteristic of MR fluid under shock loading, Japan Symposium on Magnetic Fluid, Hikone, Japan, 1–2 December 2011.

5. A. Isnikurniawan*, J. Kuroiwa S. Abell and T. Sawada, Experimental analysis of cluster growth in MR fluid under magnetic field, 24th Electromagnetic and Dynamic Symposium, Toyama, Japan, 16–18 May 2012.

6. Y. Fujita*, A. Isnikurniawan, S. Tanimoto and T. Sawada, Ultrasonic propagation properties of a magnetic fluid under high pressure, JSME on Fluids Engineering Division, Kyoto, Japan, 17–18 November 2012 (in Japanese).

7. A. Isnikurniawan*, H. Kaneko, R. Yoshizawa and T. Sawada, Investigation on damping characteristic of different volume fraction of MR fluids subjected to shock loading, 21st Magnetodynamics Conference, Sendai, Japan, 21–23 November 2012.

8. H. Kaneko*, A. Isnikurniawan, H. Ohba, R. Yoshizawa and T. Sawada, Influence of the particle concentration on the resistance of the shock absorber using MR fluid, The Japan Symposium on Magnetic Fluid, Kyoto, Japan 29 November–1 December 2012 (in Japanese).

9. I. P. Purwanto*, A. Isnikurniawan, T. Sawada and M. A. Bramantya, Experimental study of magnetorheological fluids under impact loading for low magnetic field, The Japan Symposium on Magnetic Fluid, Kyoto, Japan 29 November–1 December 2012.

10. S. Tanimoto*, A. Isnikurniawan, Y. Fujita and T. Sawada, Ultrasonic propagation properties in magnetorheological fluid under alternating magnetic field, 25th Symposium on Electromagnetics and Dynamics, Hakone, Japan, 15–17 May 2013 (in Japanese).

Others

1. T. Sawada*, A. Isnikurniawan, M. A. Bramantya and M. Motozawa, Ultrasonic propagation properties of magnetic and MR fluids, Japan-Taiwan International Conference on Magnetic fluid, Kyoto, Japan, 30 November–1 December 2012.

2. T. Sawada, A. Isnikurniawan, M. Motozawa and M. A. Bramantya, Application of ultrasonic technique for magnetic functional fluids, Final report of research committee on integration of fluid power systems with functional fluids, (2012), pp. 65–69 (in Japanese).

Award

1. Young Author's Award, 20th Magnetodynamics Conference, Taiwan, 2011.